AD NUMBER

AD809305

LIMITATION CHANGES

TO:

Approved for public release; distribution is unlimited.

FROM:

**Distribution authorized to U.S. Gov't. agencies and their contractors;
Administrative/Operational Use; 22 MAR 1967.
Other requests shall be referred to U.S. Army Signal Propagation Agency, Fort Monmouth, NJ 07703.**

AUTHORITY

ITSA ltr dtd 7 Sep 1967

Technical Report

INSTITUTES FOR ENVIRONMENTAL RESEARCH IER 8-ITSA 8

Linear High Frequency Antennas over a Finitely Conducting Spherical Earth

LESLIE A. BERRY

MARY E. CHRISMAN

SEPTEMBER, 1966
Boulder, Colorado

THE INSTITUTES FOR ENVIRONMENTAL RESEARCH

The mission of the Institutes is to study the oceans, and inland waters, the lower and upper atmcsphere, the space environment, and the earth, seeking the understanding needed to provide more useful services. These research Institutes are:

- The Institute for Earth Sciences
  conducts exploratory and applied research in geomagnetism, seismology, geodesy, and related earth sciences.

- The Institute for Oceanography
  works to increase knowledge and improve understanding of the ocean and its interaction with the total physical environment of the globe.

- The Institute for Atmospheric Sciences
  seeks the understanding of atmospheric processes and phenomena that is required to improve weather forecasts and related services and to modify and control the weather.

- The Institute for Telecommunication Sciences and Aeronomy
  supports the Nation's telecommunications by conducting research and providing services related to radio, infrared, and optical waves as they travel from a transmitter to a receiver. The Institute is also active in the study and prediction of periods of solar activity and ionospheric disturbance.

monitor:
USA STRATCOM,
Radio Propagation
Agency, Ft Monmouth,
N.J. 07703.
attn:
22 March 1967

Environmental Science Services Administration

Boulder, Colo.

U. S. DEPARTMENT OF COMMERCE
John T. Connor, Secretary
ENVIRONMENTAL SCIENCE SERVICES ADMINISTRATION
Robert M. White, Administrator
INSTITUTES FOR ENVIRONMENTAL RESEARCH
George S. Benton, Director

(18) IER (19) 8

ESSA TECHNICAL REPORT IER8ITSA8

(14) ITSA-8

(6)

Linear High Frequency Antennas over a Finitely Conducting Spherical Earth.

(9) Technical rept.,

(10)
LESLIE A. BERRY
MARY E. CHRISMAN

(11) Sep 66 (12) 117p.

THIS RESEARCH WAS SPONSORED BY THE U.S. ARMY STRATEGIC COMMUNICATIONS COMMAND, RADIO PROPAGATION DIVISION, FORT MONMOUTH, NEW JERSEY, UNDER USARPA PROJECT 10108.

(16) ARPA-10108

INSTITUTE FOR TELECOMMUNICATION SCIENCES AND AERONOMY (078 045)
BOULDER, COLORADO
September, 1966

mt

(2)

Table of Contents

Abstract

Vertical radiation patterns of vertical quarter-wave monopoles, and of vertical and horizontal half-wave dipoles located at various heights up to twenty wavelengths over several typical types of ground are shown. Vertical antennas have the best low-angle patterns at low heights and at medium heights over land. For low and medium antenna heights, only vertically polarized antennas over water radiate appreciable energy at zero or negative elevation angles.

The propagation factor used to calculate the antenna patterns can be accurately evaluated with the simple two-ray theory for elevation angles greater than one or two degrees. For smaller, and negative, elevation angles the full wave theory for diffraction by a sphere must be used.

Key Words: Antenna patterns, HF antennas, low-angle radiation, propagation factor.

Linear High Frequency Antennas Over a Finitely Conducting Spherical Earth

Leslie A. Berry and Mary E. Chrisman

1. Introduction

Recently there has been increased interest in using low elevation angle paths for HF ionospheric communications. Utlaut [1961] measured HF signals propagated over 6800 km and 8400 km paths. On the average, more energy arrived at low angles (<5°) than at high angles (~15°), even though the transmitting antenna favored high angles. For a given signal threshold, Utlaut found that low-angle reception provided service a greater percentage of the time. Other reports by various workers suggesting the same result are listed and discussed by Utlaut.

Because of the possible usefulness of low-angle propagation, the calculation of low-angle radiation patterns of HF antennas is desirable. Commonly, antenna patterns are computed assuming that the earth is flat and smooth (and, often, perfectly conducting). Both of these assumptions are questionable at low elevation angles, and are certainly invalid at zero or negative elevation angles. In this report, the model of a flat, smooth earth is replaced by a spherical, smooth earth, and some consideration is given to the effect of a large surface irregularity.

The necessary solution of Maxwell's equations has existed for some time, since the basic problem is just that of diffraction by a conducting sphere. The first useful solution for a large sphere

was given by Watson [1918]. Bremmer [1949][1] and Fock [1965][2] made significant progress in providing useful approximations for numerical work. The functions now most frequently used to express the solution were defined by Fock although equivalent solutions were given by Pryce [1953]in a different notation. Norton [1941] published graphs which made simple engineering calculations of the ground wave possible. Wait and Conda [1958] gave numerical values of the current induced on a curved conductor by an incident plane wave -- corresponding to a short dipole on the surface receiving a downcoming sky wave. In 1959, they considered the far field diffraction by a cylinder of an incident plane wave [Wait and Conda, 1959]. Logan [1959] gives an excellent historical review of previous work, lists over 80 original contributions to the problem, and shows the relations between the functional notations used by the various authors.

In this paper, the antenna is within a few wavelengths of the surface and a target source is located in the far field. The vertical radiation patterns of practical antennas are found by integration over the field for a current element. Example calculations are made for vertical and horizontal half-wave dipoles, and vertical quarter-wave monopoles for a frequency of 10 MHz.

The conclusions are: In the HF band, the curvature of the earth is important only for elevation angles less than one or two degrees. Except for vertical antennas over water and very high antennas, little energy is received at these angles, so the curvature of the earth is at best a second order effect. As expected, the best low-angle radiation by

---

1. The book by Bremmer summarizes and extends the work done by Bremmer and Van Der Pol.
2. Fock's research was done in the 1940s. The book referenced is an excellent English translation of his earlier papers on diffraction theory.

low antennas is by vertical polarization over sea water. The low-angle patterns of low horizontal antennas improve as the ground conductivity decreases. For high antennas, the low-angle patterns of horizontal antennas are as good as those of vertical antennas.

2. The Propagation Factor

The formulas for the antenna patterns are conveniently written in terms of the "propagation factor", which is the ratio of the electric field at a point to the field which the same source would excite at that point if all boundaries were removed; i.e., the ratio of the actual field to the free space field. This factor has also been called the reflection factor, Laitinen [1949], the cutback factor [Wait and Conda, 1958], and the attenuation function [Norton, 1936; Furutsu, 1965].

2.1 Flat Earth, Plane Wave Example

As a simple example, consider a probe antenna located at height h above a plane earth as shown in figure 1. A plane wave E_o is incident from the right at an angle Δ with the horizontal. When the lower ray strikes the ground some of its energy is absorbed, and some is reflected with a phase shift. The ratio of the reflected wave to the incident wave is the reflection coefficient, R, i.e., $E_{reflected} = RE_o$. In general, R is a complex number. Then the total field received at A is

$$E = E_o + e^{-i\varphi}RE_o = E_o(1 + e^{-i\varphi}R), \qquad (1)$$

where φ is the difference in phase path between the direct and reflected rays. From geometry,

$$\varphi = k\, 2h \sin \Delta, \qquad (2)$$

where $k = 2\pi/\lambda$ and λ is the free space wavelength. For this case $F(\Delta,h) = 1 + e^{-i\varphi}R$ is the propagation factor.

The reflection coefficient R is a function of the angle Δ, the polarization and frequency of the incident wave, and the electrical properties of the reflecting surface. For a surface with relative dielectric constant ϵ, and conductivity, σ mho/m, the reflection coefficient for "vertical polarization" (electric vector in the plane of incidence) is [Norton, 1936]

$$R_V = \frac{\sin\Delta - \frac{k}{k_2}\sqrt{1 - (\frac{k}{k_2}\cos\Delta)^2}}{\sin\Delta + \frac{k}{k_2}\sqrt{1 - (\frac{k}{k_2}\cos\Delta)^2}} \quad , \qquad (3)$$

where

$$k_2 = k\sqrt{\epsilon - i\frac{\sigma\mu_0 c^2}{\omega}} \cong k\sqrt{\epsilon - i\frac{18\sigma(10^3)}{f_{MHz}}} \quad ,$$

and $\mu_0 \cong 4\pi(10^{-7})$ is the permeability of free space, c is the speed of light, $\omega = 2\pi f$ is the angular frequency, and f_{MHz} is the frequency in megahertz. For horizontal polarization (electric vector perpendicular to the plane of incidence),

$$R_h = \frac{\sin\Delta - \frac{k_2}{k}\sqrt{1 - (\frac{k}{k_2}\cos\Delta)^2}}{\sin\Delta + \frac{k_2}{k}\sqrt{1 - (\frac{k}{k_2}\cos\Delta)^2}} \quad . \qquad (4)$$

Some characteristics of ground reflection coefficients will be discussed later. The most important thing for HF is that if $|k_2| >> k$ (high conductivity), $R_h \cong -1$, and except for very small Δ, $R_V \cong 1$. If $\Delta = 0$, $R_h = R_V = -1$.

2.2 Spherical Earth, Vertical Component in the Plane of Incidence

We will now develop formulas for the propagation factor for a sky wave incident on a spherical earth. The geometry of the spherical model is shown in figure 2. The receiving antenna is an elementary dipole at A, h_A meters above a smooth, homogeneous, spherical earth of radius a whose center is the origin of the spherical coordinate system (r, θ, φ). To model waves reflected from the ionosphere, a target source T is located at ionospheric reflection height h_T, a distance D from A. Throughout this report we assume $h_T > h_A$. The direct ray TA makes an angle Δ with the local horizontal at A -- i.e., Δ is the elevation angle. The reflected ray travels the path $D_1 + D_2$. The angular distance between A and T is $\theta = \frac{d}{a}$.

For large elevation angles, the flat earth approximation developed above may be used by defining the equivalent height $\hat{h}_T = h_A + D \sin \Delta$. Let the target source at T be a vertically polarized elementary dipole with current moment I dh, where dh is along the radius of the sphere. Then the radial electric field E_r at A (assuming time dependence $\exp(i\omega t)$ which is not written) is [Feldman, 1933; Laitinen, 1949]

$$E_r \cong -30ik \frac{e^{-ikD}}{D} I\, dh \cos^2\Delta \left(1 + R_V e^{-ik(D_1+D_2-D)}\right). \qquad (5)$$

This equation is $(-\cos \Delta)$ times the one usually given because it gives the E_r component for a coordinate system originating at the earth's center instead of the E_θ component for a coordinate system centered on the antenna. For large D and $h_T \gg h_A$,

$$D_1 + D_2 - D \cong 2 h_A \sin \Delta \quad , \qquad (6)$$

which reduces (5) to (1).

As Δ approaches zero, the notion of distinct direct and reflected rays breaks down. Waves coming from T graze the horizon and travel some distance near the curved ground to get to A. In fact there is a continuum of waves which reach A in this manner, and they must be summed to obtain the resultant field. Thus we must integrate over this continuum and use wave functions appropriate to a spherical geometry. Exactly how this should be done would not be clear without referring to the rigorous direct solutions given by, for example, Fock [1965] and Wait [1962]. Since the intent here is to stress the physical interpretation, the appropriate wave functions and form of the integral are taken from these references without derivation.

Wave functions appropriate to the problem are the Airy functions $W_n(t)$ used by Fock [1965], Wait [1962], and others. The functions are linearly independent solutions of the differential equation,

$$W_n''(t) = tW_n(t) \quad ; \tag{7}$$

for n = 1 or 2, and for $-t \gg 1$,

$$\left.\begin{aligned} W_1(t) &\cong (-t)^{-\frac{1}{4}} \exp\left[\mp i(z + \pi/4)\right], \\ \text{and} \qquad & \\ W_2(t) &\cong (-t)^{\frac{1}{4}} \exp\left[\mp i(z - \pi/4)\right], \end{aligned}\right\} \tag{8}$$

where $z = \frac{2}{3}(-t)^{3/2}$. Equation (8) shows that the functions act like plane waves for large (-t) and $W_1(t)$ is an upgoing wave and $W_2(t)$ a downgoing wave.

The relation of the variable t to the geometry is

$$t \cong -v^2 \sin^2\Delta \,, \quad \Delta > 0 \,, \tag{9}$$

where $$v = (ka/2)^{1/3} . \tag{10}$$

The so-called natural units of distance and height are [Pryce, 1953]

$$x = v\theta, \quad \text{and} \quad y = kh/v. \tag{11}$$

Then the integral which sums the continuum of waves reaching A from T at small angles Δ is (compare Wait and Conda [1958] and Fock [1965])

$$E_r \cong e^{-i3\pi/4} KU \frac{e^{ikd}}{\sqrt{\sin\theta}} I_r, \text{ and} \tag{12a}$$

$$I_r = \oint_\Gamma e^{-ixt}\left(1 + \frac{t}{2v^2}\right)^{5/2} W_1(B_T) W_2(B_A) \left\{1 + \frac{W_1(B_A)}{W_2(B_A)} \frac{W_2(t)}{W_1(t)} \hat{R}_V\right\} dt. \tag{12b}$$

In (12), $$K = 12\ v^2\sqrt{k/a^3}\ I\ dh , \tag{13}$$

$$U = \left(\frac{a^2}{rb}\right)^{11/6} \cong 1 - \frac{11}{6}\frac{h_T}{a} \cong 1, \tag{14}$$

where $r = a + h_A$, $b = a + h_T$, and Γ is a contour enclosing the poles of the integrand in the lower half plane. For discussion here, Γ can be taken along the real axis from ∞ to $-\infty$.

$$B_n = \left(\frac{a}{a+h_n}\right)^{1/3}(t - y_n), \quad n = A \text{ or } T ,$$

$$\cong (t - y_n), \text{ since } h_n << a.$$ Most authors use the latter form, and it will be used for the rest of this section, but the more accurate form was necessary for some of the numerical calculations.

Finally, $\hat{R}_V$ is the spherical reflection coefficient,

$$\hat{R}_V = - \frac{W_2'(t)/W_2(t) - q_V}{W_1'(t)/W_1(t) - q_V}, \tag{15}$$

where

$$q_V = - iv \frac{k}{k_2} \sqrt{1 - \left(\frac{k}{k_2}\right)^2} \quad . \tag{16}$$

Equation (12) has only a superficial resemblance to (5), so the first thing to do is to show that it indeed reduces to (5) for large Δ. This demonstration will also show the roles of the various factors in (12). Referring to (9), if Δ is large, $(-t) \gg 1$, since $v > 10$ at high frequencies. So substitute (8) into (12) and simplify:

$$I_r \cong \int_{-\infty}^{\infty} \frac{\left(1+\frac{t}{2v^2}\right)^{5/2}}{(Y_A - t)^{1/4} (Y_T - t)^{1/4}} e^{-i\Omega(t)} \left(1 + e^{-i\frac{4}{3}\left((Y_A - t)^{3/2} - (-t)^{3/2}\right)} \hat{R}_V\right) dt, \tag{17}$$

$$\text{where } \Omega(t) = xt + \tfrac{2}{3}(Y_T - t)^{3/2} - \tfrac{2}{3}(Y_A - t)^{3/2}. \tag{18}$$

This integral can be evaluated by the saddle point method [Morse and Feshbach, 1953]. The result is

$$I_r \cong e^{i\pi/4} \sqrt{\frac{\pi}{x}} \left(1+\frac{t_o}{2v^2}\right)^{5/2} e^{-i\Omega(t_o)} \left(1 + e^{-i\hat{\varphi}} \hat{R}_V\right), \tag{19}$$

where

$$\hat{\varphi} = \tfrac{4}{3}(Y_A - t_o)^{3/2} - \tfrac{4}{3}(-t_o)^{3/2}, \text{ and}$$

t_o is the solution of $\Omega'(t_o) = 0$, or

$$t_o = \frac{2x^2(y_A+y_T) - (y_A-y_T)^2 - x^4}{4x^2} . \tag{20}$$

Then

$$E_r \cong \frac{-2iKT}{\sqrt{\sin\theta}} \sqrt{\frac{\pi}{x}}\, e^{-i(kd+\Omega(t_o))}\left(1 + e^{-i\hat{\varphi}_{\hat{R}_V}}\right) \tag{21}$$

which now has a form much like (5).

First, we want to verify that (20) is equivalent to (9) to justify the transformation of variables. Substitute (11) into (20) and simplify to get

$$t_o = -v^2\left\{\frac{(h_T-h_A)^2}{d^2} + \frac{d^2}{4a^2} - \frac{h_A+h_T}{a}\right\}$$

$$\cong -v^2\left(\frac{h_T-h_A}{d}\right)^2, \text{ if } d^2 \ll 4a(h_T-h_A) , \tag{22}$$

which corresponds to Δ being somewhat greater than 0.

From the geometry of figure 2, if $h_A \ll h_T$ (the antenna is much lower than the ionospheric reflection height),

$$\sin^2\Delta = 1 - \cos^2\Delta \cong 1 - \frac{d^2}{D^2} \cong \frac{D^2-d^2}{D^2} .$$

Since $D^2 \cong d^2 + (h_T-h_A)^2$,

$$\sin^2\Delta \cong \frac{(h_T-h_A)^2}{d^2}\left(1 - \left(\frac{h_T-h_A}{d}\right)^2\right) \cong \frac{(h_T-h_A)^2}{d^2} , \tag{23}$$

if Δ is not too large.

Substitution of (23) into (22) yields (9).

Now, using (8) in (15),

$$\hat{R}_V \cong -\frac{-i(-t)^{\frac{1}{2}} - q_V}{i(-t)^{\frac{1}{2}} - q_V},$$

or, using (16) and (9),

$$\hat{R}_V \cong \frac{\sin\Delta - \frac{k}{k_2}\sqrt{1 - \left(\frac{k}{k_2}\right)^2}}{\sin\Delta + \frac{k}{k_2}\sqrt{1 - \left(\frac{k}{k_2}\right)^2}}. \tag{24}$$

Thus $\hat{R}_V \cong R_V$ if $\cos\Delta \cong 1$, which is true for small Δ. This justifies identifying $\hat{R}_V$ as the reflection coefficient and shows that a more accurate definition of q_V would include the $\cos^2\Delta$ as a factor of $\left(\frac{k}{k_2}\right)$. But since the integral is to be used only for very small Δ and since $(k/k_2)^2$ is usually quite small, it does not seem necessary.

Next consider the phase term $kd + \Omega(t_o)$ in (21). By putting (11) and (20) into (18) and grinding through some tedious algebra, we get

$$\Omega(t_o) = k\left(\frac{d(h_A+h_T)}{2a} + \frac{(h_A-h_T)^2}{2d} - \frac{d^3}{24a^2}\right). \tag{25}$$

By the law of cosines, $D^2 = r^2 + b^2 - 2rb\cos\theta$. Using Taylor's series for $\cos\theta$, after working out the algebra,

$$D-d \cong \frac{d(h_A+h_T)}{2a} + \frac{(h_A-h_T)^2}{2d} - \frac{d^3}{24a^2} + \text{terms in}\left(\frac{d}{a}\right)^3.$$

Thus, to a close approximation, $\Omega(t_o) = k(D-d)$ and

$$e^{-i(kd - \Omega(t_o))} = e^{-ikD}. \qquad (26)$$

Similarly, $\hat{\varphi} \cong \varphi$.

Finally, consider the coefficient:

$$\frac{-2iKU}{\sqrt{\sin\theta}}\sqrt{\frac{\pi}{x}}\left(1 + \frac{t_o}{2v^2}\right)^{5/2} \cong \frac{-24i\, v^2\sqrt{k/a^3}\,\sqrt{\pi/x}\left(1 - \frac{\sin^2\Delta}{2}\right)^{5/2}}{\sqrt{d/a}}\, I\, dh$$

$$\cong -24i\,\frac{k}{d}\sqrt{\frac{\pi}{2}}\left(1 - \frac{\Delta^2}{2}\right)^{5/2} I\, dh$$

$$\cong -30i\,\frac{k}{d}\left(1 - \frac{\Delta^2}{2}\right)^{5/2} I\, dh \qquad (27)$$

for $\theta = \frac{d}{a} \ll 1$ and $\Delta \ll 1$. But for small Δ, $d \cong D\cos\Delta$ and $1 - \frac{\Delta^2}{2} \cong \cos\Delta$, so the coefficient is approximately

$$-30ik\,\frac{\cos^2\Delta}{D}\, I\, dh\,.$$

This reduces (21) and hence (12) to (5) for the range of Δ in which both are valid. It may seem contradictory that we have required the elevation angle Δ to be both "not too small" and "not too large". This is because we are trying to show that two formulas, one for large Δ and one for small Δ, have an overlap region in which both give the same answer. Careful examination of the inequalities above show that they require Δ to lie between about 2° and 10°. Numerical calculation of (5) and (12) has shown that they do indeed give the same result in this region.

Comparison of (19) and (26) shows that if I_r is calculated directly then the propagation factor is given by

$$F_r(\Delta, h_A) = -\tfrac{1}{2}\sqrt{\frac{x}{\pi i}}\, e^{-ik(D-d)}\, I_r \,. \tag{28}$$

Reviewing the results of this section so far, it has been shown that the simple two ray formula for the propagation factor can be derived from the rigorous full wave solution for sufficiently large elevation angles in accordance with physical intuition. For very small and negative elevation angles, a continuum of waves must be summed with the integral shown in (12). The integral can be evaluated numerically on a computer by swinging the ends of the contour down into the lower half plane to get convergence, being careful not to cross any poles of the integrand.

The integral in (12) can also be evaluated with the calculus of residues for negative take-off angles. Rewrite (12) as

$$I_r \cong 2i \int \frac{(1+\frac{t}{2v^2})\, e^{-ixt}}{W_1'(t)/W_1(t) - q_V}\, H_1(y_T)\, H_2(y_A)\, dt \tag{29}$$

where $H_1(y_T) = \dfrac{W_1(t-y_T)}{W_1'(t)}$, and

$$H_2(y_A) = \frac{W_2(t-y_A)\,[W_1'(t) - q_V W_1(t)] - W_1(t-y_A)\,[W_2'(t) - q_V W_2(t)]}{2i} \,.$$

This form has two advantages: first, the $H_n(y)$ are height gain functions such that if $h = 0$, $y = 0$ and $H_n(0) = 1$. This is obvious for $H_1(y)$. For $H_2(y)$ it is shown by using the Wronskian [Wait, 1962],

$$W_1'(t)W_2(t) - W_1(t)W_2'(t) = 2i. \tag{30}$$

The second advantage is that this form shows that the integrand has poles at the points t_s which are solutions of

$$W_1'(t_s) = q_V W_1(t_s). \tag{31}$$

Then the field is given by

$$E_r \cong -4\pi e^{-3\pi i/4} KT \frac{e^{-ikd}}{\sqrt{\sin\theta}} \sum_{s=0}^{\infty} \frac{\left(1+\frac{t_s}{2v}\right)^{5/2} e^{-ixt_s}}{t_s - q_V^2} \frac{W_1(t_s - y_T)}{W_1(t_s)} \frac{W_1(t_s - y_A)}{W_1(t_s)} \tag{32}$$

which is the well-known series for the ground wave (shown in this notation by Wait [1962] and Fock [1965]). Equations (30) and (31) were used to simplify H_2. In this case, the propagation factor is

$$F_r(\Delta, h_A) = 2\pi \sqrt{\frac{x}{\pi i}}\, e^{-ik(D-d)} \sum_s (\text{residues}). \tag{33}$$

2.3 Horizontal Component in the Plane of Incidence

The propagation factor for the horizontal component in the plane of incidence of an incoming wave is [Laitinen, 1949]

$$F_\theta(\Delta, h) = 1 - e^{-i\varphi} R_V. \tag{34}$$

In the spherical geometry of figure 2, the E_θ component is such a wave. The integral corresponding to (29) for E_θ is (for $h_T > h_a$)

$$E_\theta \cong e^{i\pi/4} 2K \left(\frac{r}{a}\right)^{2/3} U \frac{e^{-ikd}}{v\sqrt{\sin\theta}} \int_\Gamma \frac{\left(1+\frac{t}{2v^2}\right)^{3/2} e^{-ixt}}{W_1'(t)/W_1(t) - q_V} H_1(y_T) H_3(y_A)\, dt \tag{35}$$

where

$$H_3(y_A) = \frac{W_2'(t-y_A)\left[W_1'(t)-q_V W_1(t)\right] - W_1'(t-y_A)\left[W_2'(t)-q_V W_2(t)\right]}{-2iq_V} . \tag{36}$$

By evaluating (35) with the saddle point approximation it can be shown that it reduces to the plane wave formula just as in the previous case. The propagation factor is

$$F_\theta(\Delta, h_A) = \sqrt{\frac{ix}{\pi}}\ \frac{x}{y_T - y_A - x^2}\ I_\theta \tag{37}$$

where I_θ is the integral of (35). The denominator of (37) is zero when

$$d = \sqrt{2a(h_T - h_A)} \tag{38}$$

which occurs when $\Delta = 0$. But there is no infinity in the field E_θ = E (free space) $\cdot$ F_θ because the θ-component of E (free space) is proportional to sin Δ.

2.4 Horizontal Component Perpendicular to Plane of Incidence

The term "horizontal polarization" usually indicates that the electric vector is perpendicular to the plane of incidence. In the coordinate system of figure 2, this corresponds to the E_φ component. For large Δ, the propagation factor is

$$F_\varphi(\Delta, h) = (1 + e^{-i\varphi} R_h) \tag{39}$$

where R_h is given by (4). Since (39) has the same form as (1) it seems reasonable that the analysis of section 2.2 should apply here just by

replacing R_V by R_h. This is indeed the case, and the integral for F_φ has the same form as (29) except that q_V, (16), is replaced by

$$q_h = - iv \frac{k_2}{k} \sqrt{1 - \left(\frac{k}{k_2}\right)^2} \quad . \tag{40}$$

2.5 Relation to Other Problems and Special Cases

The integral in (12) and (29) and the residue series (32) are the same as those given by Fock [1965] and by Wait and Conda [1958] except for the factor $\left(1 + \frac{t}{2v^2}\right)^{5/2} \cong 1$ for small t (small Δ). Wait [1962] showed that it is equivalent to the ground wave series of Bremmer [1949]. If the receiving antenna is put on the surface ($h_A = 0$), and the source is raised very high, the formulas correspond to those given for the cut-back factor by Wait and Conda [1958]. If both antennas are raised very high, (12) is equivalent to the diffraction integral denoted $\hat{G}(X)$ by Wait and Conda [1959] and also given by Fock [1965]. Thus the solution used here is the general solution for electromagnetic wave propagation near and around a large, finitely conducting sphere. It contains implicitly both the space wave and the surface wave [Norton, 1936], although it has not been written to display them separately.

As a final check, the wave tilt $\left(= \frac{E_\theta}{E_r}\right)$ [Norton, 1937] will be calculated. Let $h_A = 0$, so that the fields are found on the surface, and $H_3 = H_1 = 1$. For $\Delta < 0$, only a diffracted wave is present. Then since $\left(1 + \frac{t}{2v^2}\right) \cong 1$, dividing (35) by (29),

$$\frac{E_\theta}{E_r} \cong \frac{iq_V}{v} \frac{\int \ldots dt}{\int \ldots dt} \cong \frac{iq_V}{v} \cong \frac{k}{k_2} \sqrt{1 - \left(\frac{k}{k_2}\right)^2} \quad , \tag{41}$$

because the integrands are now the same. The result on the right is the correct value for the wave tilt [Norton, 1937].

2.6 Calculation and Discussion of the Propagation Factor

The propagation factor was calculated for frequencies from 1 to 25 MHz, for the types of ground shown in table 1, and for heights h_A = .05, .1, .25, .375, .5, .75, 1, 2, 5, and 10 λ.

Table 1. Ground Constants Used in this Report

Ground type	Conductivity, mho/m	Relative dielectric constant
sea water	5.0	80
good ground	0.01	10
poor ground and sea ice	0.001	4
polar ice cap	0.0001	1
fresh water	0.002	80

The values for sea water, fresh water, good and poor ground are fairly standard; that for sea ice is an average taken from Wentworth and Cohen [1964]. The constants for "polar ice cap" are speculative -- they at least represent the extreme of poor conductivity.

Printed tables and magnetic tapes containing the data are available. To illustrate the properties of the propagation factor, the amplitude has been plotted for f = 1, 5, 15, and 25 MHz for sea water and poor ground for both vertical and horizontal polarization. They will be discussed later in this section, after explanation of some details of the calculations.

The integral formulas for the propagation factor for small elevation angles (29, 35) apparently depend on the height h_T of the target

source, an undesirable feature. In fact, the propagation factor depends on h_T only when T is below the horizon. This occurs when $-\Delta > 2h_A/a$. Even then, the dependence on h_T is very slight over a reasonable range of h_T. Still, h_T must be given some value in the formulas, and in this report, h_T = 200 km.

For a number of test cases calculated for h_T = 300 km and h_T = 100 km, the difference in $|F|$ was less than 0.5 dB if $-1.5° < \Delta < 0.5°$, and there was no difference if $\Delta > 0.5°$. This error is hardly significant since the antenna patterns shown in section 3 are all more than 20 dB below an isotropic radiator if $\Delta < -1.5°$.

The decrease in the refractive index of air with height causes some bending of a radio wave. The amount of bending varies with time, location, and elevation angle; but on the average it is accounted for by using an equivalent earth's radius 4/3 as large as its actual mean radius [Burrows, 1935]. This standard procedure was used for the calculations of the propagation factor.

The condition for use of the saddle point approximation, and hence the two-ray model, is $-t_0 \cong (v \sin \Delta)^2 >> 1$. In practice, if $-t_0 > 4$ (i.e., $\Delta > 2'$ at 1 MHz, $\Delta > 1°$ at 10 MHz), the two-ray, plane wave calculation is correct to at least 3 significant digits, so at this value the computer program switches to numerical integration of the integral. When $\Delta < 0$, the residue series (32) is used.

Actually, the ranges of validity of the three methods overlap, providing a check on the logic and precision of each branch of the program. The program was also validated by comparing with calculations of the cutback factor by Wait and Conda [1958] and Hyovalti [1965], and with the ground wave calculations of Johler, Walters, and Lilley [1960], since these are special cases of the general solution used here. The only unresolved difficulty is the inability to make a smooth transition

from the two-ray solution to the integral for $h_A = 20\lambda$ at 1 MHz (h_A = 6000 m). If it is necessary to make calculations for such a high antenna, a smooth transition could be interpolated.

Figure 3.1 shows the propagation factor for the vertical and horizontal components for $h_A = 0.05\lambda$ over sea water[3]. The lines are labeled with the frequency in MHz. At first glance, the most striking feature is that there is almost no frequency dependence for horizontal polarization, and very little for vertical polarization above $\Delta = 10°$. There are two reasons for the very weak frequency dependence: First, in the graphs the height is measured in wavelengths. If the curves were plotted for some fixed height in meters, there would be much more dependence on frequency. Second, there is no frequency dependence for a perfect conductor, and sea water is a good conductor.

Another noticeable feature is that the amplitude of the propagation factor is much greater for vertical polarization than for horizontal polarization. For good conductivity, $R_V \cong 1$, except for very small elevation angles, and $R_h \cong -1$. For horizontal polarization the reflected ray nearly cancels the direct ray, while for vertical polarization the two reinforce each other and $|1 + R_V| \cong 2$.

Finally, note that the vertically polarized wave is not cut off at $\Delta = 0$ as it would be for a flat model of the earth, but is merely cut back. For negative elevation angles, the amplitude of the propagation factor decreases exponentially with frequency, just as the ground wave does.

Figures 3.2 and 3.3, for heights of 0.1λ and 0.25λ are similar to figure 3.1.

The propagation factor for a perfect plane reflector is [Laitinen, 1949]

---

3. In the figure legend, HT is the height h_A.

$$F_V = 2\, e^{-ikh\sin\Delta} \cos(kh\sin\Delta), \text{ and}$$

$$F_h = 2i\, e^{-ikh\sin\Delta} \sin(kh\sin\Delta).$$

For small Δ, the first null of F_V is at $\sin\Delta = \frac{\lambda}{4h}$, and the first null of F_h is at $\sin\Delta = \frac{\lambda}{2h}$. If $h = \lambda/2$, as in figure 3.4, F_V should have a null near $\Delta = 30°$ -- and it does. For the same height, F_h should have a null near $\Delta = 90°$. The null is near $\Delta = 85°$, because Δ is large enough that the exponential factor must be considered. At greater heights, shown in figures 3.5, 3.6, etc., the lobes are closer together as expected.

Figures 3.7 and 3.8 have an expanded angle-of-elevation scale to show the detail at small angles. At these heights, there is more low-angle frequency dependence, and even horizontal polarization shows appreciable amplitude for $\Delta < 0$. For $0 < \Delta < 5°$, the propagation factor is greater for horizontal polarization than for vertical polarization; vertical polarization is better at negative angles.

The propagation factors for poor land are shown in figure 4 for the same set of heights. There is a little more frequency dependence at low heights, and the difference between the polarizations is not so great. At medium heights the behavior of the propagation factor for vertical polarization is complicated by the psuedo-Brewster angle of the ground reflection coefficient [Jordan, 1950]. This occurs near $\Delta = 6°$ at 1 MHz and near $\Delta = 17°$ at 15 and 25 MHz.

For greater heights, the lobe structure is similar to that for sea water but the range between a maximum and an adjacent minimum is not so great. Horizontal polarization is slightly better than vertical polarization at low angles.

2.7 The Effect of a Large Irregularity

So far, it has been assumed that the earth is smooth and homogeneous. All parts of the real world do not satisfy this requirement so the natural question is: How much will irregularities affect the propagation factor? A complete answer to this question is not available, although a number of special cases have been treated in the literature. In general, it is assumed that surface irregularities very small compared to a wavelength can be accounted for by using "effective" ground constants. Structures and irregularities comparable to a wavelength may act as scatterers, and large irregularities result in shadowing and diffraction. A limited attempt to compute the effect of a certain class of large irregularities is described in this section.

The nature of the irregularity, a large box-like ridge or mesa, is illustrated in figure 5. The antenna is at A, d_H kilometers from the hill of height h_H. The solution for this model, given by Furutsu [1965], is a triple residue series with terms similar to those in (32). This solution, developed for VHF tropospheric paths, is not well-adapted to antenna pattern calculations because the numerical procedures will not work except for very small elevation angles. However, it can be used to determine how small and how remote an irregularity must be before the propagation factor calculations are correct at low angles.

The propagation factor was calculated for low antennas and for elevation angles less than one degree for hill sizes ranging from $h_H = \lambda/3$ to $h_H = 10\lambda$ and for distances d_H ranging from 2.5 km to 10 km. The results were divided by the propagation factor for a spherical earth of the same conductivity to minimize the influence of ground conductivity. (This also removed the polarization dependence.) The results indicated the following empirical rule: For the small angles where the two-wave theory cannot be used, an irregularity of the kind pictured in figure 5 will cause

the propagation factors to be in error by 1 dB or more if the ratio h_H/d_H exceeds 0.01, i.e., if the elevation angle to the horizon is more than one-half degree.

For larger angles, no calculations could be made, but since the two-wave theory is valid for large angles, the notion of requiring a smooth unobstructed first Fresnel zone, or portion thereof, as outlined by Utlaut [1962] can probably be used. In this regard, Anderson [1964] has found that the Fresnel zone is considerably smaller over poorly conducting ground than it is over perfectly conducting ground.

Much more research on the effect of terrain irregularities is needed.

3. Antenna Patterns

In the preceding section, formulas were developed for propagation factors for very short dipoles. Most HF antennas are comparable to a wavelength, and it is necessary to integrate along their length to find the radiation pattern. This was done for several HF antennas located above a flat earth by Laitinen [1949]. In this section, the equations for vertical and horizontal linear antennas over curved earth will be derived, with sample patterns shown for $\lambda/2$ vertical and horizontal dipoles and $\lambda/4$ vertical monopoles.

3.1 Vertical Antenna Pattern Formulas

A thin current-carrying wire of length $L = h_2 - h_1$ is located on a radial of the earth (h_2 is the height to the top of the antenna; h_1 is the height to the bottom of the antenna). The current in the wire is assumed to be distributed sinusoidally, i.e.,

$$I(h) = I_m \sin k\,(h_2 - h)\,, \tag{42}$$

where I_m is the current maximum and $h = r - a$. From section 2, the radial field due to an element dh is [3]

$$dE_r \cong E_0 \cos^2\Delta\, I_m \sin[k(h_2 - h)]\, F_r(\Delta, h)\, dh, \tag{43}$$

where $E_0 = -30\, ik \dfrac{e^{-ikD}}{D}$.

The phase path to T is a function of position along the antenna, and this is accounted for by multiplying (43) by $e^{ikh \sin\Delta}$, i.e., the phase is referred to the surface of the earth. Then

$$E_r \cong E_0 \cos^2\Delta\, I_m \int_{h_1}^{h_2} e^{ikh\sin\Delta} \sin[k(h_2 - h)]\, F_r(\Delta, h)\, dh. \tag{44}$$

When the elevation angle Δ is large enough to use (5), the integral can be evaluated in closed form, and

$$E_r \cong E_0 \frac{e^{ikh_2 \sin\Delta}}{\cos\Delta}\, I_m \Big[1 + e^{-ik2h_2 \sin\Delta} R_V$$

$$- e^{-ikL\sin\Delta} \Big\{ i \sin\Delta \sin kL \left(1 - e^{-ik2h_1 \sin\Delta} R_V \right)$$

$$+ \cos kL \left(1 + e^{-2ikh_1 \sin\Delta} R_V \right) \Big\} \Big]$$

$$\cong E_0 \frac{e^{ikh_2 \sin\Delta}}{\cos\Delta}\, I_m \Big[F_r(\Delta, h_2) - e^{-ikL\sin\Delta} \Big\{ i \sin\Delta \sin kL\, F_\theta(\Delta, h_1)$$

$$+ \cos kL\, F_r(\Delta, h_1) \Big\} \Big] \quad . \tag{45}$$

3. The formulas in this section are not complete if Δ is too near 90°.

For a half-wave dipole ($L = \lambda/2$), (45) reduces to

$$E_r \cong E_0 \frac{e^{ikh_2 \sin\Delta}}{\cos\Delta} I_m\left[F_r(\Delta, h_2) + e^{-i\pi \sin\Delta} F_r(\Delta, h_1)\right]. \qquad (46)$$

For a quarter-wave monopole ($L = \lambda/4$),

$$E_r \cong E_0 \frac{e^{ikh_2 \sin\Delta}}{\cos\Delta} I_m\left[F_r(\Delta, h_2) - i \sin\Delta\, e^{-i\frac{\pi}{2}\sin\Delta} F_\theta(\Delta, h_1)\right]. \qquad (47)$$

These equations show that if the elevation angle is large enough, the field is proportional to the propagation factor evaluated at the top of the antenna plus the propagation factor at the bottom (with the phase shifted to account for the difference in height). This reveals the basic nature of the propagation factors. In fact, for small Δ,

$$F_r(\Delta, h_2) + e^{-i\pi \sin\Delta} F_r(\Delta, h_1) \doteq F_r(\Delta, \frac{h_1+h_2}{2}), \qquad (48)$$

i.e., the antenna pattern of a vertical half-wave dipole is approximately proportional to the propagation factor calculated at the midpoint. The accuracy of this approximation is studied later; it is very useful for understanding the qualitative behavior of the antenna pattern.

For small Δ, the propagation factor is itself an integral and (44) cannot be integrated in closed form. However, the integration is easily done numerically on a computer. Patterns of the two types of vertical antennas will be discussed after the normalization is defined.

3.2 Normalization Relative to an Isotropic Source

One common reference antenna is the (non-physically realizable) isotropic source -- an antenna that radiates equally in all directions. The E_r field of an isotropic source is [Jordan, 1950]

$$E_r(\text{isotropic}) = \sqrt{30P}\ \frac{e^{-ikD}}{D} \cos\Delta$$

where P is the radiated power in watts. Let R_{rad} be the radiation resistance of the antenna being compared. The current I is found from

$$P = I^2 R_{rad},$$

and the pattern of a vertical antenna relative to the isotropic radiator is

$$\frac{E_r}{E_r(\text{isotropic})} \cong -ik\cos\Delta\sqrt{\frac{30}{R_{rad}}}\int_{h_1}^{h_2} \ldots\, dh. \qquad (49)$$

The impedance of a half-wave dipole over ground is the sum of its free space self-impedance plus the mutual impedance Z_{12} between the antenna and its (imperfect) image in the ground. According to Jasik [1961], Z_{21} is the product of the mutual impedance between the antenna and its perfect image, and the ground reflection coefficient for vertical incidence. The real part of the impedance then is R_{rad}. The radiation resistance for a vertical half-wave dipole as a function of height of the midpoint above the ground is shown in figure 6 for the types of ground in this report. The resistance does not differ much from the free space value above $h \sim 1\frac{1}{4}\lambda$, and the variation is greater for better conducting ground.

3.3 Radiation Patterns of Vertical Half-wave Dipoles

Vertical radiation patterns of half-wave dipoles over the five types of ground were calculated for feed-point heights ranging from .375 λ to 20 λ for f = 10 MHz and are shown in figures 10-14. The power gain, relative to an isotropic radiator, in the direction Δ is

$$G(\Delta) = 10 \log_{10} \left| \frac{E_r(\Delta)}{E_r(\text{isotropic})} \right|^2 \quad \text{dB.} \quad (50)$$

This is the function plotted in the figures.

The characteristics of the antenna patterns are largely determined by the behavior of the ground reflection coefficient R_V. The amplitude and phase of R_V for the frequency and ground constants of interest are shown in figure 8. For all types of land $|R_V| = 1$ for $\Delta = 0°$, and decreases to a minimum as Δ increases to the pseudo-Brewster angle [Jordan, 1950]. (For brevity, the pseudo-Brewster angle will hereafter be called the Brewster angle.) The Brewster angle is less than 1° for sea water (at 10 MHz) and increases with decreasing conductivity. Above the Brewster angle $|R|$ recovers and approaches its value for vertical incidence, which is greater for higher conductivity. The phase of the reflection coefficient is -180° for $\Delta = 0$ ($R_V = -1$ when $\Delta = 0$), and, except for the curve marked "polar ice", the phase increases slowly until it reaches the vicinity of the Brewster angle. There it increases quickly, passing through -90° at the Brewster angle, and then flattens out to its value for vertical incidence. For polar ice, the phase decreases at first to -245°, then increases quickly to about -90°. This different behavior of the phase of R_V for polar ice, together with the negligible amplitude of R_V above $\Delta = 30°$, explains some apparently anomalous antenna patterns to be seen later.

Now, using (48) and (1), the qualitative behavior of the antenna patterns can be deduced. First, for very small heights h,

$$F_r(h, \Delta) \cong 1 + R_V . \tag{51}$$

When Δ is less than the Brewster angle, R_V partially cancels the 1 (the reflected wave partially cancels the direct wave) since the phase of R_V is between -180° and -90°. The extent of the cancellation depends on $|R_V|$, so in this region $|F_r|$ is smaller for higher conductivities. Above the Brewster angle, the reflected wave reinforces the direct wave, and the field exceeds the free space value.

For larger heights, the phase factor,

$$e^{-i\varphi} = e^{-ik2h \sin \Delta},$$

is important in determining whether the reflected ray reinforces or cancels the direct ray. Even if $R_V = -1$, the reflected ray adds if $2kh \sin \Delta = (2n - 1)\pi$ for $n = 1, 2, \ldots$. For great heights, the first lobe of the antenna pattern is near

$$\sin \Delta \cong \frac{\lambda}{4h} \tag{52}$$

if Δ is below the Brewster angle. If Δ is above the Brewster angle, the solution of (52) is near a null.

This general qualitative behavior of F_r can now be used in the interpretation of the vertical half-wave dipole patterns in figures 10-14. Figure 10 shows the vertical radiation patterns in dB above an isotropic radiator for the antenna over sea water for various heights of the feed-point, $\frac{1}{2}(h_1 + h_2)$. Figure 10.1 is for the lowest height, $\frac{3}{8}\lambda$; figures 10.2 10.3, 10.4, 10.5, 10.6, 10.7, and 10.8 are for feed point heights of $\frac{1}{2}$, $\frac{3}{4}$, 1, 2, 5, 10, and 20λ, respectively. The frequency is 10 MHz. The

calculations were made with both the flat and spherical earth formulas in the region $0 < \Delta < 5°$, and the flat earth values are indicated by a diamond. In figure 10.1, the maximum of the pattern is about 7 dB at $\Delta = 6°$. The Brewster angle for sea water is at $\Delta < 1°$, so the reflected wave is reinforcing the direct wave and the gain is well above the 2.15 dB gain of a half-wave dipole in free space. It does not reach the 8.17 dB gain expected over perfect ground because R_V approaches unity only for large Δ.

Note that there is appreciable power at $\Delta = 0$ -- about equal to an isotropic -- and even some for negative elevation angles.

The picture is very different for the same height antenna over good ground, shown in figure 11.1. Here the Brewster angle is near $\Delta = 14°$, so at lower angles the reflected wave is partially cancelling the direct wave. The pattern reaches its maximum of 0 dB near 14° where $|R_V|$ is smallest and there is least cancellation. One might expect the gain to be greater than the free space value for $\Delta > 14°$, since the phase of R_V is such that $|1 + R_V| > 1$. However, Δ is now large enough that the phase path difference is now significant. For example, at $\Delta = 20°$, $\varphi = 2kh \sin \Delta \cong 1.61$ radians $\cong 92°$. The propagation factor is then about $1 + |R_V| e^{-i\,142°}$; its amplitude is less than one, and the gain is therefore less than in free space. This illustrates a simple rule: When both Δ and h are very small, the behavior of $1 + R_V$ qualitatively describes the antenna pattern fairly well, but if either Δ or h is large (more precisely, if h sin Δ is greater than, say, $\frac{\lambda}{10}$) the phase path difference factor, $e^{-i\varphi}$, must also be considered.

The antenna at the same height over poor ground has the same general behavior as shown in figure 12.1. The maximum gain is slightly greater than for good ground since $|R_V|$ is smaller and less

of the direct wave is cancelled. The maximum gain occurs at a higher angle, $\Delta \cong 19°$, since the Brewster angle is at a larger Δ.

This trend is continued as shown in figure 13.1 where the conductivity is very low. The maximum gain, about 3 dB, now exceeds the gain in free space because of the different behavior of the phase of R_V that was mentioned earlier. The pattern is very near to that for free space above $\Delta = 30°$ because $|R_V|$ is so small.

The Brewster angle for fresh water is near 7°, so the gain is less than it is in free space for $\Delta < 7°$ in figure 14.1. The maximum is about 3.5 dB above an isotropic radiator at $\Delta = 12°$.

For a feedpoint height of $\lambda/2$, (52) predicts a null at $\Delta = 30°$, which can be seen in figure 10.2 There is a minimum here in figures 11.2 and 14.2, although it is not so deep because $|R_V|$ is smaller and less of the direct wave is cancelled. In figures 12.2 and 13.2 the effect can hardly be seen because $|R_V|$ is so small.

The pattern of a vertical dipole fed $\frac{3}{4}\lambda$ above the ground has the same general characteristics as those for the two lower heights. In the conclusions, these three cases are grouped as "low heights".

Similarly, heights of λ and 2λ are grouped as "medium heights" and only the one wavelength case will be discussed. If Δ is above the Brewster angle, (52) predicts a null near $14\frac{1}{2}°$ which can be seen in figures 10.4 and 14.4 for sea water and fresh water, respectively. The pattern for sea water has a good lobe at 3° which is above the Brewster angle. The fresh water pattern has a relative maximum near 7°, where the gain is about that in free space because this is also the location of the Brewster angle. The Brewster angle for good ground is about 12°, so the pattern for this case (figure 11.4) does not have a relative minimum there and is almost equal to the free space value. As expected, the pattern for poor ground is between those for good ground and polar ice.

The patterns for feed point heights of 5, 10, and 20λ have similar characteristics and are grouped as "high heights". The highest, h = 20λ shown in figures 10.8, 11.8, etc., will be discussed as typical. The phase of the reflected ray, $e^{-i\varphi}R_V$, is now dominated by the phase path difference φ. Thus, all cases except sea water have a lobe near 0.7° predicted by (52), with a gain of about 7 dB. The Brewster angle for sea water is near 0.6°, and this moves the position of the first lobe above 1°. At these high heights, the pattern oscillates around the free space value, and the envelope of the pattern is also of interest. The Brewster angle is indicated by a narrowing of the envelope, since the interference is proportional to $|R_V|$. Figures 12.8 and 14.8 are especially good examples.

The success in explaining the behavior of the antenna patterns using the propagation factor for the midpoint of the vertical dipole suggests that this may be a very good approximation. The approximation (48) was tested numerically for small take-off angles, with the additional assumption that the radiation resistance of the antenna is approximately its free space value. The formula is

$$G(\Delta) \cong 2.15 + 20 \log_{10} \left| F_r\left(\Delta, \frac{h_1 + h_2}{2}\right) \right|. \qquad (53)$$

For $0 < \Delta < 5°$, the error was less than 1 dB, and less than 2 dB for negative elevation angles. The approximation was not tested above $\Delta = 5°$ since low angles are of most interest here, but the approximation is probably adequate up to $\Delta = 30°$.

3.4 Radiation Patterns of Quarter-Wave Monopoles

Equation (47) gives the field of a quarter-wave grounded antenna over flat earth, and (44) can be integrated numerically over curved earth. We assume a perfect counterpoise or ground screen large enough to sustain the sinusoidal current distribution, but too small to affect the pattern. The radiation resistance is 36.6 ohms, so that the pattern relative to an isotropic radiator is

$$\frac{E_r(\lambda/4)}{E_{r(\text{isotropic})}} \cong -0.905\, i\, k \cos\Delta \int_{h_1}^{h_2} \ldots\, dh$$

$$\cong \frac{-0.905\, i}{\cos\Delta} e^{i k h_2 \sin\Delta}$$

$$\times \left\{ F_r(h_2) - i \sin\Delta\, e^{-i\frac{\pi}{2}\sin\Delta} F_\theta(h_1) \right\} . \qquad (54)$$

The second line is for flat earth. The term involving F_θ can be interpreted as the field reradiated by the horizontal ground system since it is the same as the propagation factor for the vertical field off the end of a horizontal electric dipole [Laitenen, 1949].

Patterns were calculated for a frequency of 10 MHz for all ground types (including perfectly conducting ground) for two heights of the feedpoint: $h_1 = 0$, figure 15, and $h_1 = \lambda/4$, figure 16. For these low heights the pattern is roughly proportional to $1 + R_V$ for small Δ. Thus, below the Brewster angle, the reflected ray tends to cancel the direct ray; above the Brewster angle it reinforces the direct ray. The gain for sea water is almost as good as for perfect ground but comes at a higher angle. Then, for successively higher Brewster angles, come fresh

water, good ground, and poor ground. As for the half-wave dipole at low heights, the gain for good and poor ground never reaches the free space value because, by the time the Brewster angle is exceeded, Δ is large enough that the factor $e^{-i\varphi}$ causes partial cancellation. The pattern for polar ice is very similar to that for poor ground.

The patterns for a quarter-wave monopole with its counterpoise a quarter-wave above the ground are shown in figure 16. These have a relative minimum between 45° and 50°. Otherwise, they have the same features seen in figure 15. Over sea water, the power is only 3 dB below an isotropic radiator at $\Delta = 0°$, with some power at negative take-off angles.

3.5 Vertical Patterns Broadside to a Horizontal Half-Wave Dipole

When the linear antenna is horizontal, there is no variation of the current with h, and the vertical radiation pattern is given exactly by the free space pattern multiplied by the propagation factor for horizontal polarization [Wait, 1956]. The field broadside to a horizontal dipole (in the plane perpendicular to the dipole through its midpoint) relative to an isotropic radiator is

$$\frac{E_\varphi(\lambda/2)}{E_\varphi(\text{isotropic})} \cong \frac{10.954}{\sqrt{R_{rad}}} F_\varphi(h_A, \Delta). \tag{55}$$

The power gain varies inversely with the radiation resistance which is shown in figure 7 for a horizontal half-wave dipole over various types of ground. The variation from the free space value is greater than that for the vertical antenna.

To help understand the patterns, the behavior of the reflection coefficient for horizontal polarization, R_h, is reviewed. The amplitude and phase of R_h are shown in figure 9 as a function of Δ for a frequency of 10 MHz and for the ground types of table 1. There is no psuedo-Brewster angle for this polarization, and the most important feature is that R_h is not too different from -1 for any take-off angle less than 20°, except for polar ice. Therefore, if the phase path difference φ is small, the reflected ray nearly cancels the direct ray. The extent of the cancellation will depend on $|R_h|$ so that the antenna will have a better low angle pattern over lower conductivity. The obvious way to increase the phase path difference and thus improve the low angle pattern is to increase h_A (raise the dipole).

The calculated vertical radiation patterns of a horizontal half-wave dipole located 0.05λ above the five ground types are shown in figure 17.1. As expected from the above discussion of reflection coefficients, very little power is radiated at low angles. For all ground types except polar ice, the power is more than 10 dB below an isotropic radiator if $\Delta < 10°$. The radiation is less over the highly conducting surfaces (such as water) because R_h is nearer to -1 and the reflected ray more nearly cancels the direct ray.

As the antenna is raised to 0.1λ, figure 17.2, and then to 0.25λ, figure 17.3, the radiation increases but has the same general characteristics. The better conducting models now have more radiation at high angles because the phase path difference is large enough that the reflected ray reinforces the direct ray. This trend continues at $h_A = 0.375\lambda$ and $\lambda/2$ as shown in figures 17.4 and 17.5. Now, φ is large enough (for some values of Δ) that the antenna gain over an isotropic is more than 8 dB.

As the antenna is raised higher and higher, as shown in figures 17.6 - 17.10, a standing wave pattern is seen with lobes at elevation angles Δ_n, such that

$$\sin \Delta_n \cong (2n-1)\frac{\lambda}{4h} .$$

The gain is best for sea water. The pattern for an antenna over polar ice is a little different from the others for large Δ because $|R_h|$ is very small for this case.

3.6 Comparison of Low-Angle Patterns of the Three Types of Antennas

All the antenna patterns show power gain relative to an isotropic radiator so they can be compared directly. In this section, their relative effectiveness at low elevation angles is discussed.

The half-wave vertical dipole fed $\frac{3}{8}\lambda$ above the ground radiates better at low angles than the quarter-wave monopole. In a sense, this comparison is not "fair", since the discussion above showed that height is a great advantage in attaining a good low-angle pattern, and this half-wave dipole is higher than the quarter-wave monopole. The quarter-wave monopole has a better low-angle pattern than the horizontal dipole if the dipole is less than a half-wave above the surface, except for polar ice. Over sea water, the monopole is better than the horizontal dipole at very low angles ($< 5°$) unless the dipole is more than 5λ high, although the maximum gain of the dipole is greater.

Now compare the low-angle patterns of horizontal and vertical dipoles fed at the same height. At the lowest height for which the vertical dipole was computed, $h = \frac{3}{8}\lambda$, the vertical dipole has a better low-angle pattern than the horizontal over all types of ground except polar ice. At the other low and medium heights, the vertical dipole is

better over water, and the horizontal is better over land. For high antennas, the horizontal dipole has a slightly better pattern at very low angles.

3.7 Remark on Frequency Dependence

The antenna patterns in this report were calculated for a frequency of 10 MHz, so it may seem that the results are of limited application. However, the graphs of the propagation factor in section 2 show that there is only a weak dependence on frequency, and these same graphs can be used to estimate the frequency dependence of the antenna patterns. When doing this, remember that all heights have been measured in wavelengths. An antenna at some fixed physical height would have more frequency dependence since its height in wavelengths changes with frequency.

4. Conclusions

Propagation factors are basic to the calculation of vertical radiation patterns of high frequency antennas over finitely conducting earth. For elevation angles greater than one or two degrees, they are given by $1 + e^{-i\varphi}R$ where R is the appropriate ground reflection coefficient and φ is the difference between the phase paths of the direct and reflected rays. For smaller elevation angles (including negative elevation angles), the full-wave solution for diffraction by a spherical earth must be used.

The calculations in this report show the effects of frequency, conductivity, polarization, and height on the propagation factor. Over sea water there is very little frequency dependence for positive elevation angles. There is more variation with frequency over land, especially for vertical polarization. The conductivity has a much greater effect on vertical polarization than on horizontal polarization. In general, for low heights, the amplitude of the vertically polarized propagation factor

grows as the conductivity increases and the amplitude of the horizontally polarized propagation factor decreases with increasing conductivity. At great heights, the propagation factors for both polarizations improve with increasing conductivity.

The vertical radiation pattern broadside to a horizontal dipole is proportional to its propagation factor. This is not exactly true for a vertical dipole, but the error is less than 1 dB for positive elevation angles if the propagation factor for the mid-point of the antenna is used. Patterns were calculated for vertical and horizontal half-wave dipoles and vertical quarter-wave monopoles. For low heights, the vertical dipole has the best low-angle radiation pattern; for medium heights, the vertical dipole has the best low-angle pattern over water, and the horizontal dipole is better over land. The horizontal dipole is better for all types of ground at great heights. The best low-angle gain, relative to an isotropic radiator is: for low antennas, about 7 dB over sea water and about 0 dB over land; for medium heights, about 6 dB; and for high antennas, about 8 dB.

Further research is required to predict the quantitative effect of irregularities on low-angle radiation patterns.

5. Acknowledgments

This research was sponsored by the U.S. Army Signal Radio Propagation Agency, and was initiated by Mr. Richard Silberstein who also contributed many ideas to the development. A. C. Stewart provided guidance on some aspects of antenna practice.

6. References

Anderson, J. B. (1964), Fresnel zones for ground-based antennas, IEEE Trans. on Ant. and Prop., AP-12, No. 4, 417-422.

Bremmer, H. (1949), Terrestrial radio waves, (Elsevier Publishing Company, Inc., N. Y., N. Y.).

Burrows, C. R. (1935), Radio propagation over spherical earth, Proc. IRE 23, No. 5, 470-480.

Feldman, C. B. (1933), Optical behavior of the ground for short radio waves, Proc. IRE 21, No. 6, 764-801.

Fock, V. A. (1965), Electromagnetic diffraction and propagation problems, (Pergamon Press, N.Y.).

Furutsu, K. (1965), Calculated curves for groundwave propagation over inhomogeneous earth with pronounced topographical features, Radio Sci., J. Res. NBS 69D, No. 7, 1011-1025.

Hyovalti, D. C. (1965), Computations of the antenna cut-back factor for LF radio waves, NBS Technical Note 330.

Jasik, H. (editor) (1961), Antenna engineering handbook, (McGraw-Hill Book Company, N.Y.).

Jordan, E. C. (1950), Electromagnetic waves and radiating systems, (Prentice-Hall, Inc., N. Y.).

Johler, J. R., L. C. Walters, and C. M. Lilley (1960), Amplitude and phase of the low- and very-low-frequency ground wave, NBS Technical Note 60.

Laitinen, P. O. (1949), Linear communication antennas, Radio Propagation Unit Technical Report No. 7, U.S. Army Signal Radio Propagation Agency.

Logan, N. A. (1959), Research in diffraction theory, Vol. 1. Lockheed Technical Report LMSD-288087.

Morse, P. M. and H. Feshback (1953), Methods of Theoretical Physics (McGraw-Hill Book Company, Inc., New York)

Norton, K. A. (1936), The propagation of radio waves over the surface of the earth and in the upper atmosphere, I, Proc. IRE 24, 1367-1388.

Norton, K. A. (1937), The propagation of radio waves over the surface of the earth and in the upper atmosphere, II, Proc. IRE 25, 1203-1236.

Norton, K. A. (1941), The calculation of ground wave field intensity over a finitely conducting spherical earth, Proc. IRE 29, 623-639.

Pryce, M. H. L. (1953), The diffraction of radio waves by the curvature of the earth, Advances in Physics, 2, 67-95.

Utlaut, W. F. (1961), Effect of antenna radiation angles upon HF radio signals propagated over long distances, J. Res. NBS 65D (Radio Prop.), No. 2, 167-174.

Utlaut, W. F. (1962), Siting criteria for HF communication centers, NBS Technical Note No. 139.

Wait, J. R. (1956), Low frequency radiation from a horizontal antenna over a spherical earth, Can. J. Phys. 34, 586-595.

Wait, J. R. (1962), Electromagnetic waves in stratified media (Pergamon Press, N. Y.)

Wait, J. R., and A. M. Conda (1958), Pattern of an antenna on a curved lossy surface, IRE Trans. Ant. and Prop. AP-6, No. 4, 348-359.

Wait, J. R., and A. M. Conda (1959), Diffraction of electromagnetic waves by smooth obstacles for grazing angles, J. Res. NBS 63D (Radio Prop.), No. 2, 181-197.

Watson, G. N. (1918), The diffraction of electric waves by the earth, Proc. Roy. Soc., London 95, 546.

Wentworth, F. L., and M. Cohen (1964), Electrical properties of sea ice at 0.1 to 30 Mc/s, Radio Science, J. Res. NBS 68D, No. 6, 681-691.

7. Index to Figures

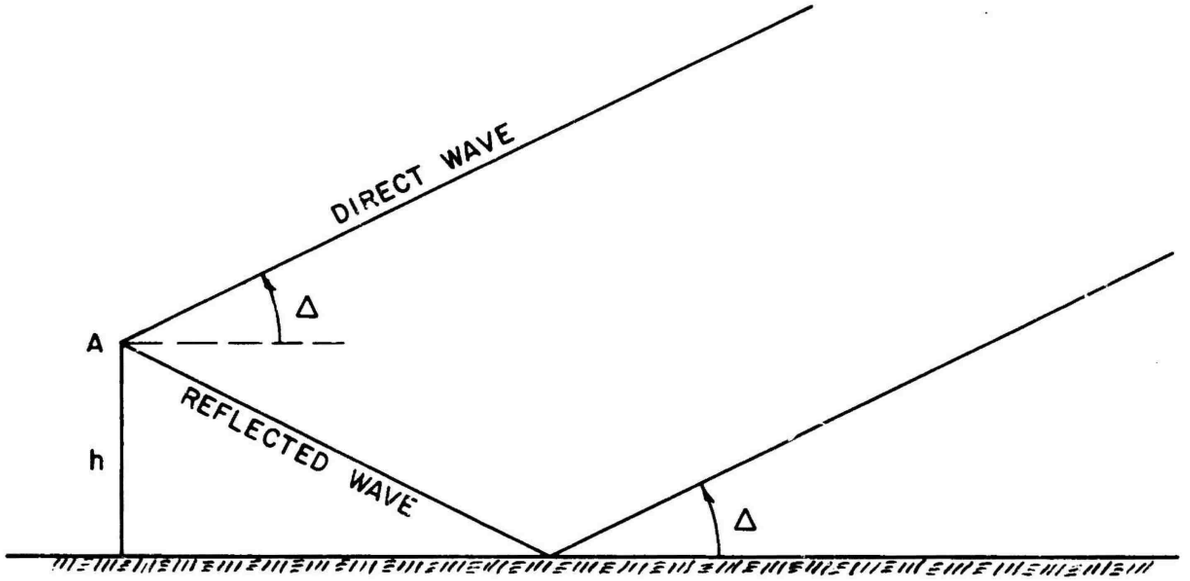

1. Geometry for flat-earth, two wave theory.

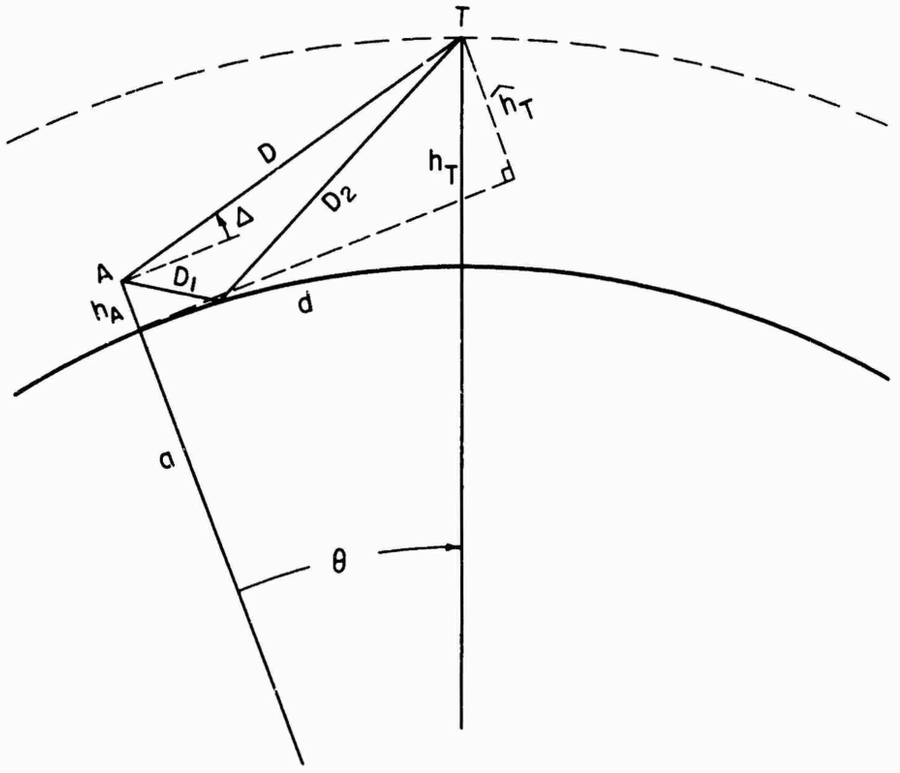

2. Illustration of the geometry for spherical earth model.

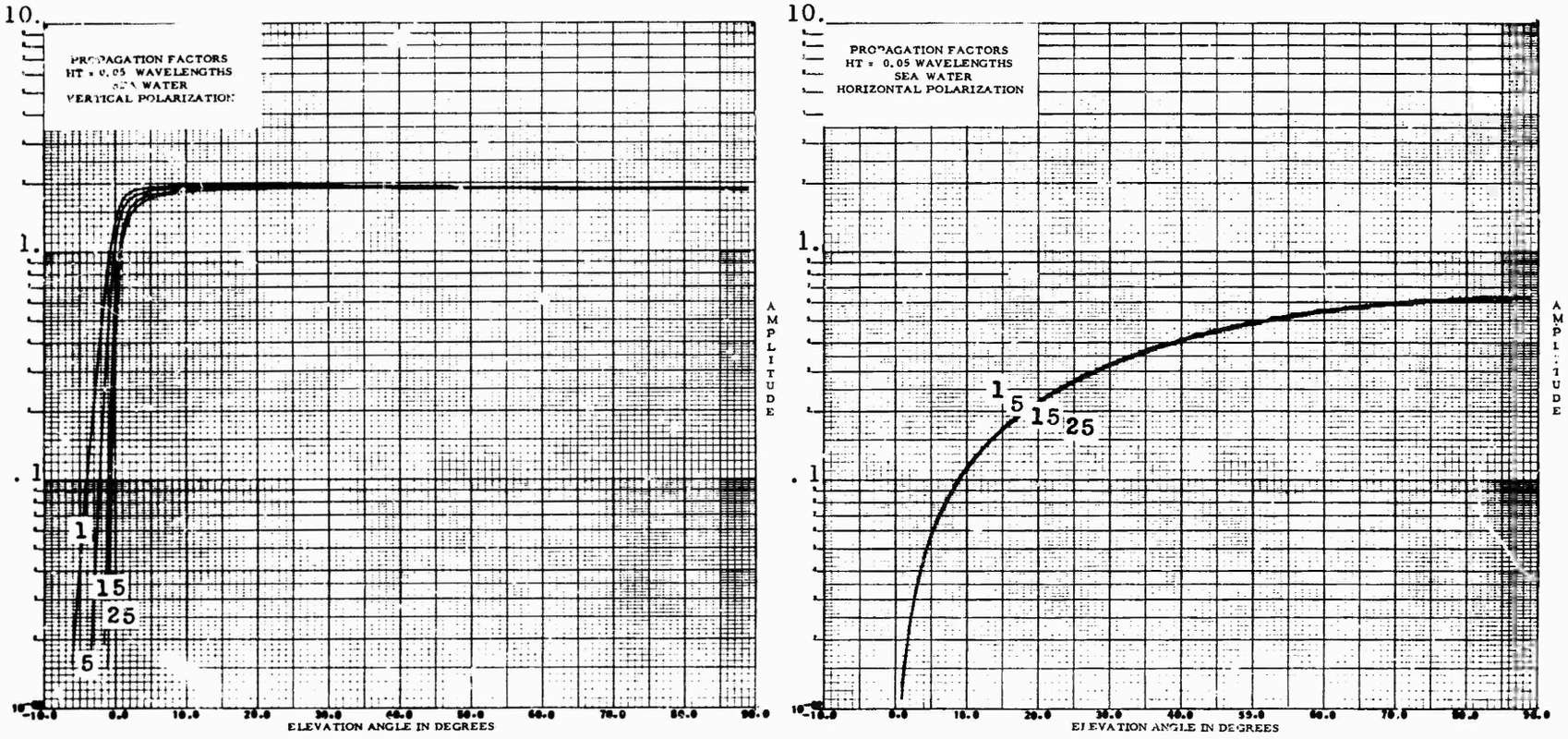

3.1. Propagation factors over sea water.
The numbers on the curves are frequency, in MHz.

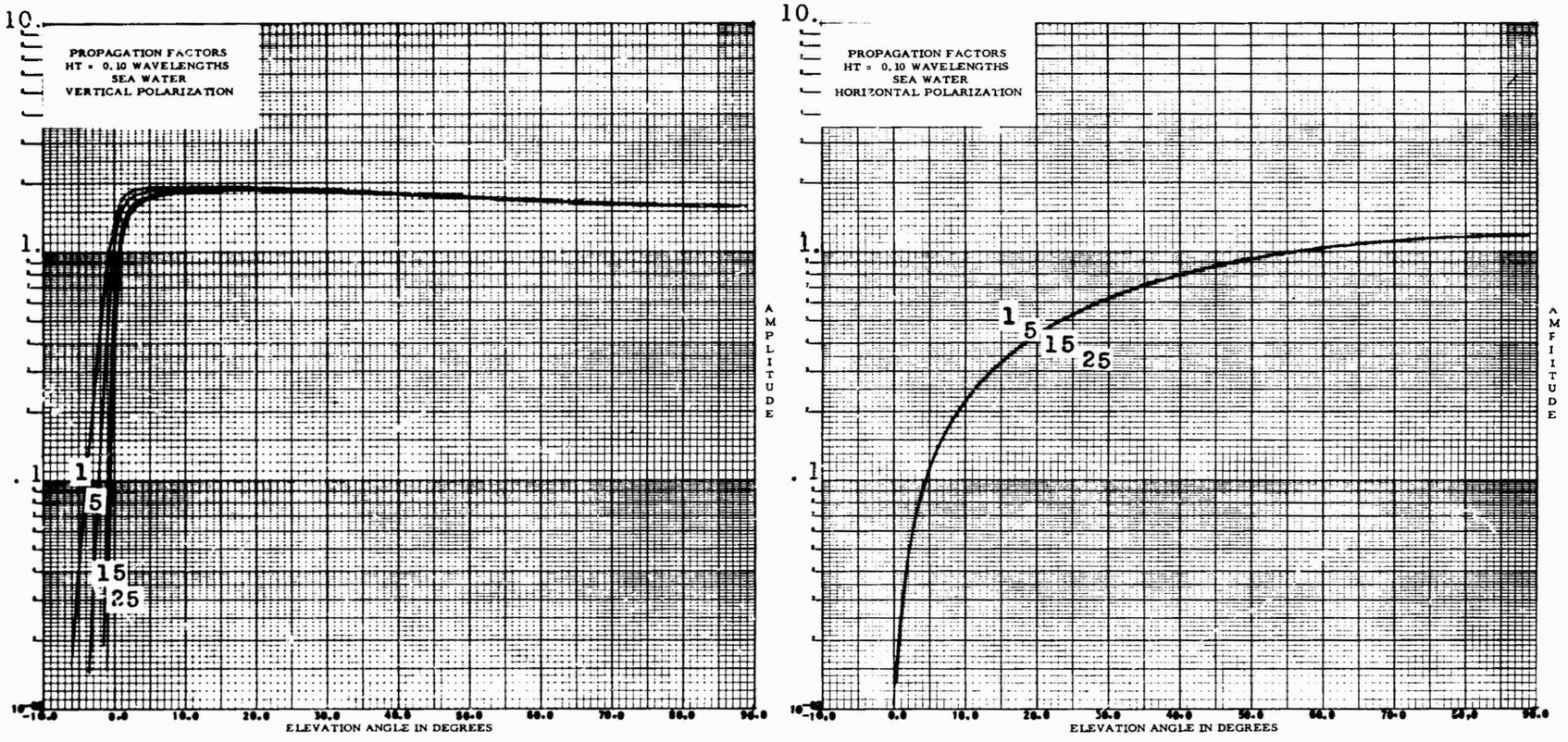

3.2. Propagation factors over sea water.
The numbers on the curves are frequency, in MHz.

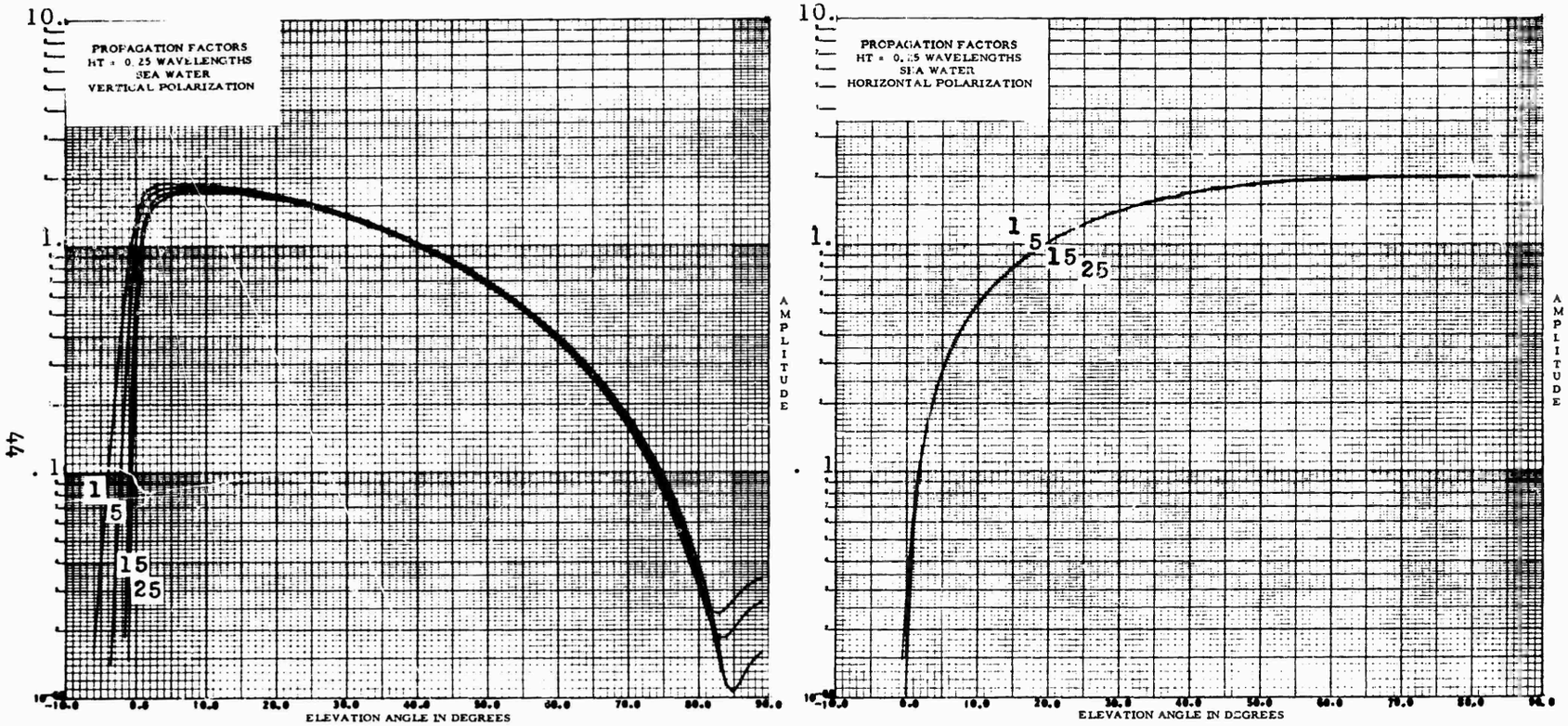

3.3. Propagation factors over sea water.
The numbers on the curves are frequency, in MHz.

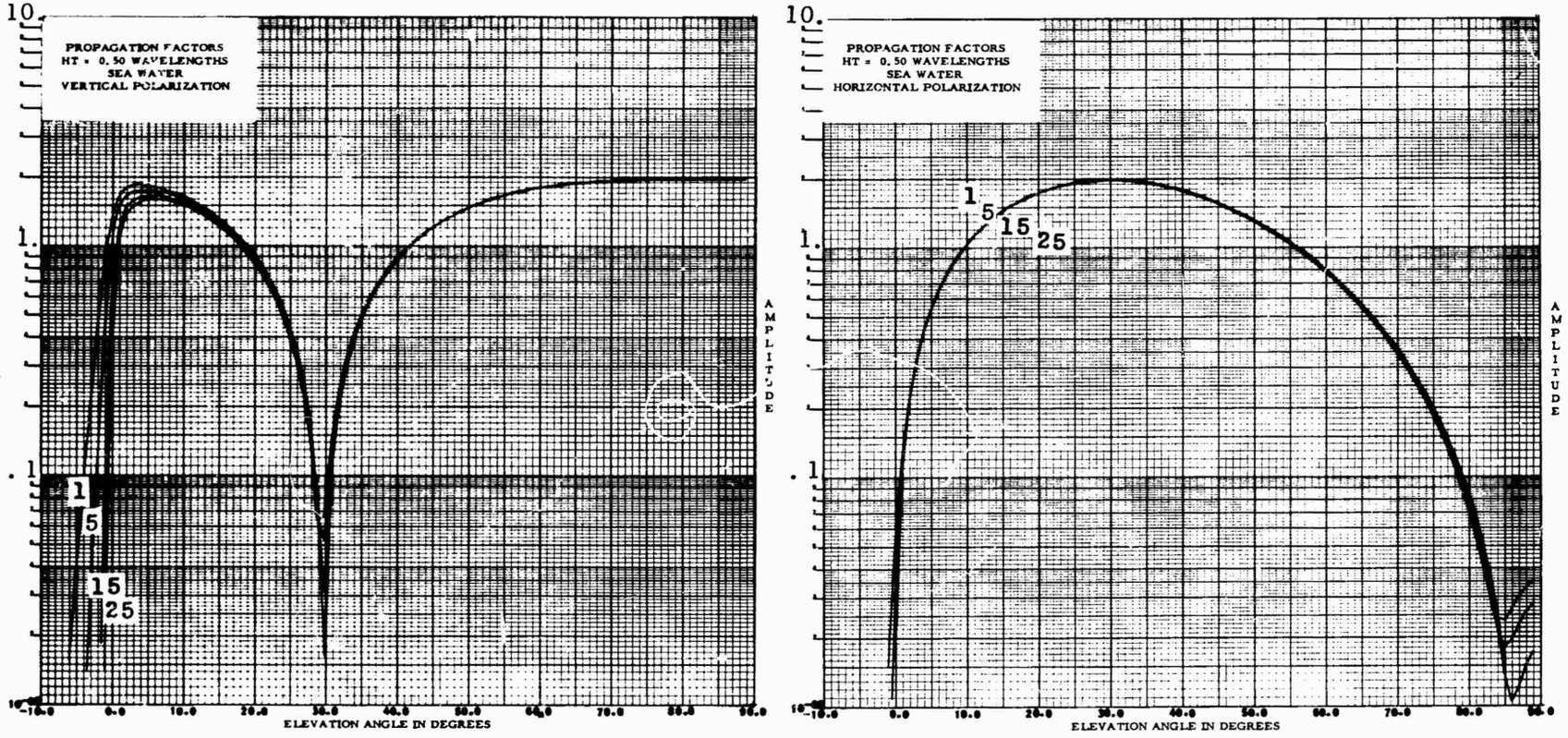

3.4. Propagation factors over sea water.
The numbers on the curves are frequency, in MHz.

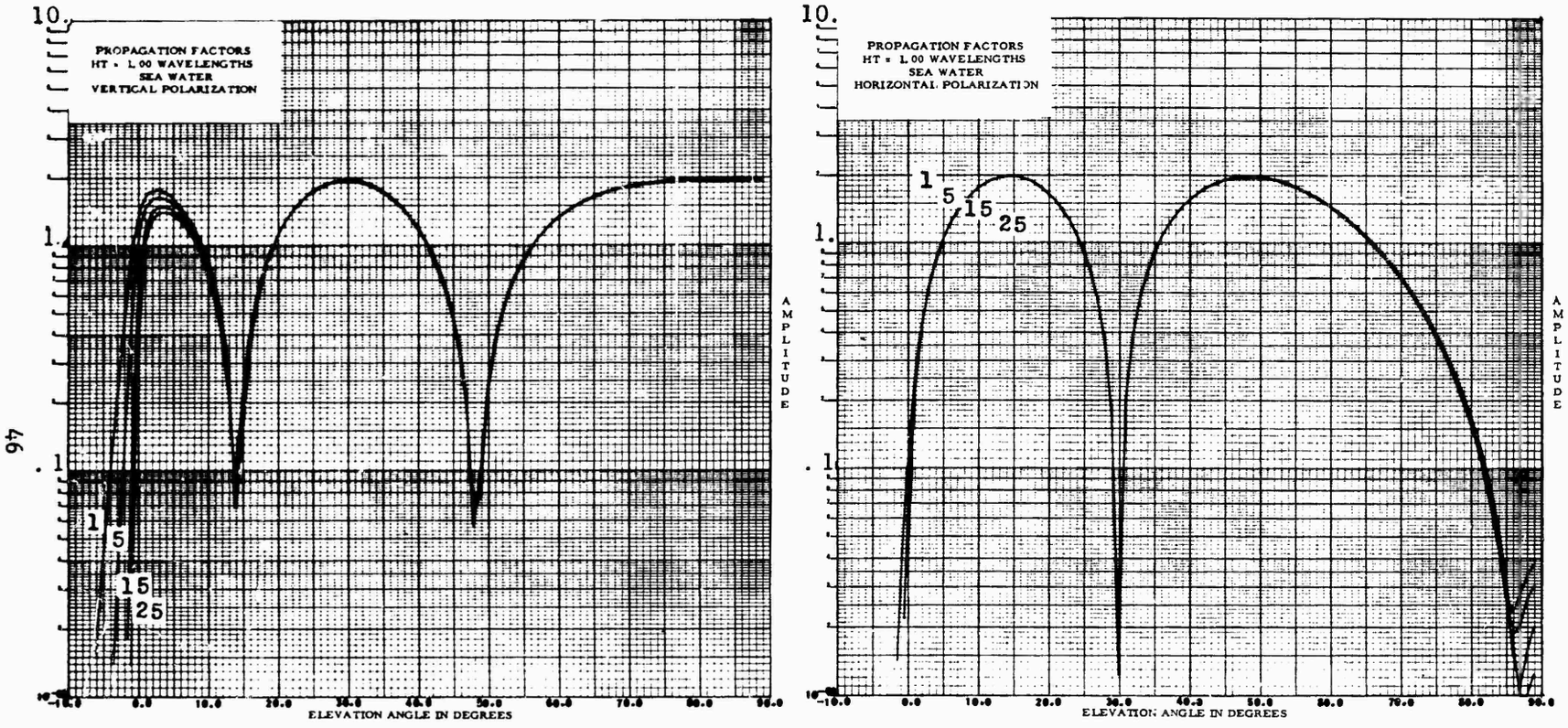

3.5. Propagation factors over sea water.
The numbers on the curves are frequency, in MHz.

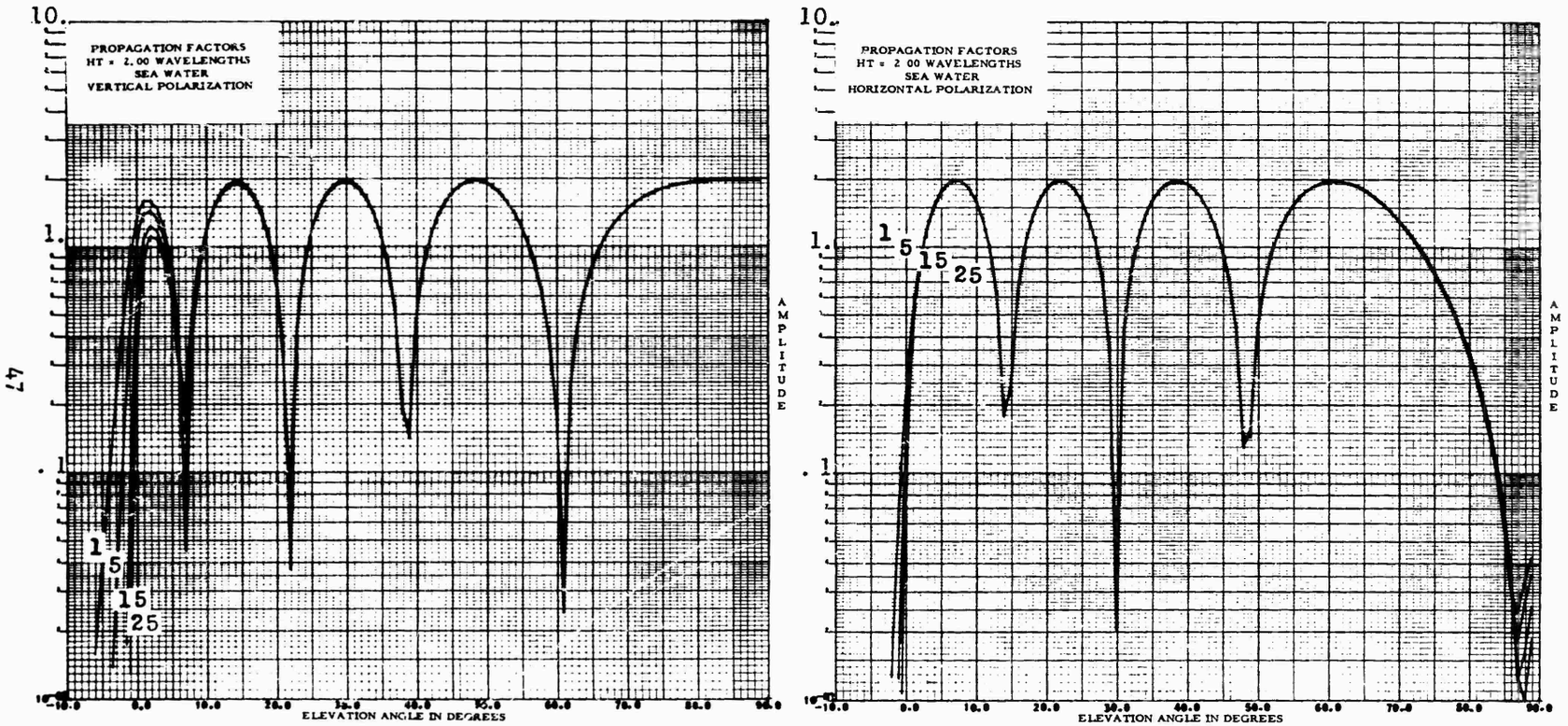

3.6. Propagation factors over sea water.
The numbers on the curves are frequency, in MHz.

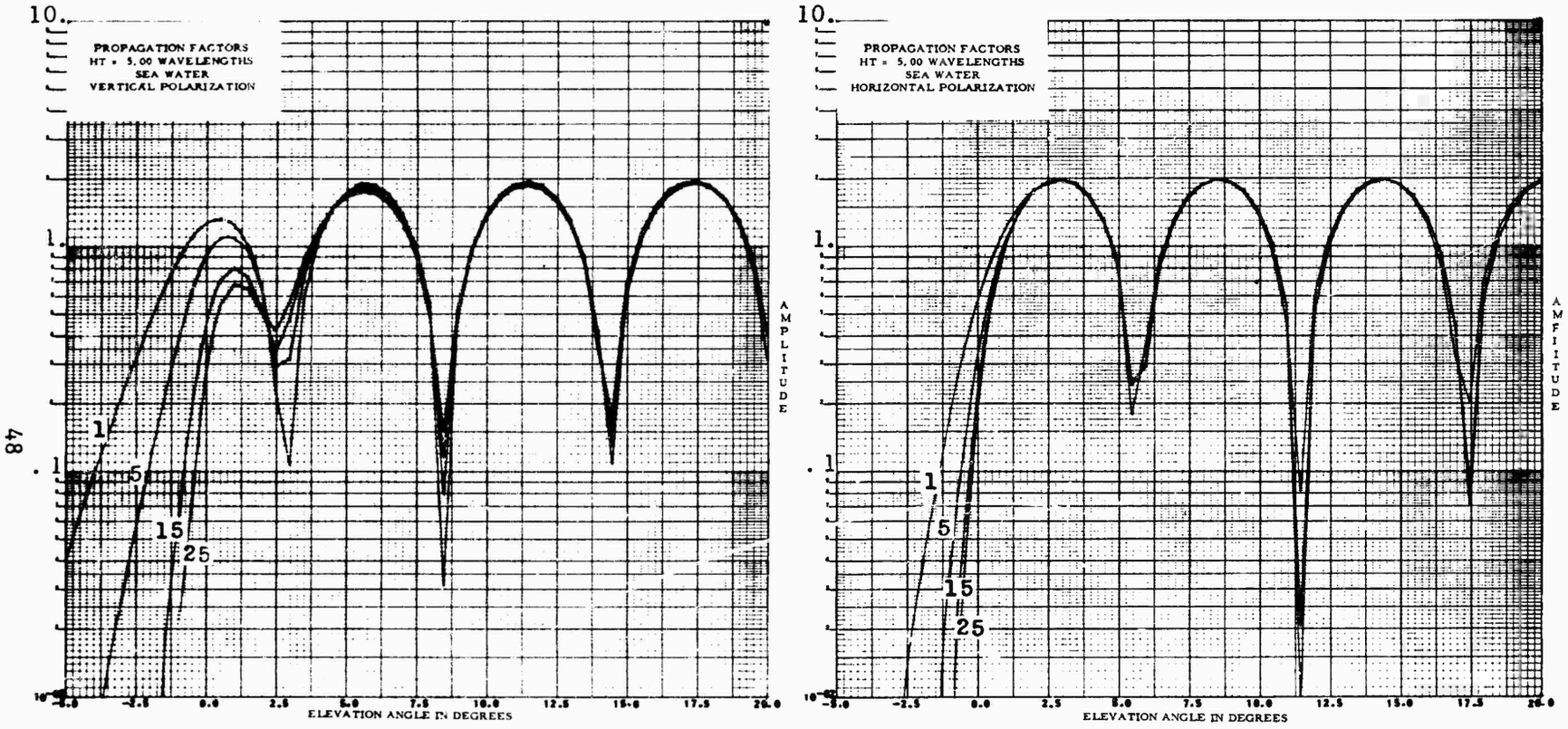

3.7. Propagation factors over sea water.
The numbers on the curves are frequency, in MHz.

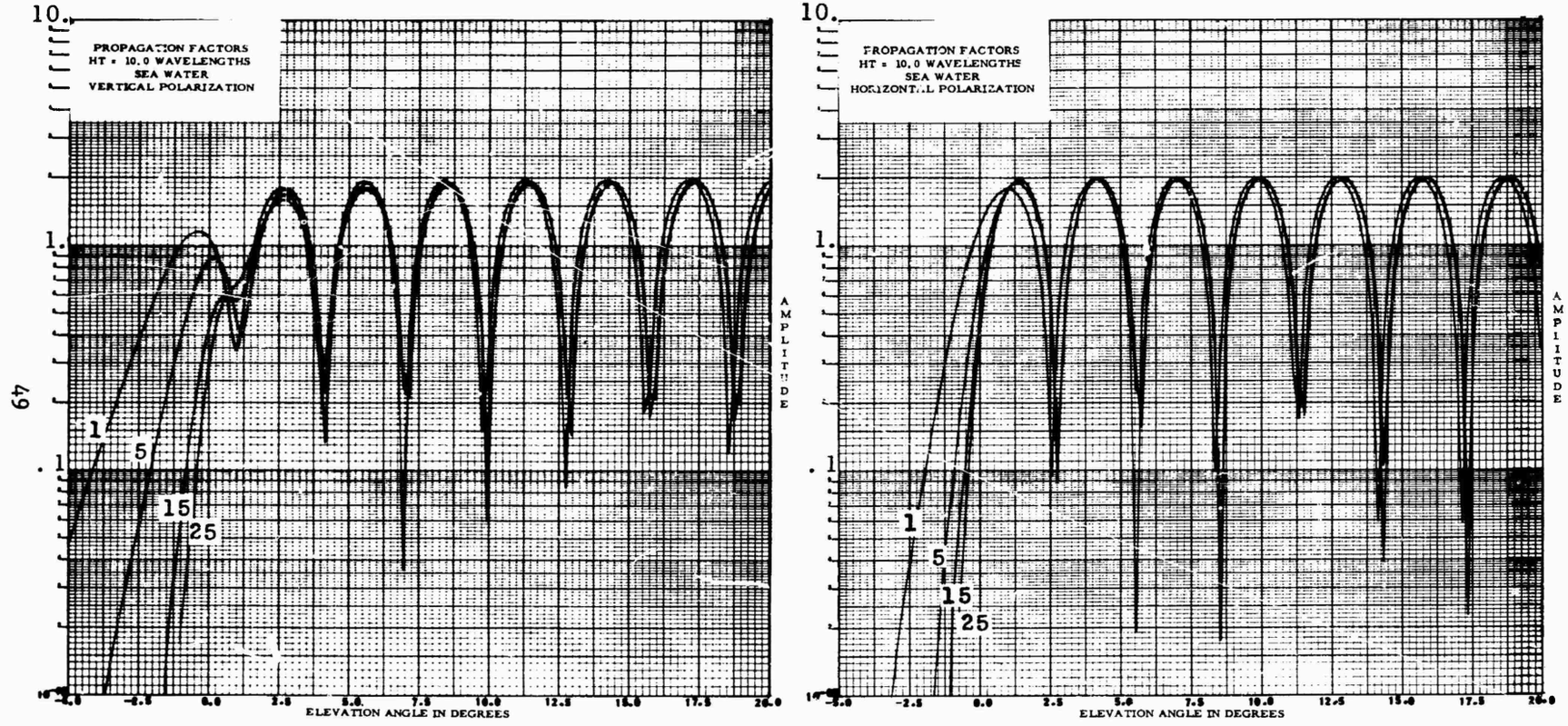

3.8. Propagation factors over sea water.
The numbers on the curves are frequency, in MHz.

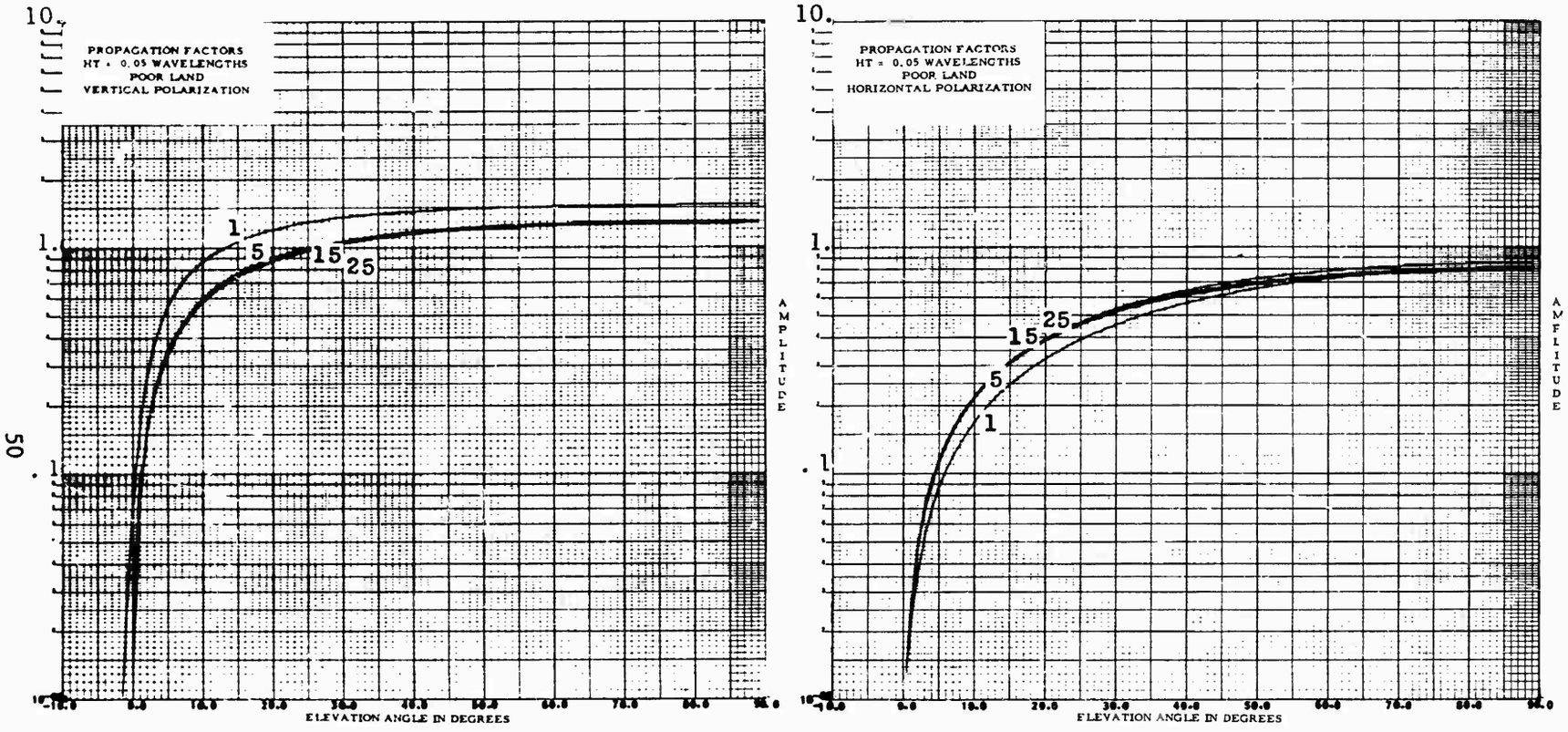

4.1. Propagation factors over poor ground.
The numbers on the curves are frequency, in MHz.

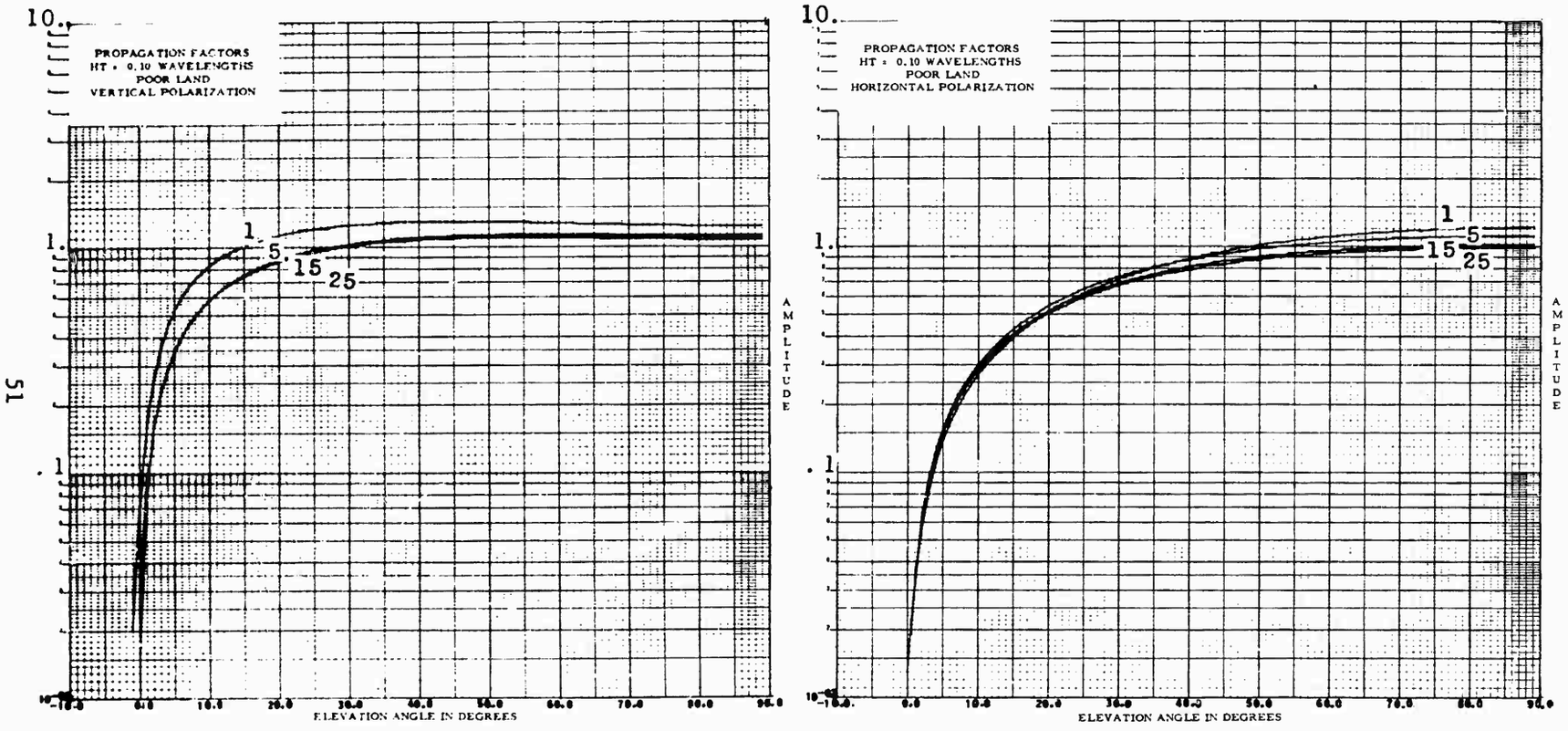

4.2. Propagation factors over poor ground.
The numbers on the curves are frequency, in MHz.

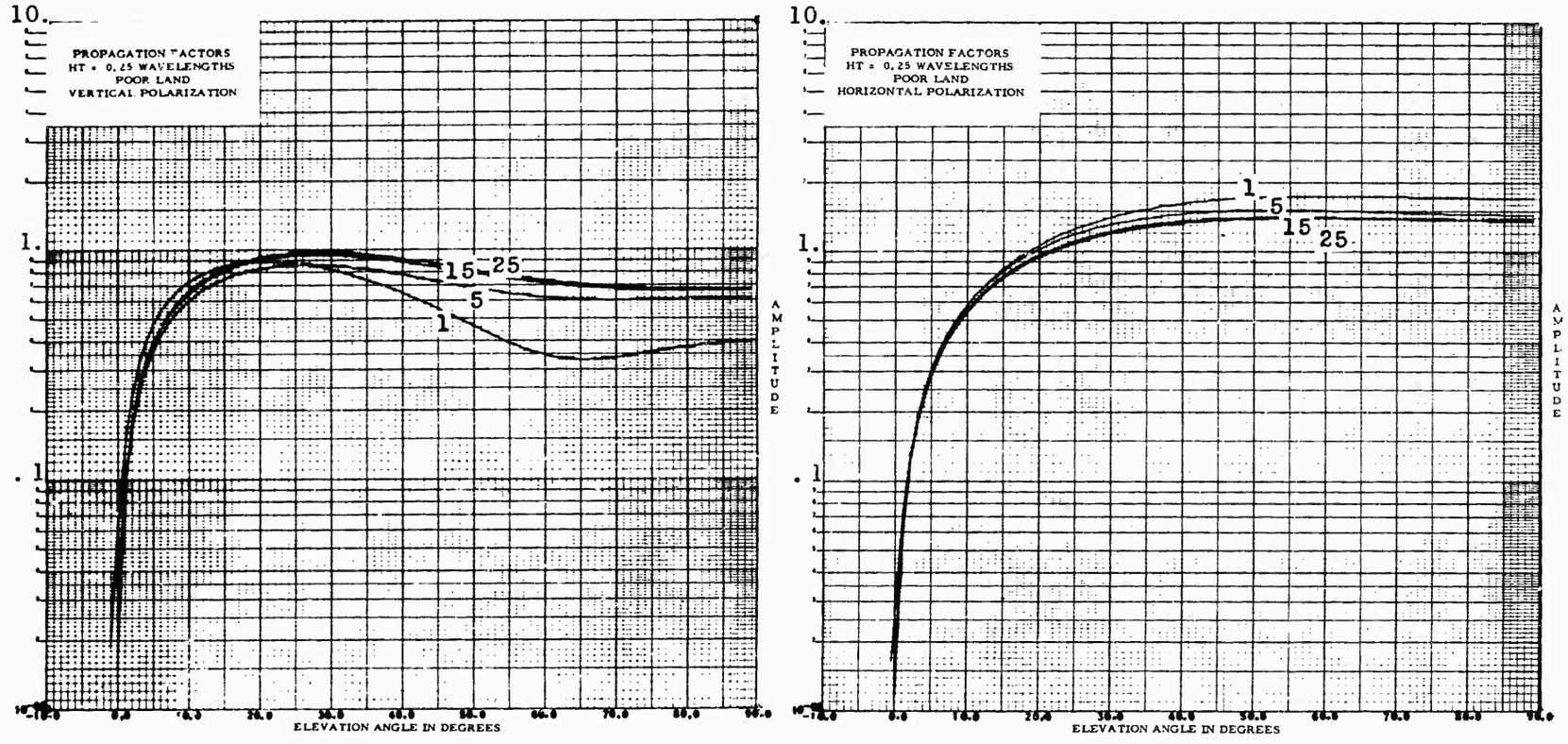

4.3. Propagation factors over poor ground.
The numbers on the curves are frequency, in MHz.

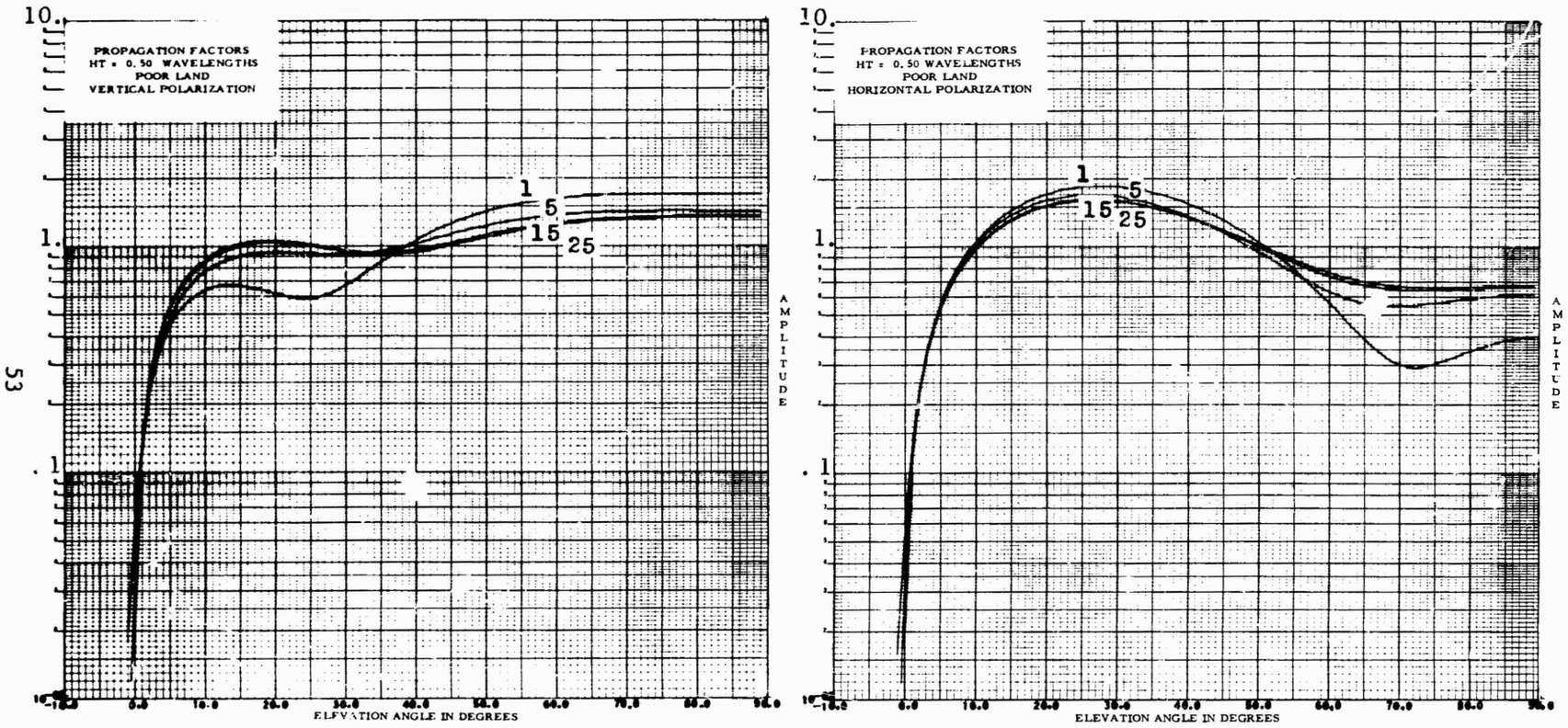

4.4. Propagation factors over poor ground.
The numbers on the curves are frequency, in MHz.

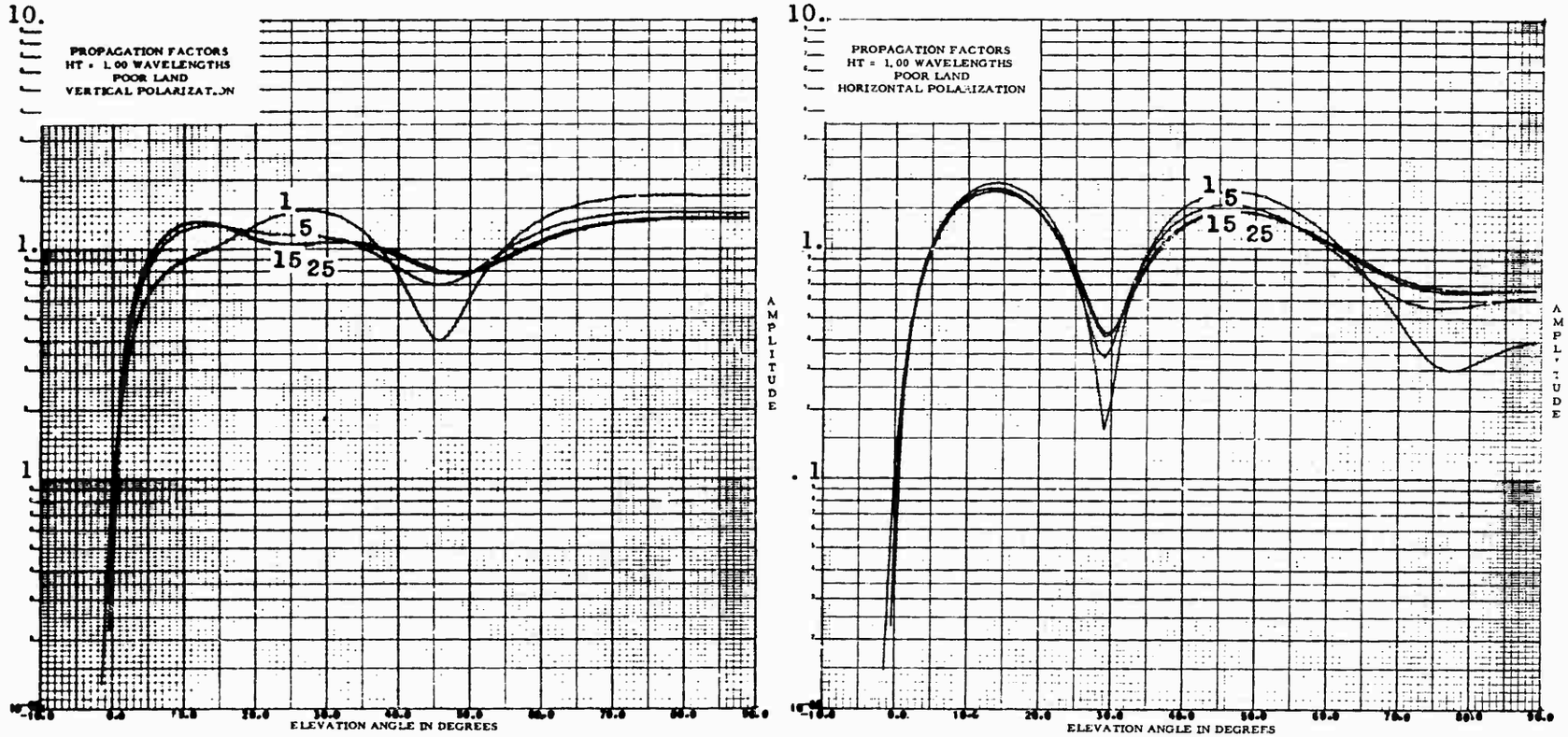

4.5. Propagation factors over poor ground.
The numbers on the curves are frequency, in MHz.

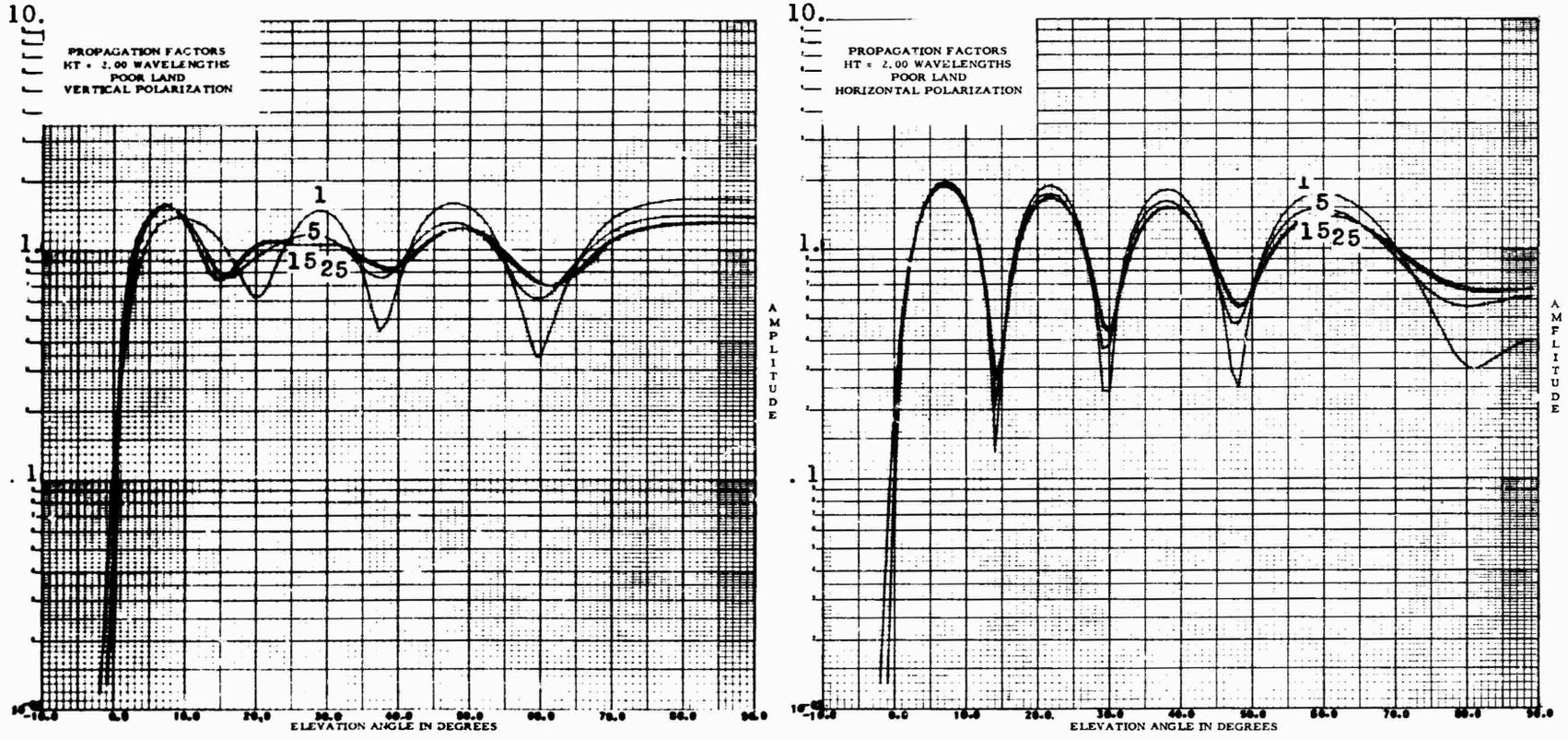

4.6. Propagation factors over poor ground.
The numbers on the curves are frequency, in MHz.

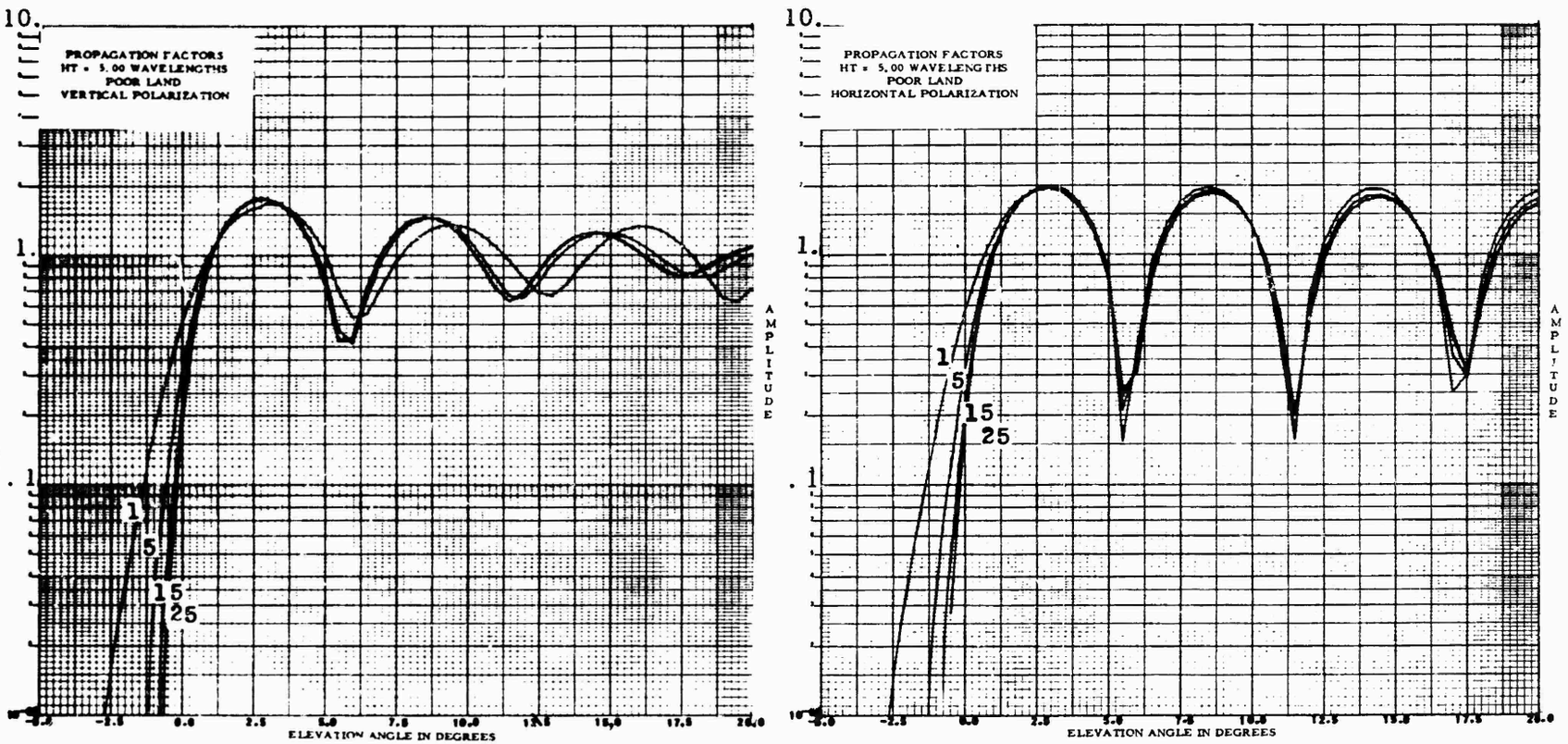

4.7. Propagation factors over poor ground.
The numbers on the curves are frequency, in MHz.

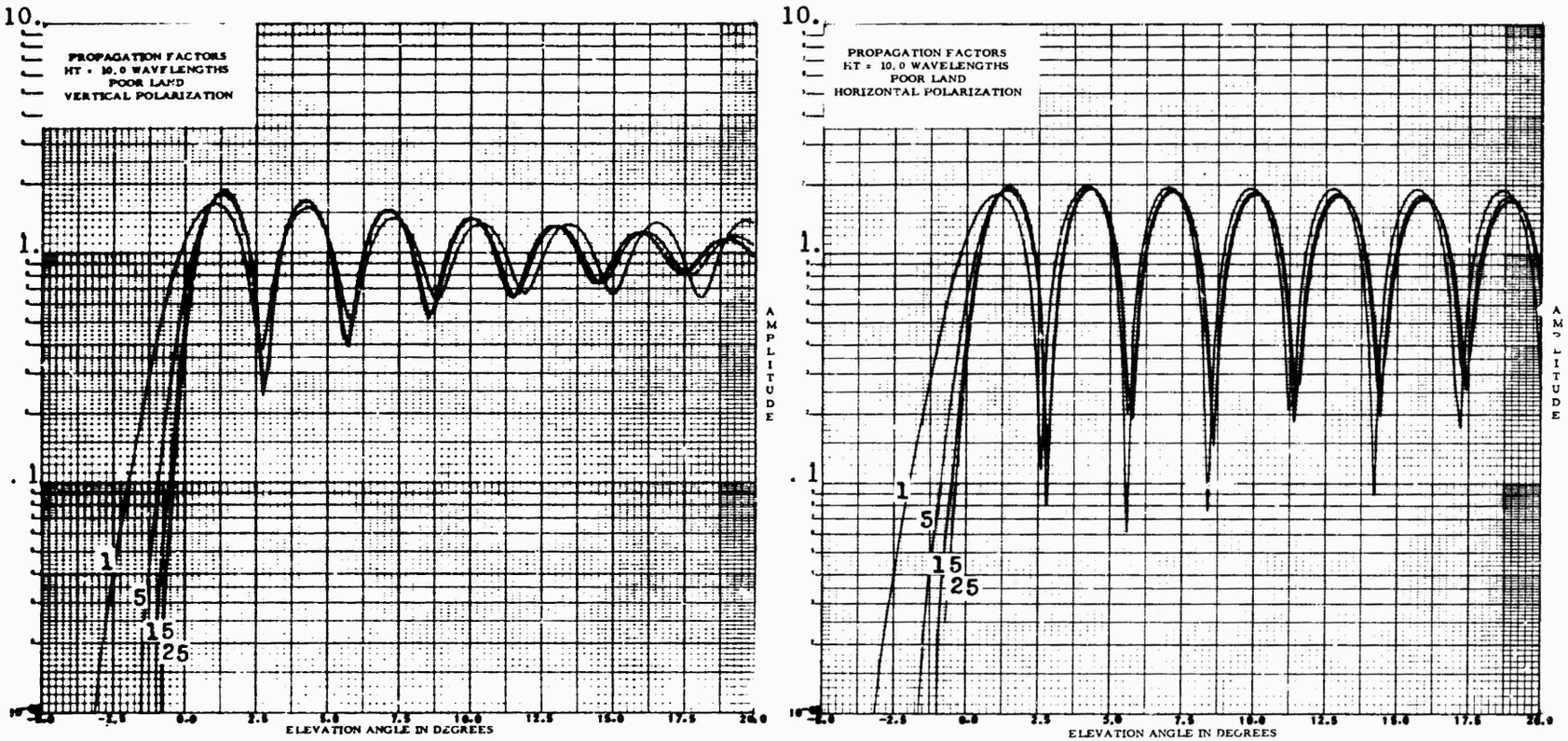

4.8. Propagation factors over poor ground.
The numbers on the curves are frequency, in MHz.

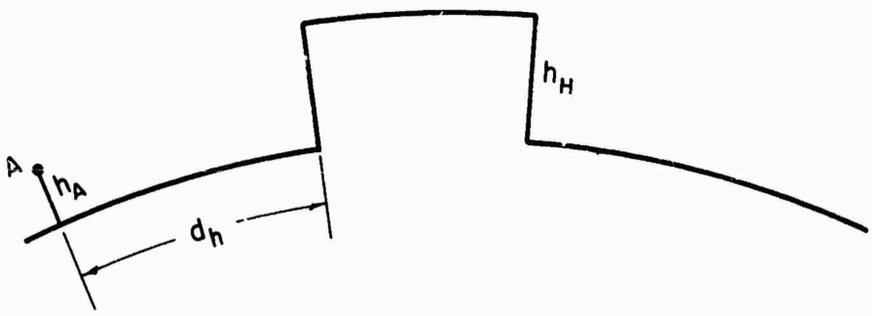

5. The "hill" used in the effect of an irregularity calculation in section 2.7.

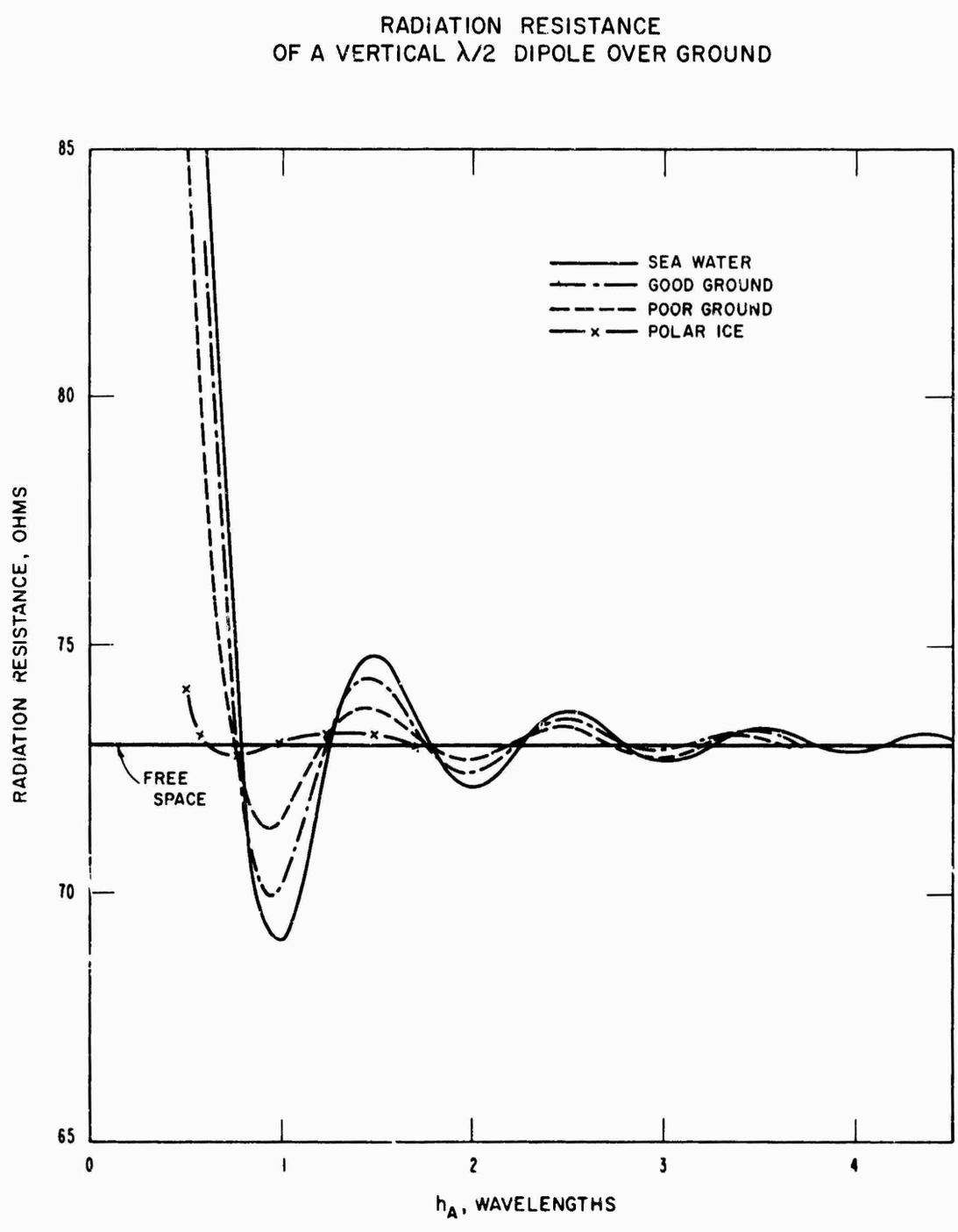

6. Radiation resistance of a vertical half-wave dipole over various types of ground as a function of height of the midpoint.

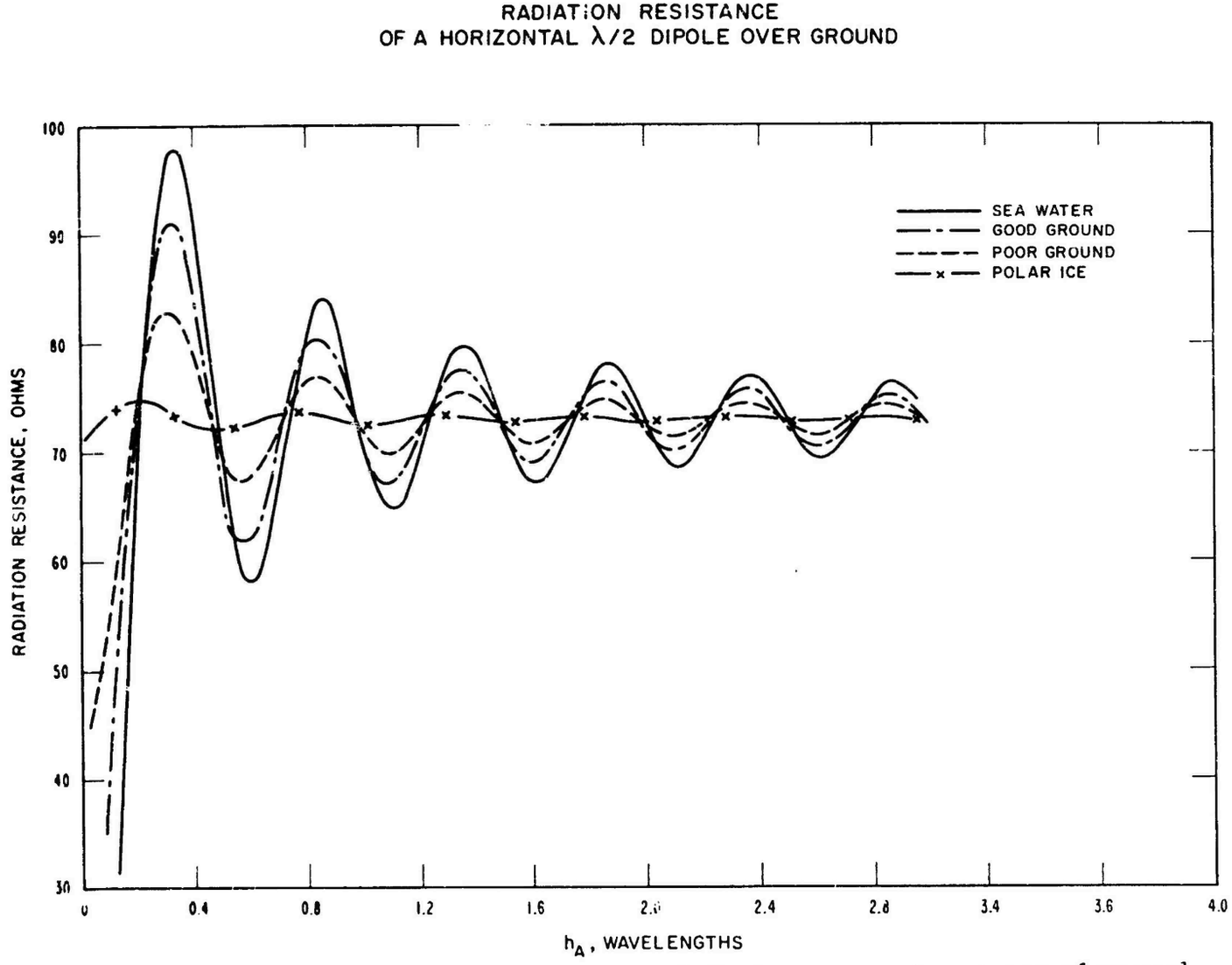

7. Radiation resistance of a horizontal dipole over various types of ground as a function of height.

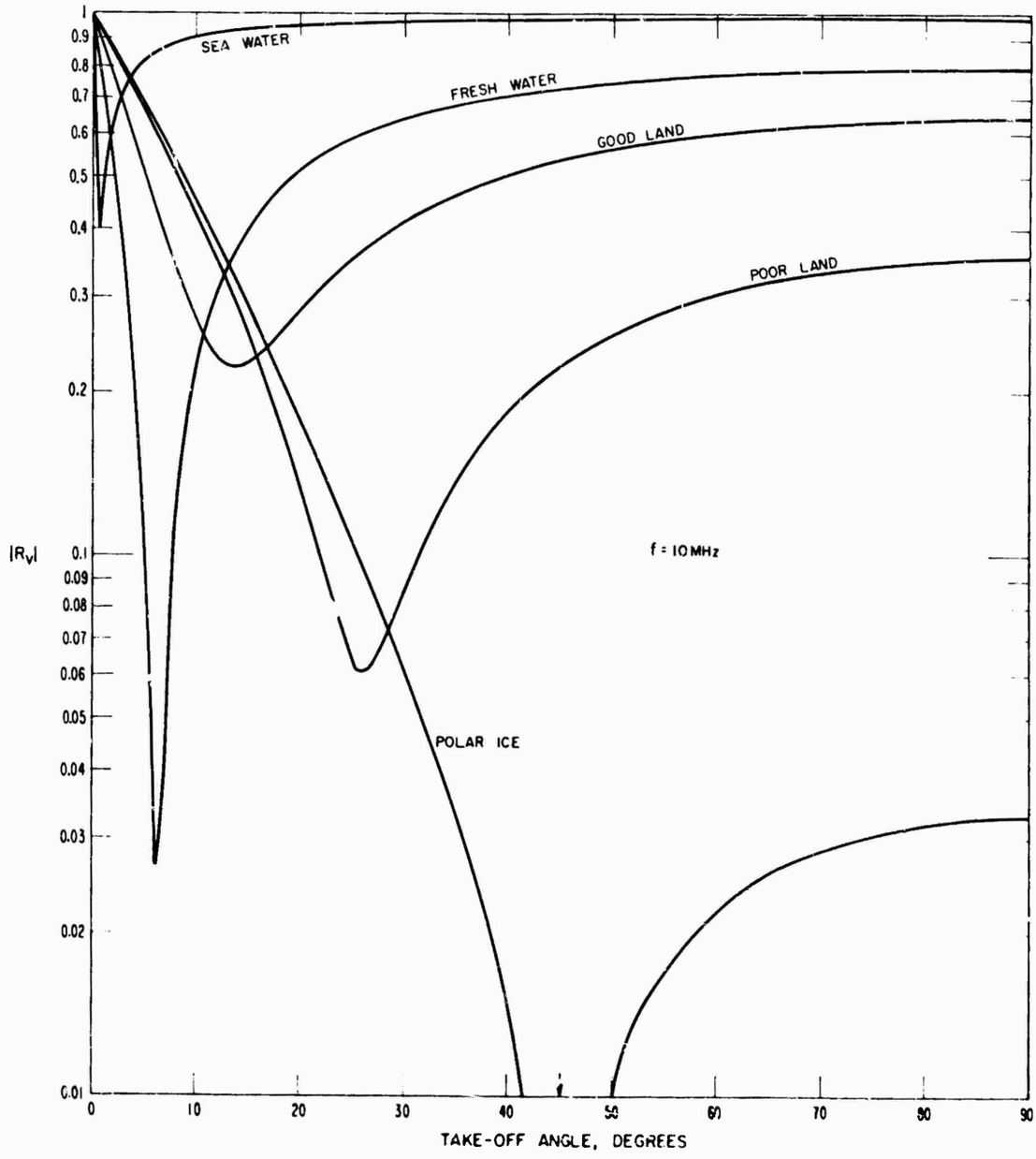

8.1. Amplitude of the ground reflection coefficient for vertical polarization, R_V, for various types of ground. The frequency is 10 MHz.

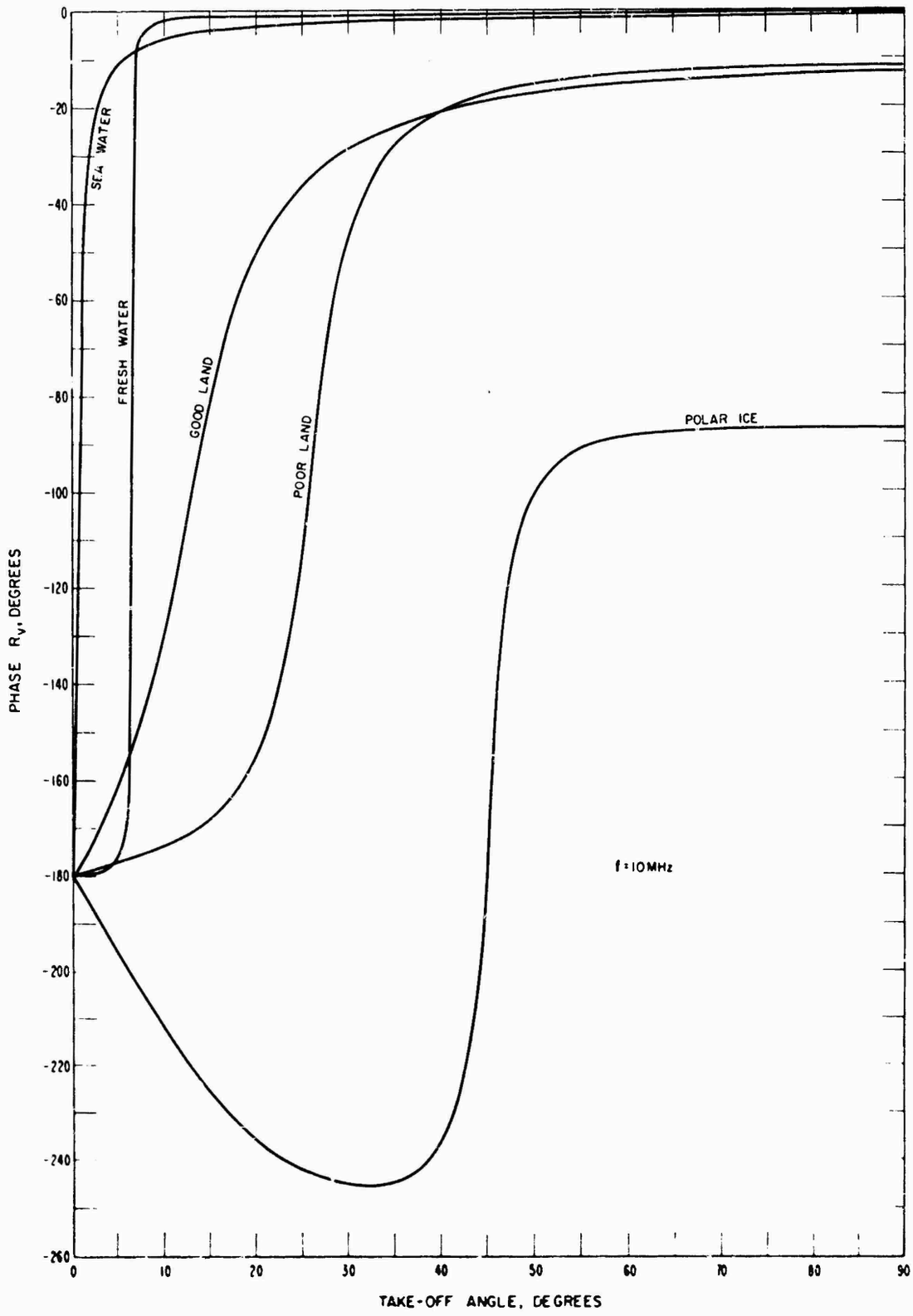

8.2. Phase of the ground reflection coefficient for vertical polarization, R_V, for various types of ground. The frequency is 10 MHz.

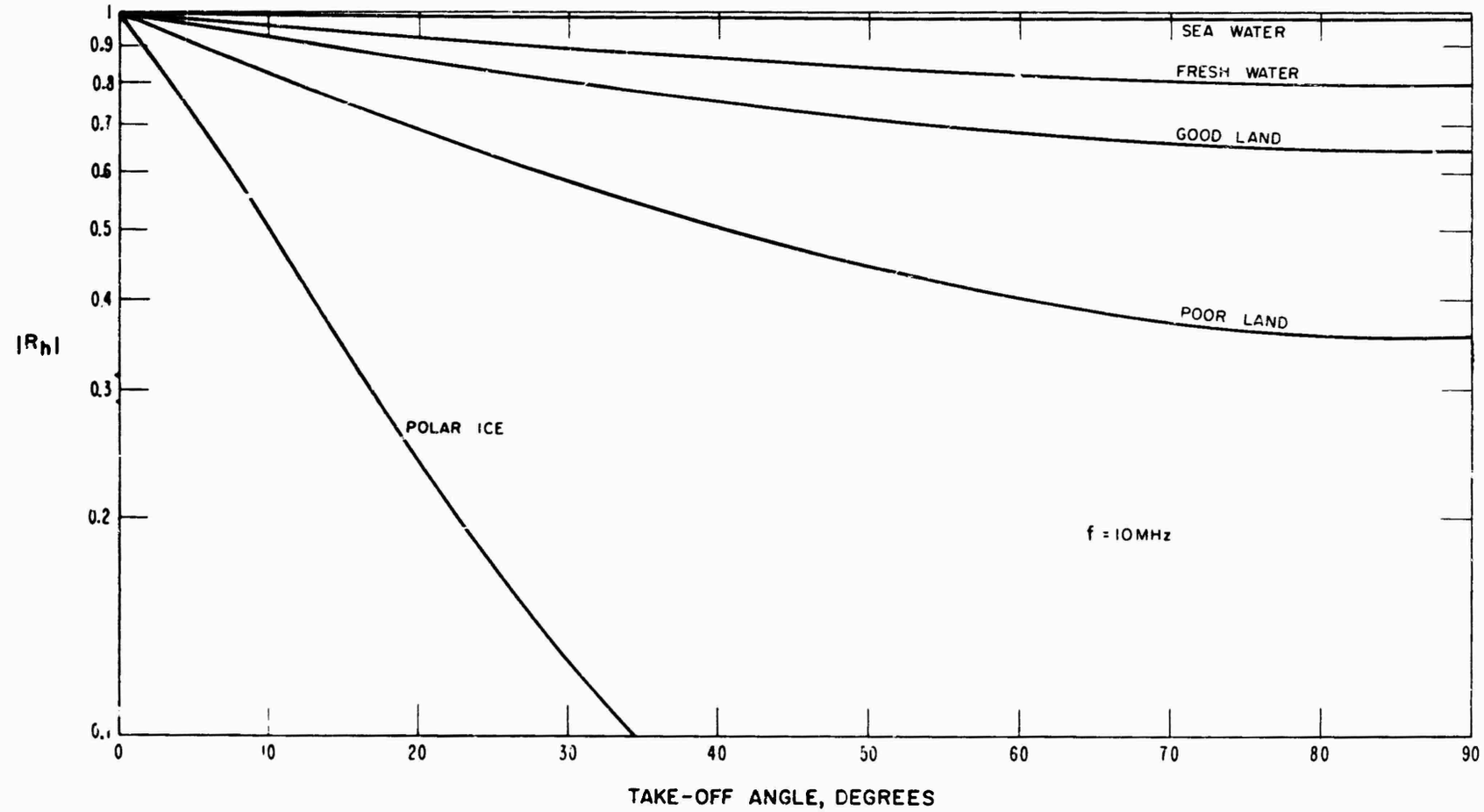

9.1. Amplitude of the ground reflection coefficient for horizontal polarization, R_h, for various types of ground. The frequency is 10 MHz.

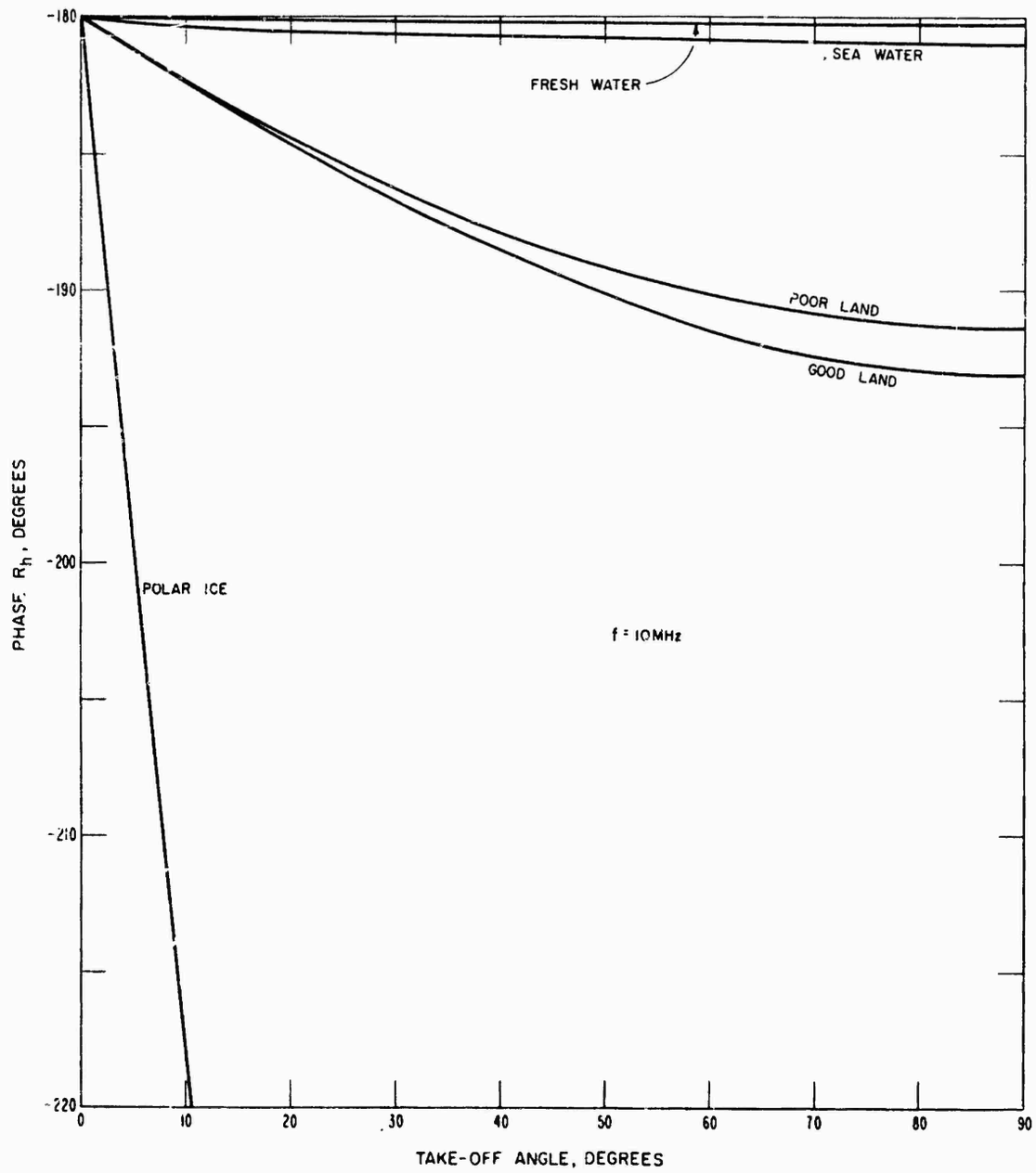

9.2. Phase of the ground reflection coefficient for horizontal polarization, R_h, for various types of ground. The frequency is 10 MHz.

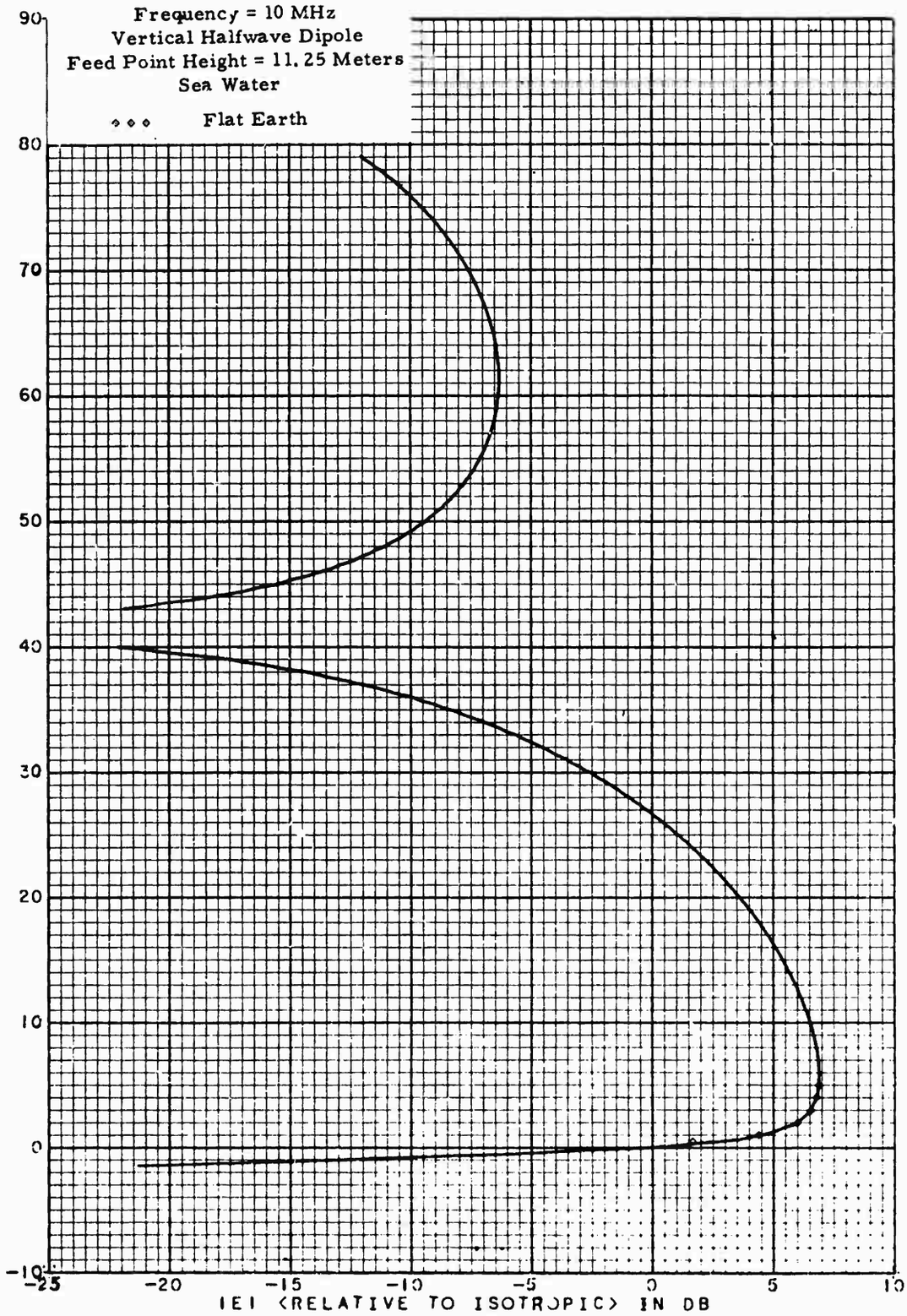

10.1. Vertical radiation pattern of a vertical half-wave dipole located $\frac{3}{8}\lambda$ above sea water. The frequency is 10 MHz.

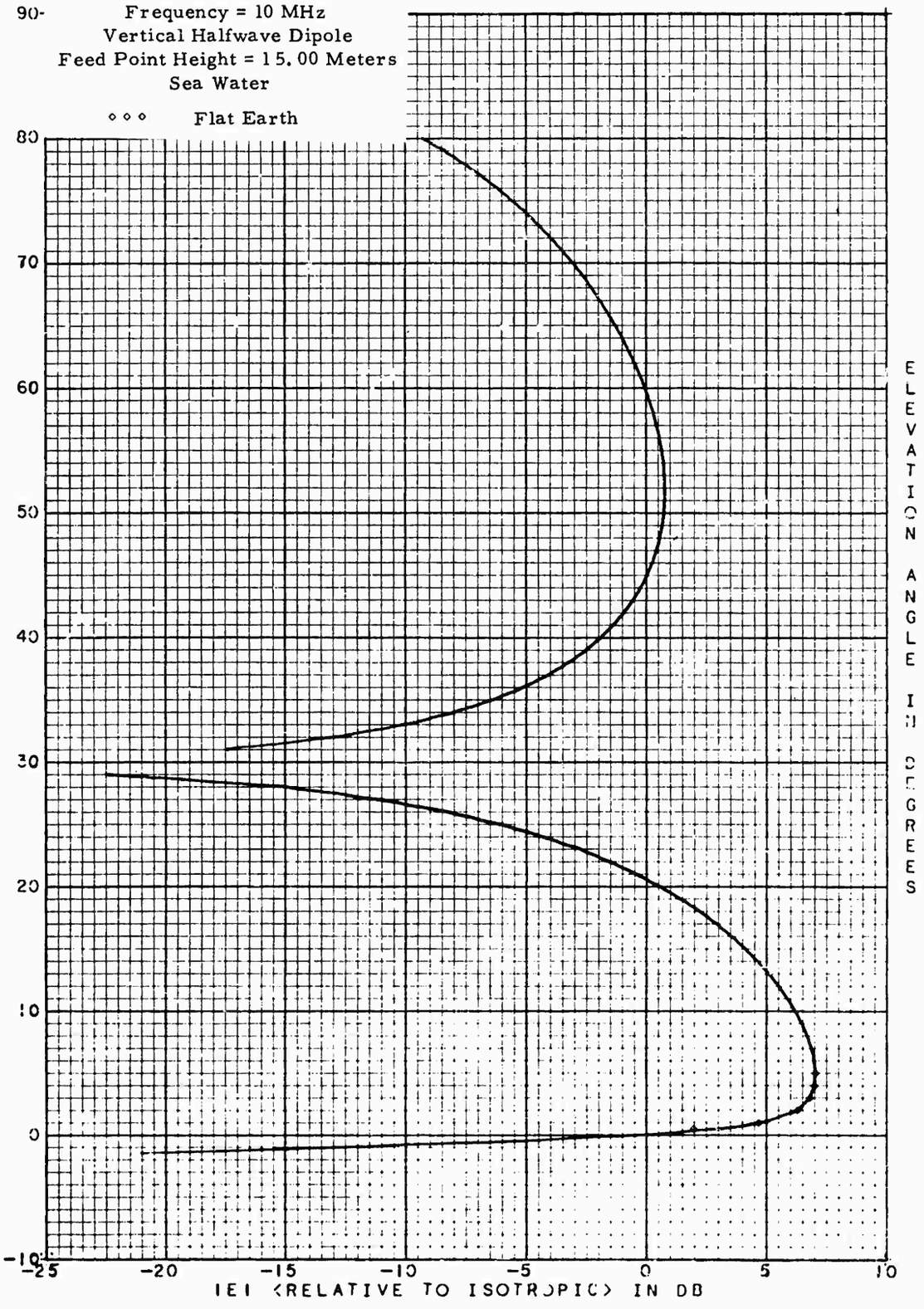

10.2. Vertical radiation pattern of a vertical half-wave dipole located $\lambda/2$ above sea water. The frequency is 10 MHz.

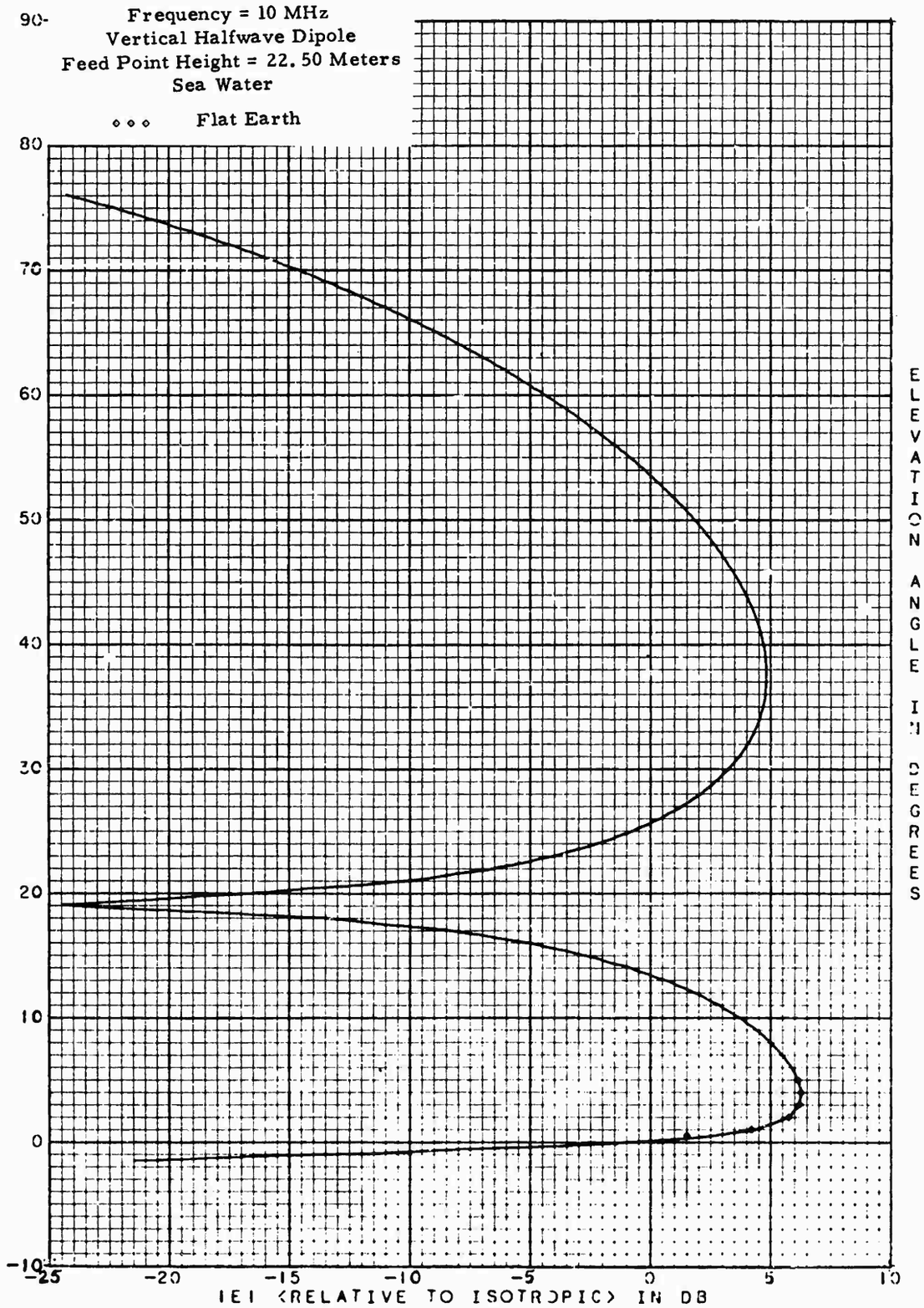

10.3. Vertical radiation pattern of a vertical half-wave dipole located $\frac{3}{4}\lambda$ above sea water. The frequency is 10 MHz.

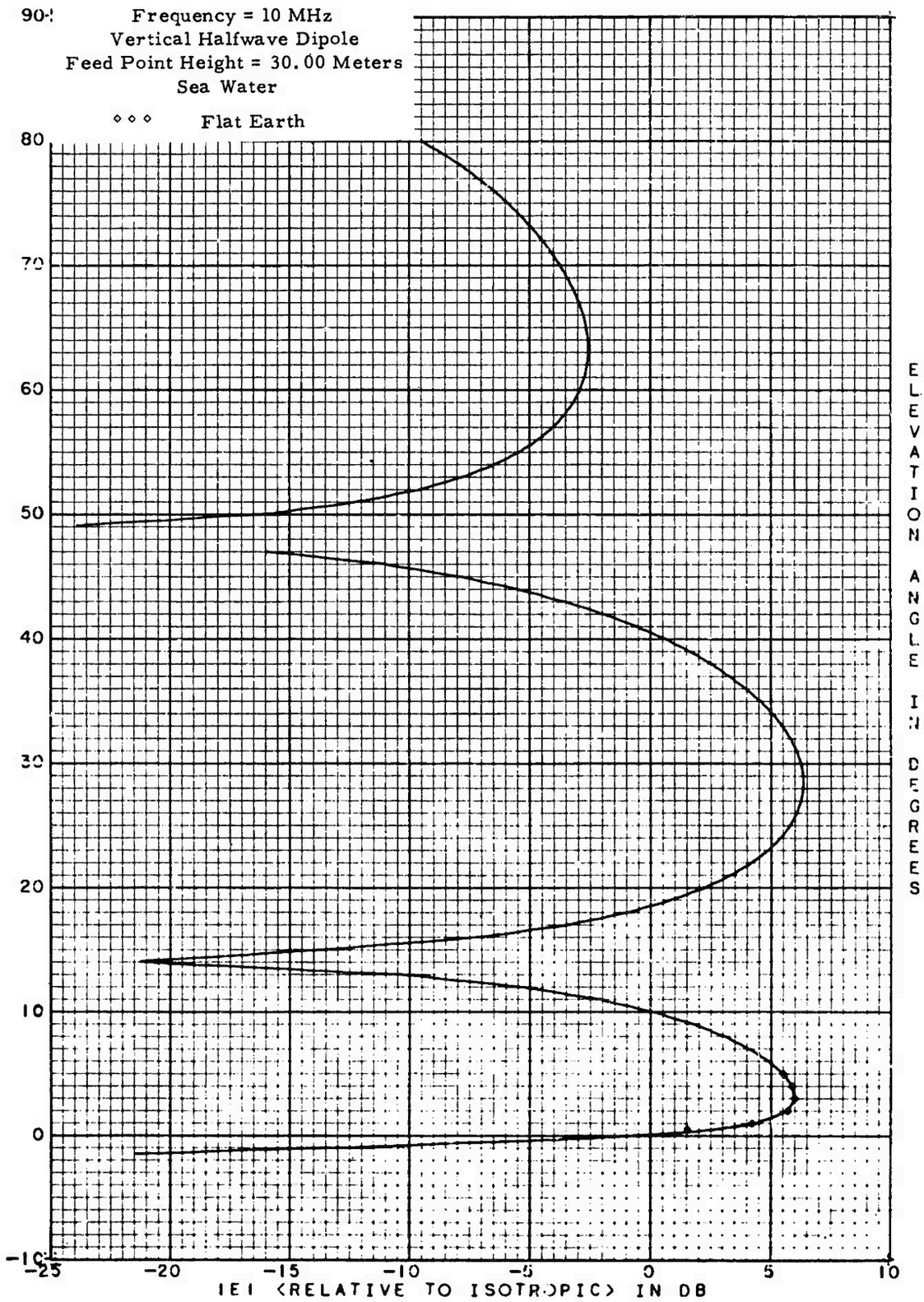

10.4. Vertical radiation pattern of a vertical half-wave dipole located λ above sea water. The frequency is 10 MHz.

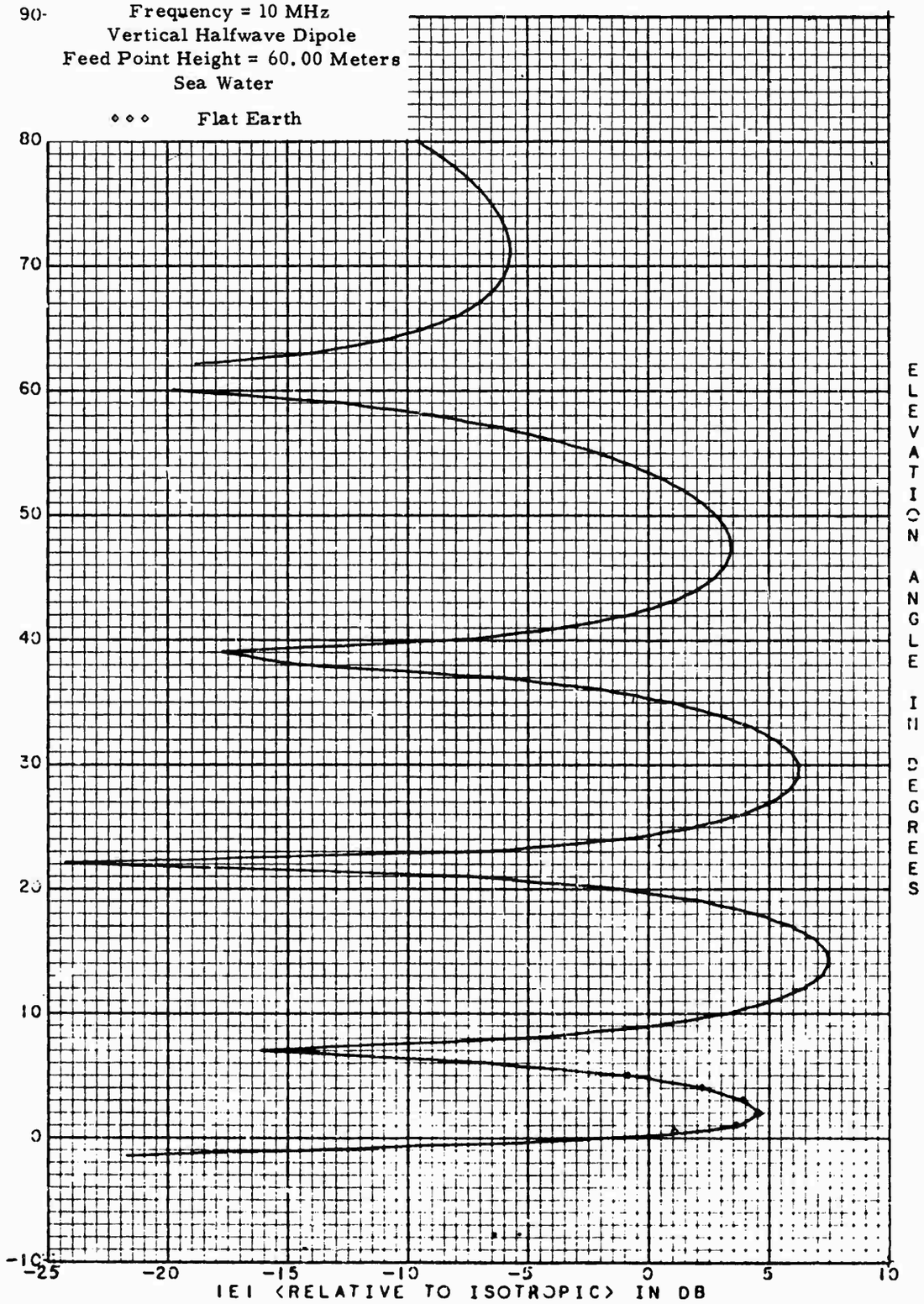

10.5. Vertical radiation pattern of a vertical half-wave dipole located 2λ above sea water. The frequency is 10 MHz.

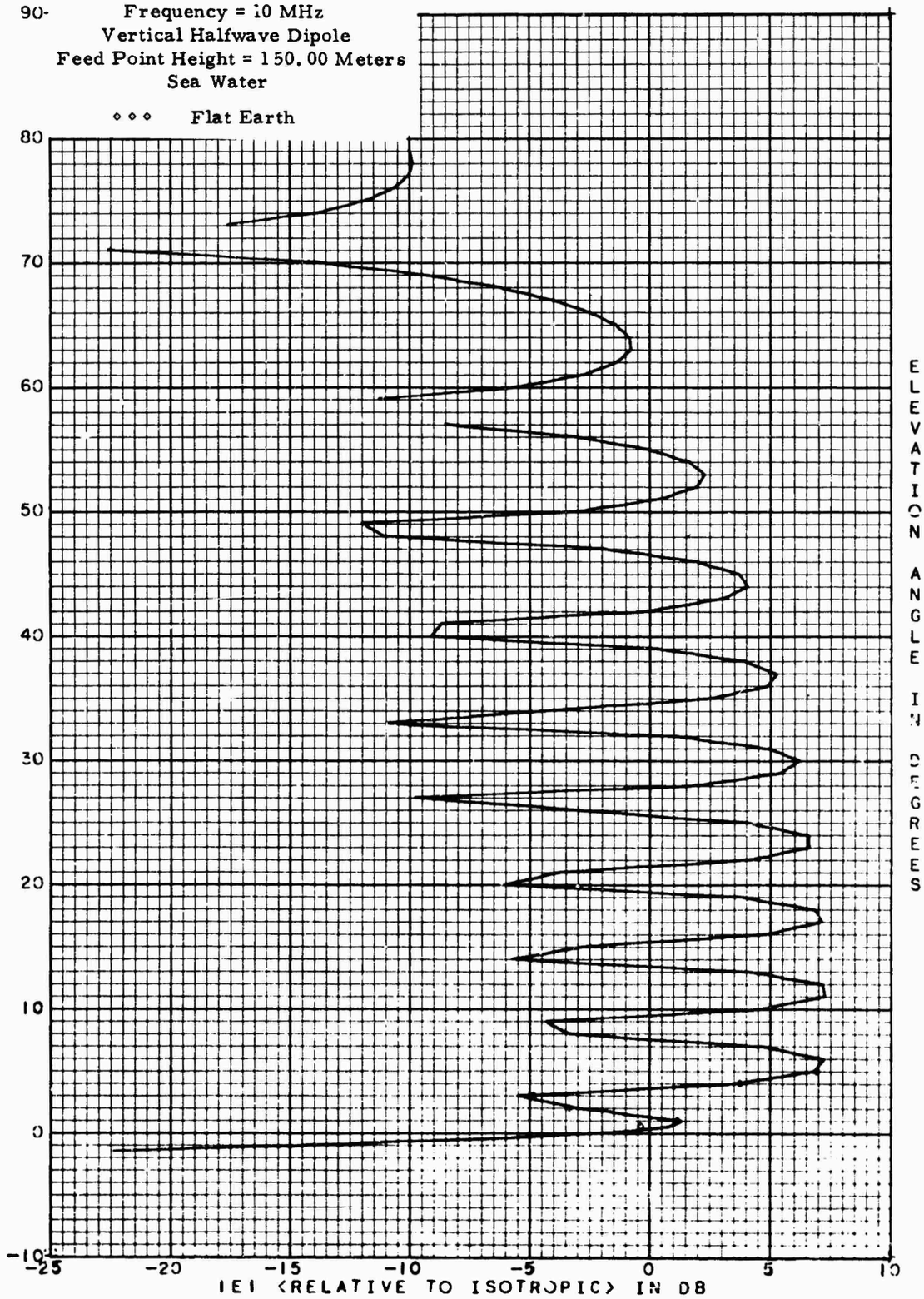

10.6. Vertical radiation pattern of a vertical half-wave dipole located 5λ above sea water. The frequency is 10 MHz.

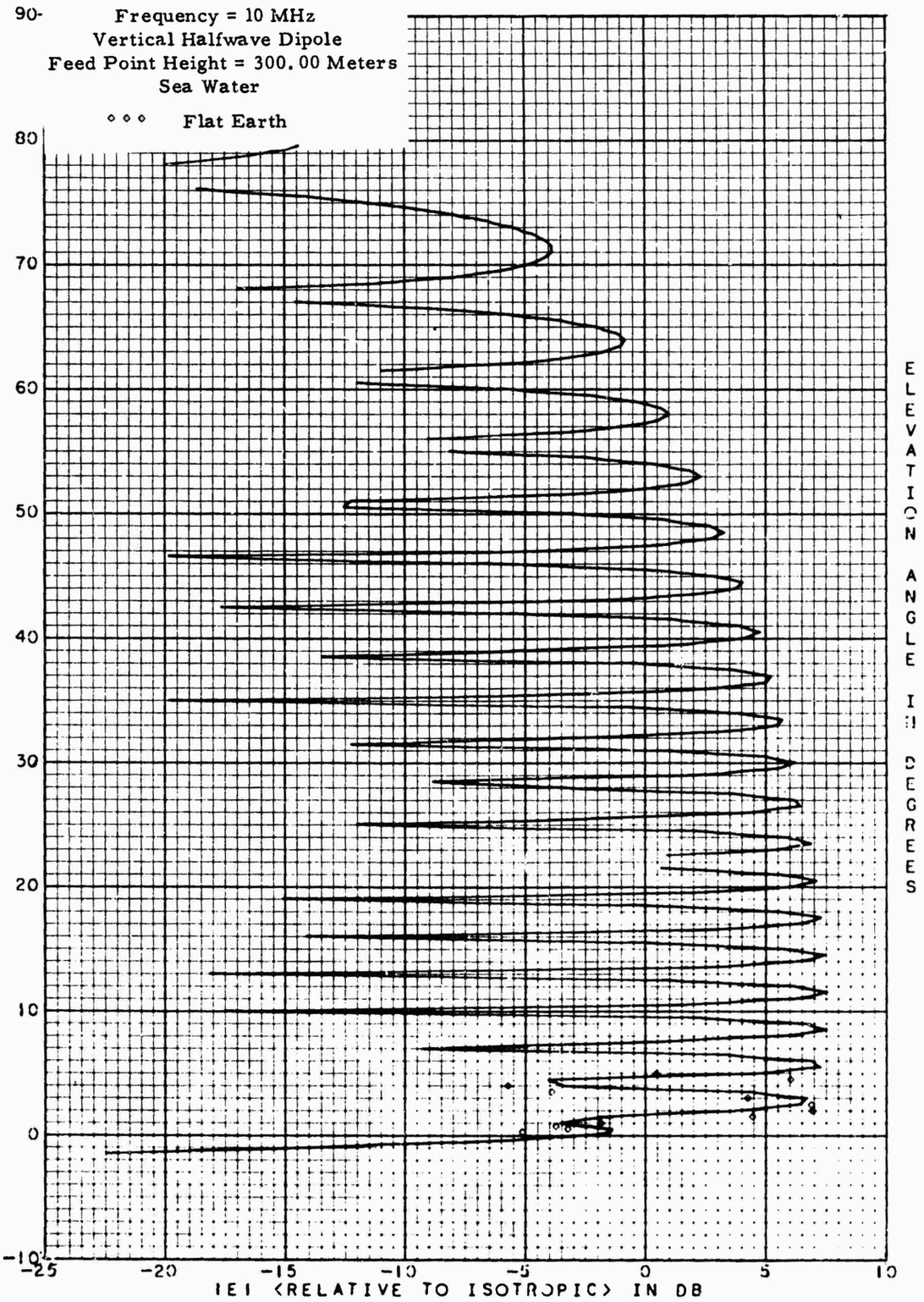

10.7. Vertical radiation pattern of a vertical half-wave dipole located 10λ above sea water. The frequency is 10 MHz.

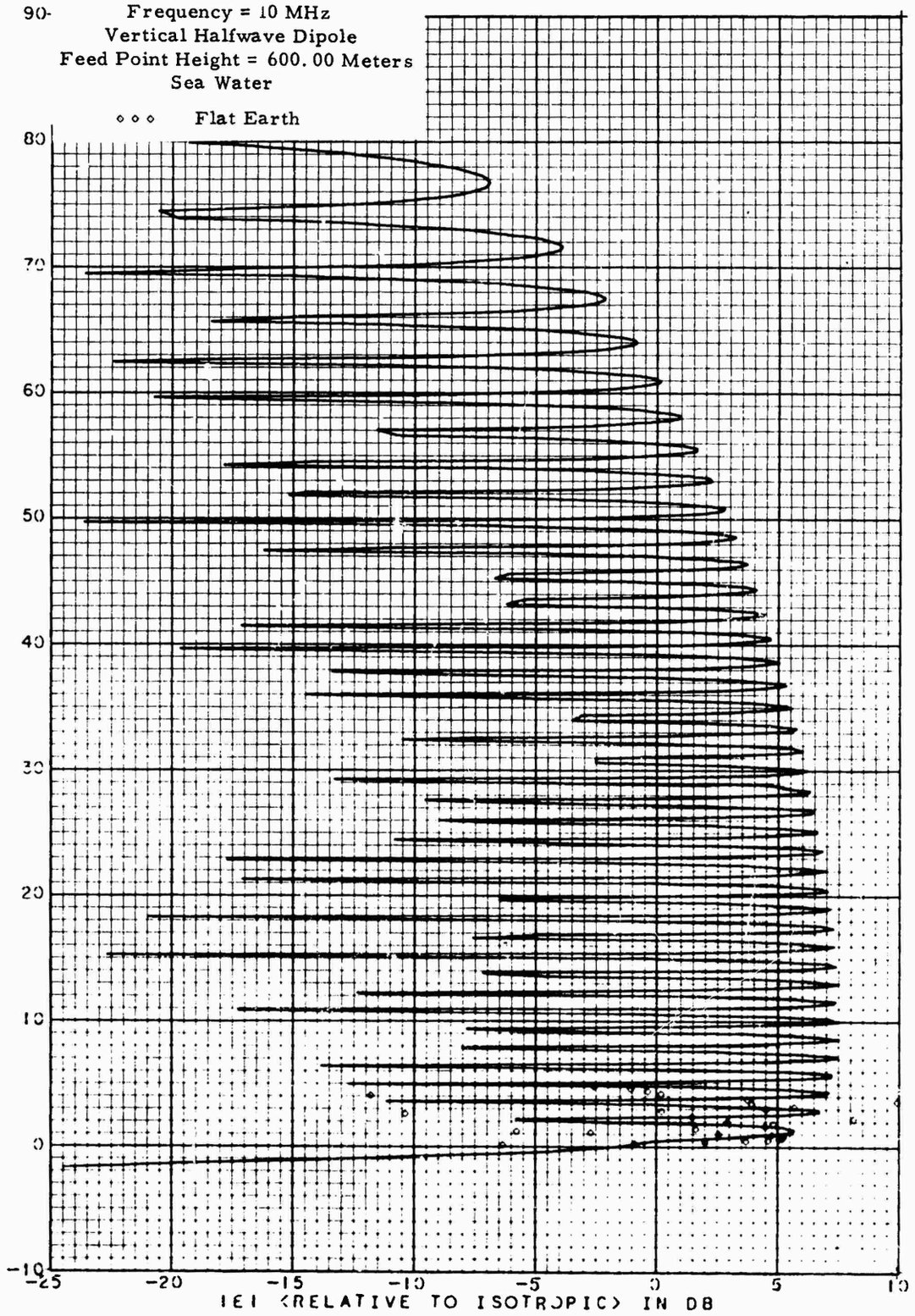

10.8. Vertical radiation pattern of a vertical half-wave dipole located 20λ above sea water. The frequency is 10 MHz.

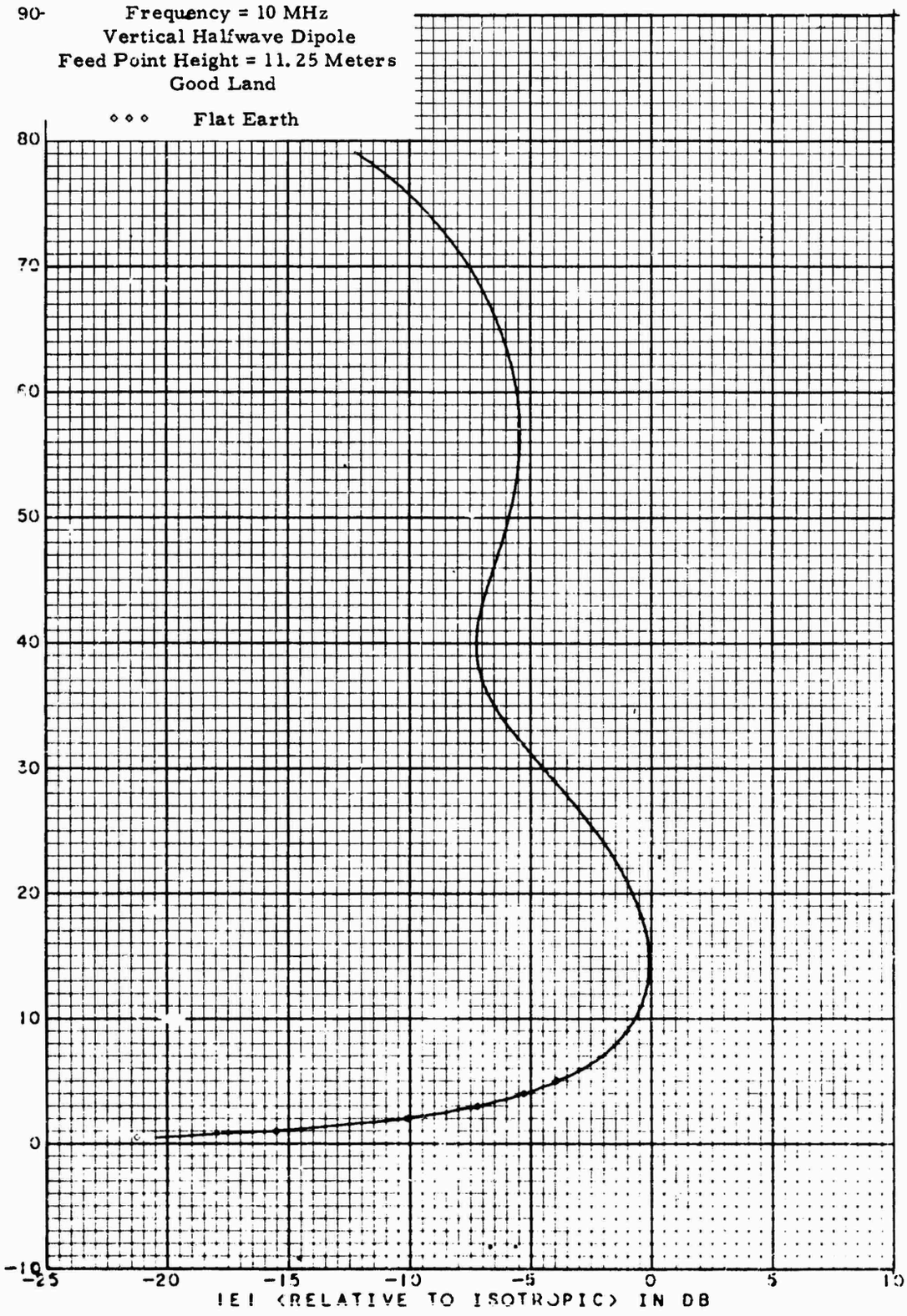

11.1. Vertical radiation pattern of a vertical half-wave dipole located $\frac{3}{8}\lambda$ above good ground. The frequency is 10 MHz.

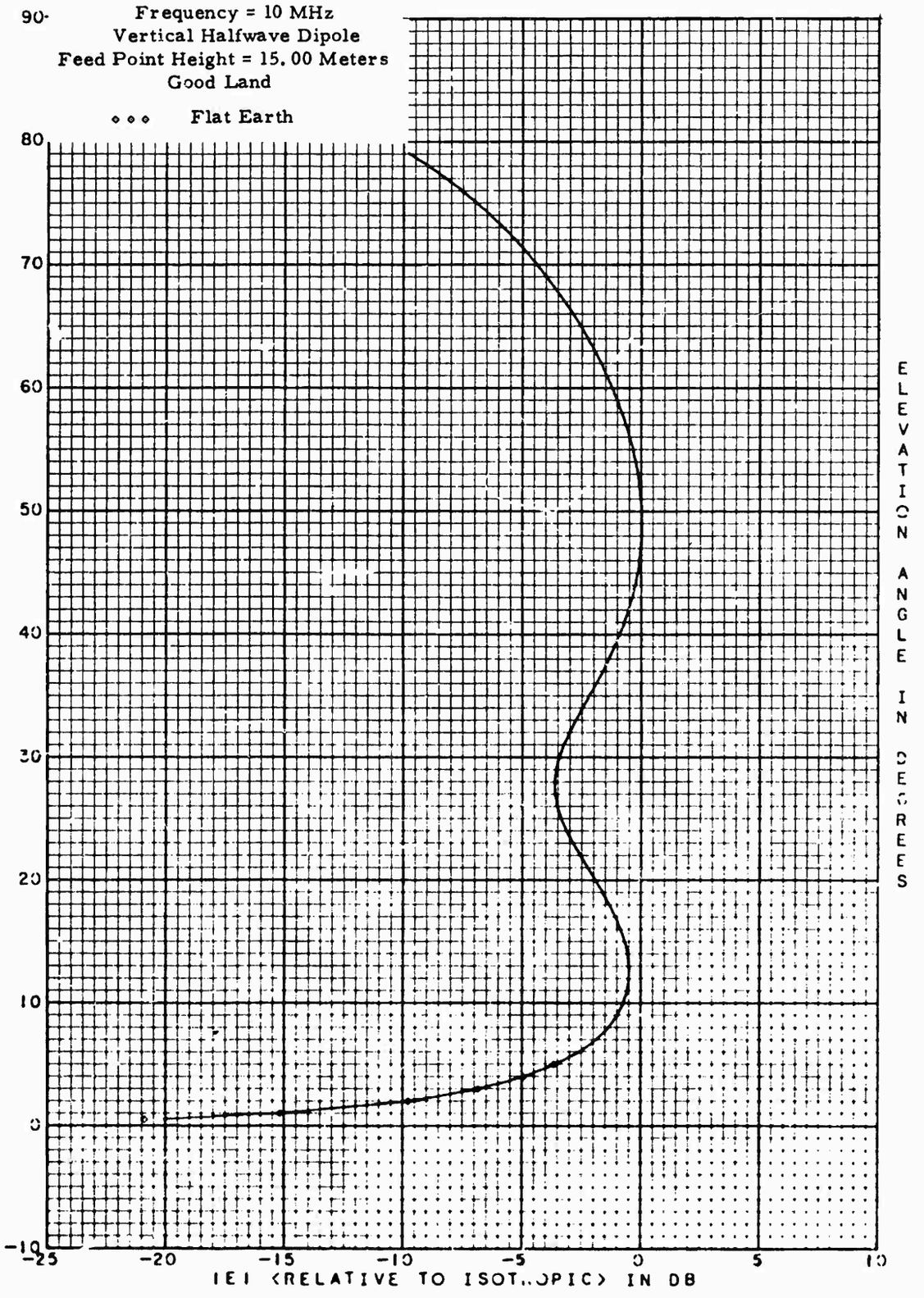

11.2. Vertical radiation pattern of a vertical half-wave dipole located $\lambda/2$ above good ground. The frequency is 10 MHz.

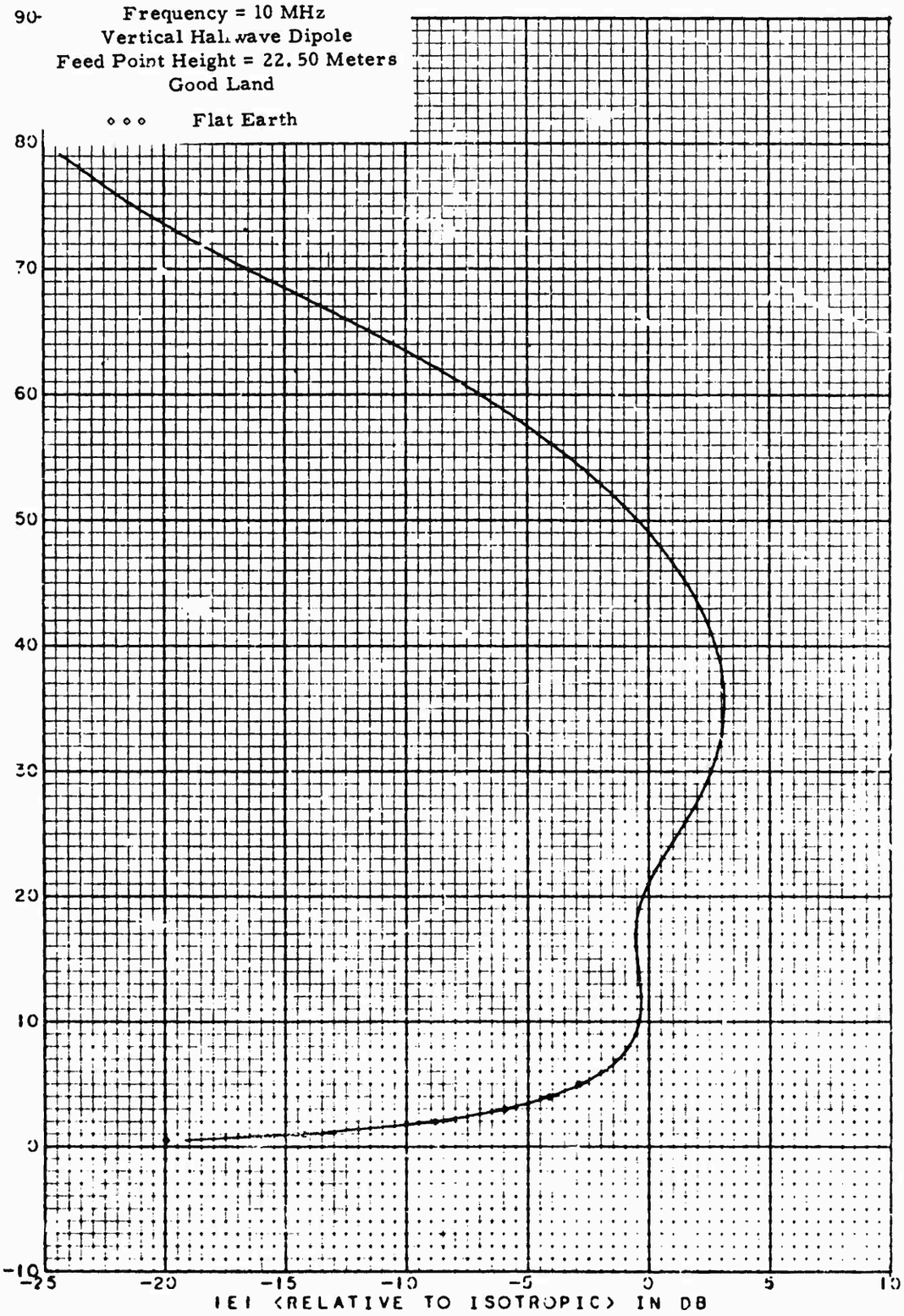

11.3. Vertical radiation pattern of a vertical half-wave dipole located $\frac{3}{4}\lambda$ above good ground. The frequency is 10 MHz.

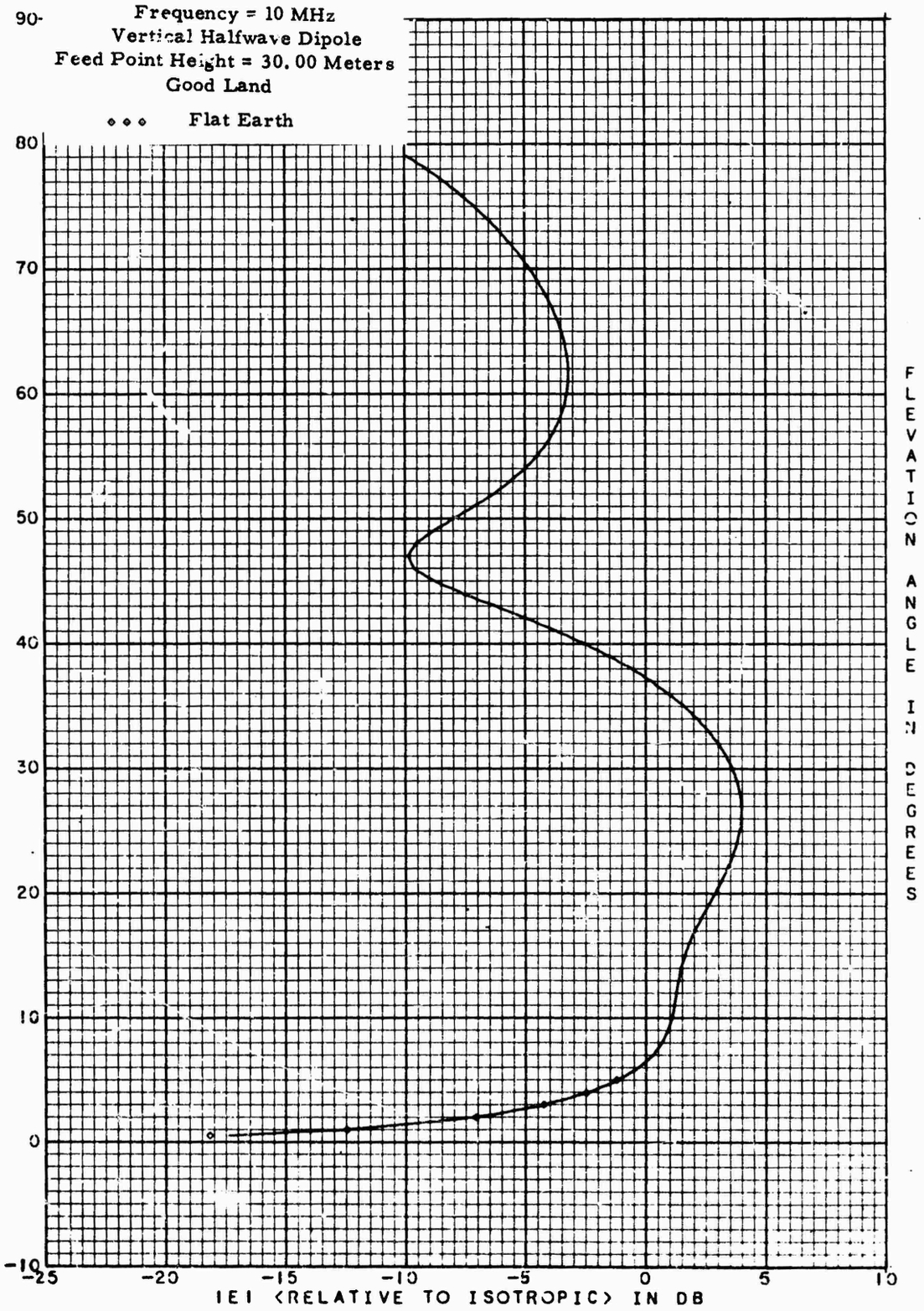

11.4. Vertical radiation pattern of a vertical half-wave dipole located λ above good ground. The frequency is 10 MHz.

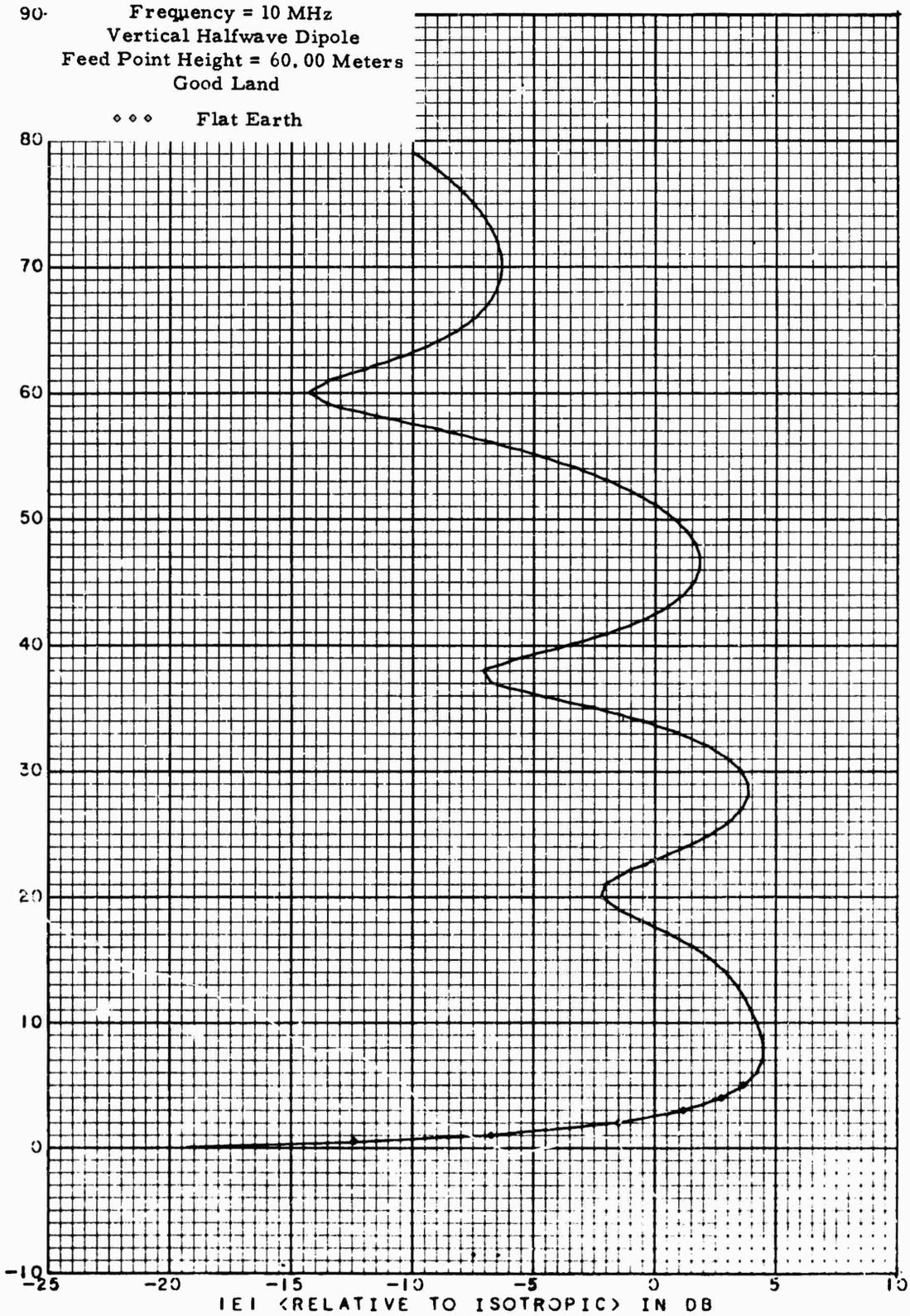

11.5. Vertical radiation pattern of a vertical half-wave dipole located 2λ above good ground. The frequency is 10 MHz.

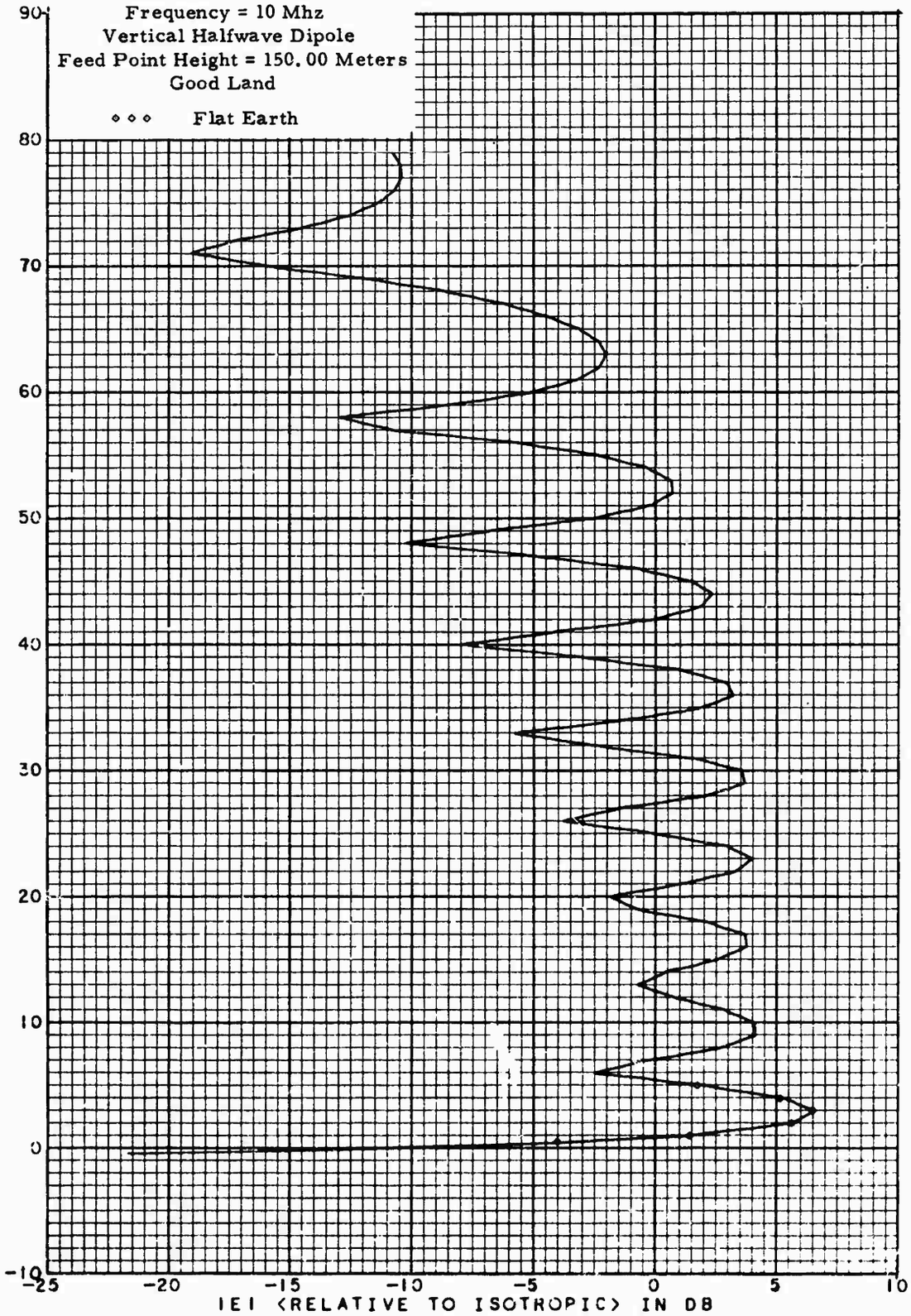

11.6. Vertical radiation pattern of a vertical half-wave dipole located 5λ above good ground. The frequency is 10 MHz.

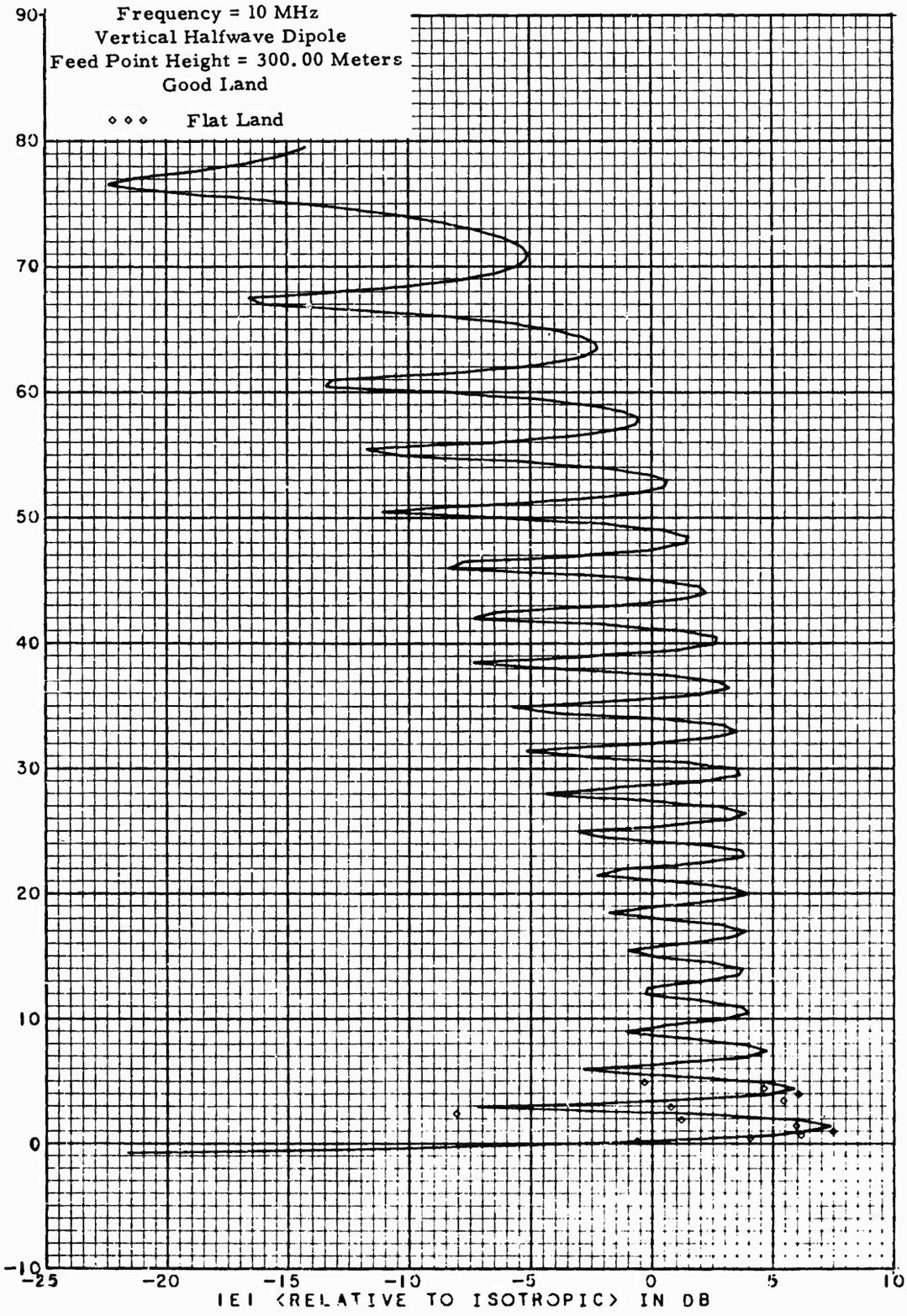

11.7. Vertical radiation pattern of a vertical half-wave dipole located 10λ above good ground. The frequency is 10 MHz.

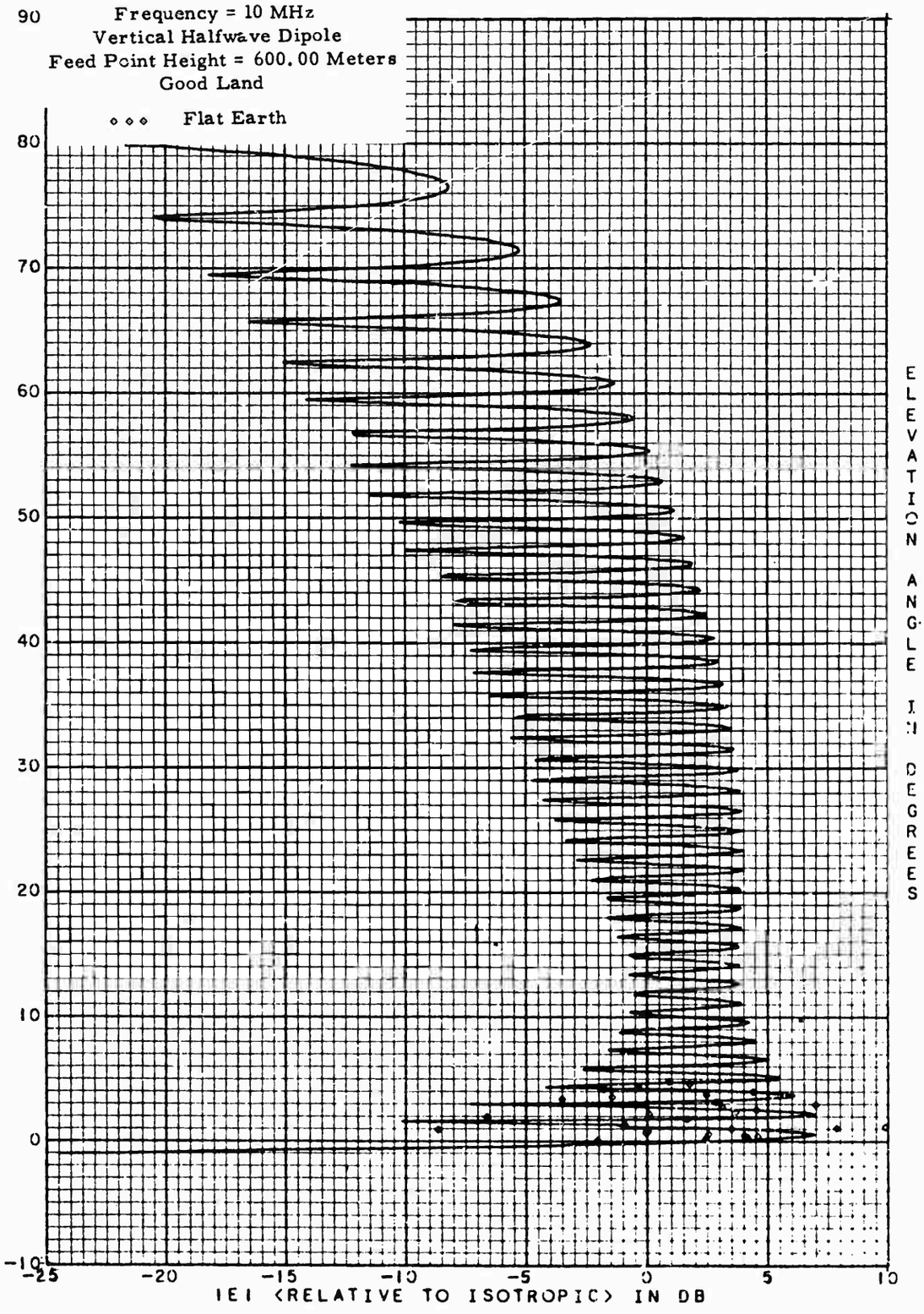

11.8. Vertical radiation pattern of a vertical half-wave dipole located 20λ above good ground. The frequency is 10 MHz.

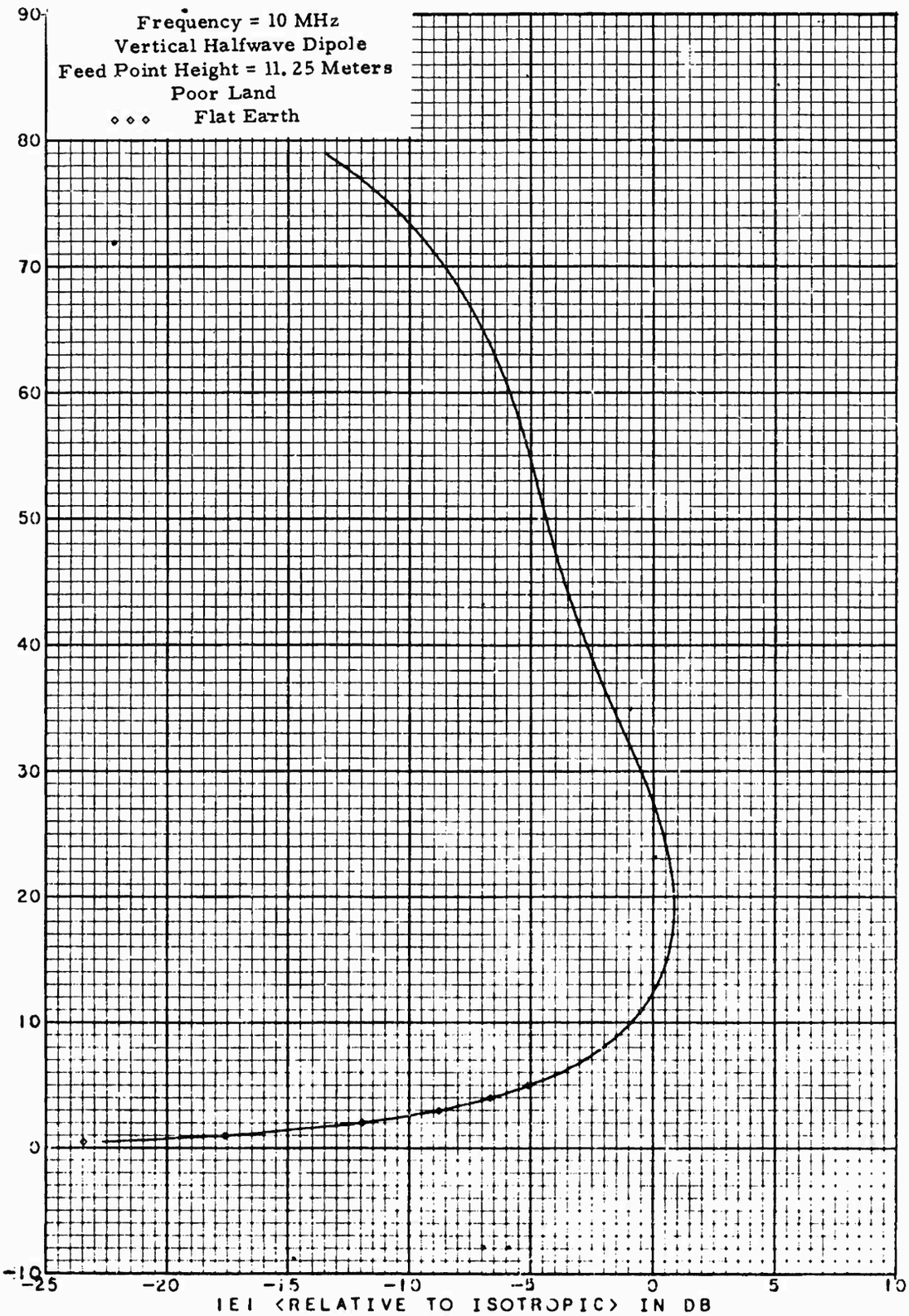

12.1. Vertical radiation pattern of a vertical half-wave dipole located $\frac{3}{8}\lambda$ above poor ground. The frequency is 10 MHz.

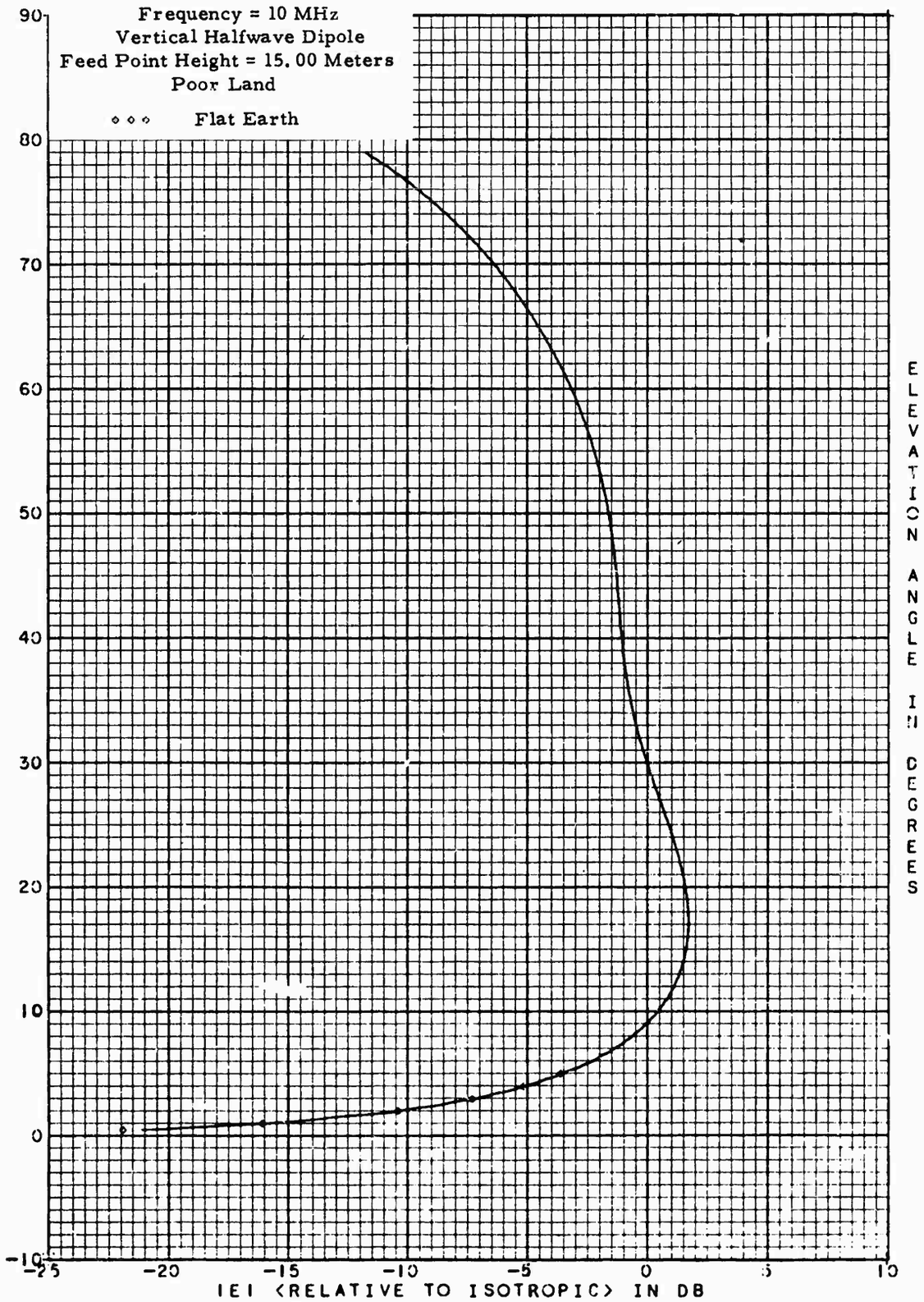

12.2. Vertical radiation pattern of a vertical half-wave dipole located $\lambda/2$ above poor ground. The frequency is 10 MHz.

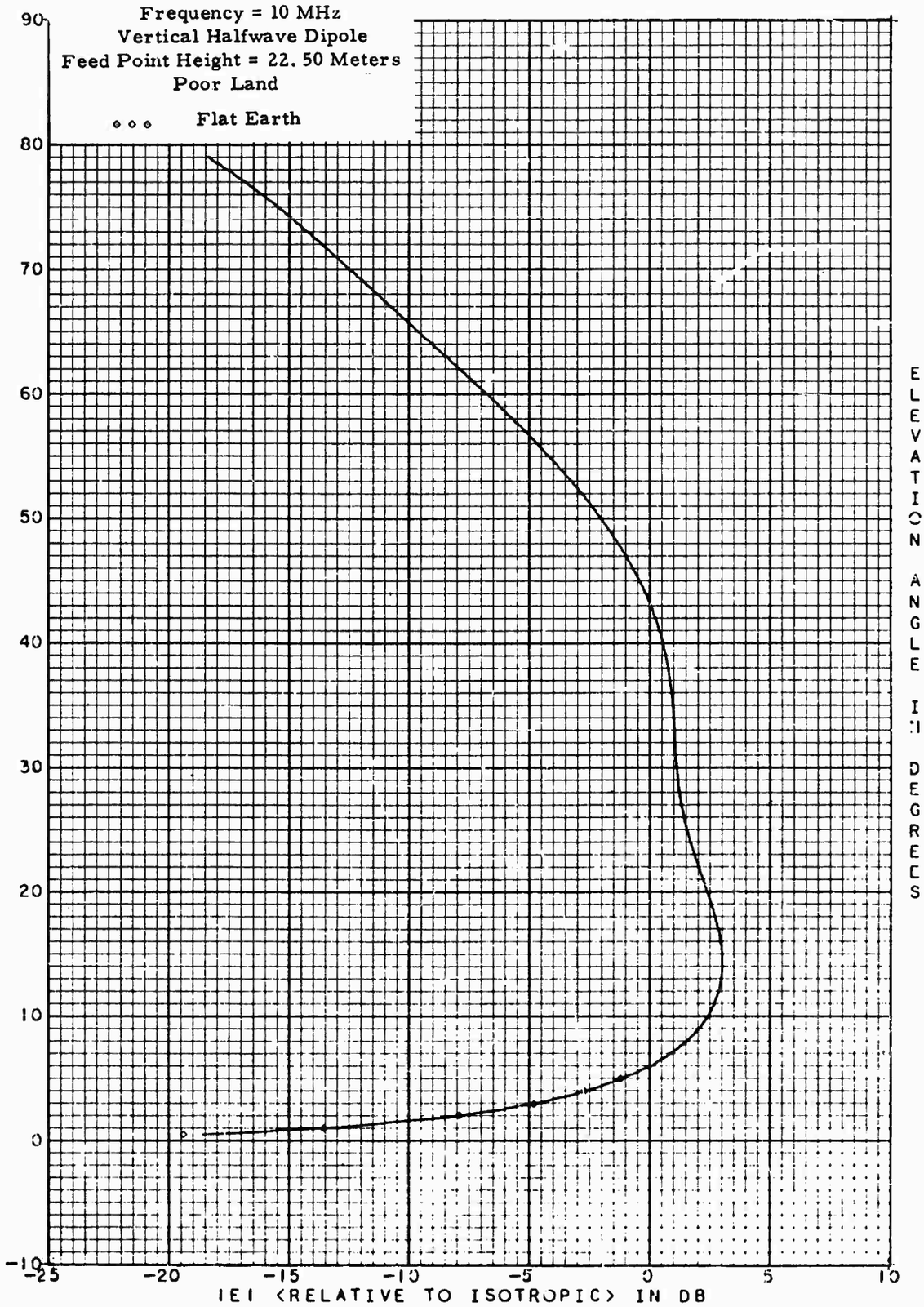

12.3. Vertical radiation pattern of a vertical half-wave dipole located $\frac{3}{4}\lambda$ above poor ground. The frequency is 10 MHz.

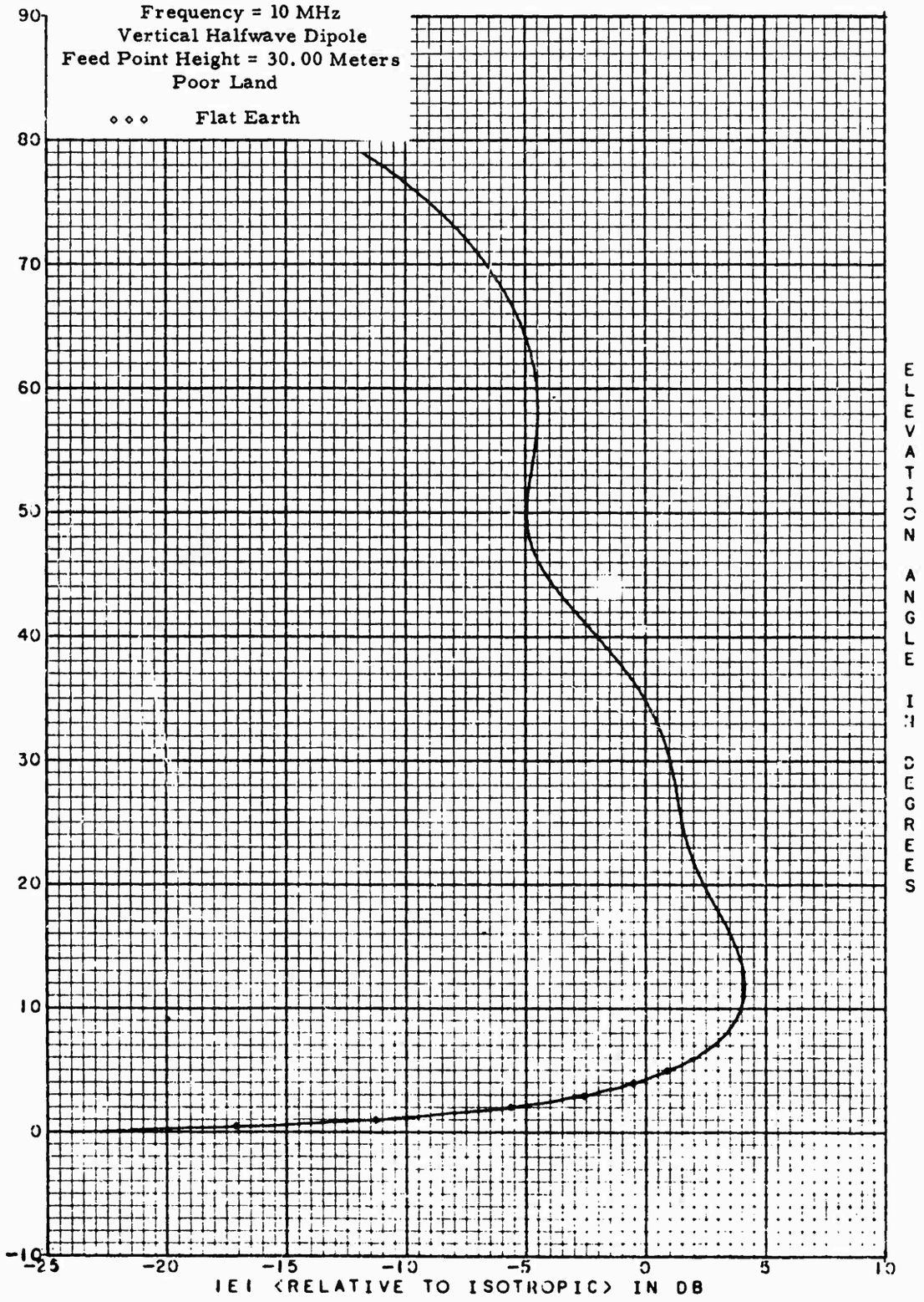

12.4. Vertical radiation pattern of a vertical half-wave dipole located λ above poor ground. The frequency is 10 MHz.

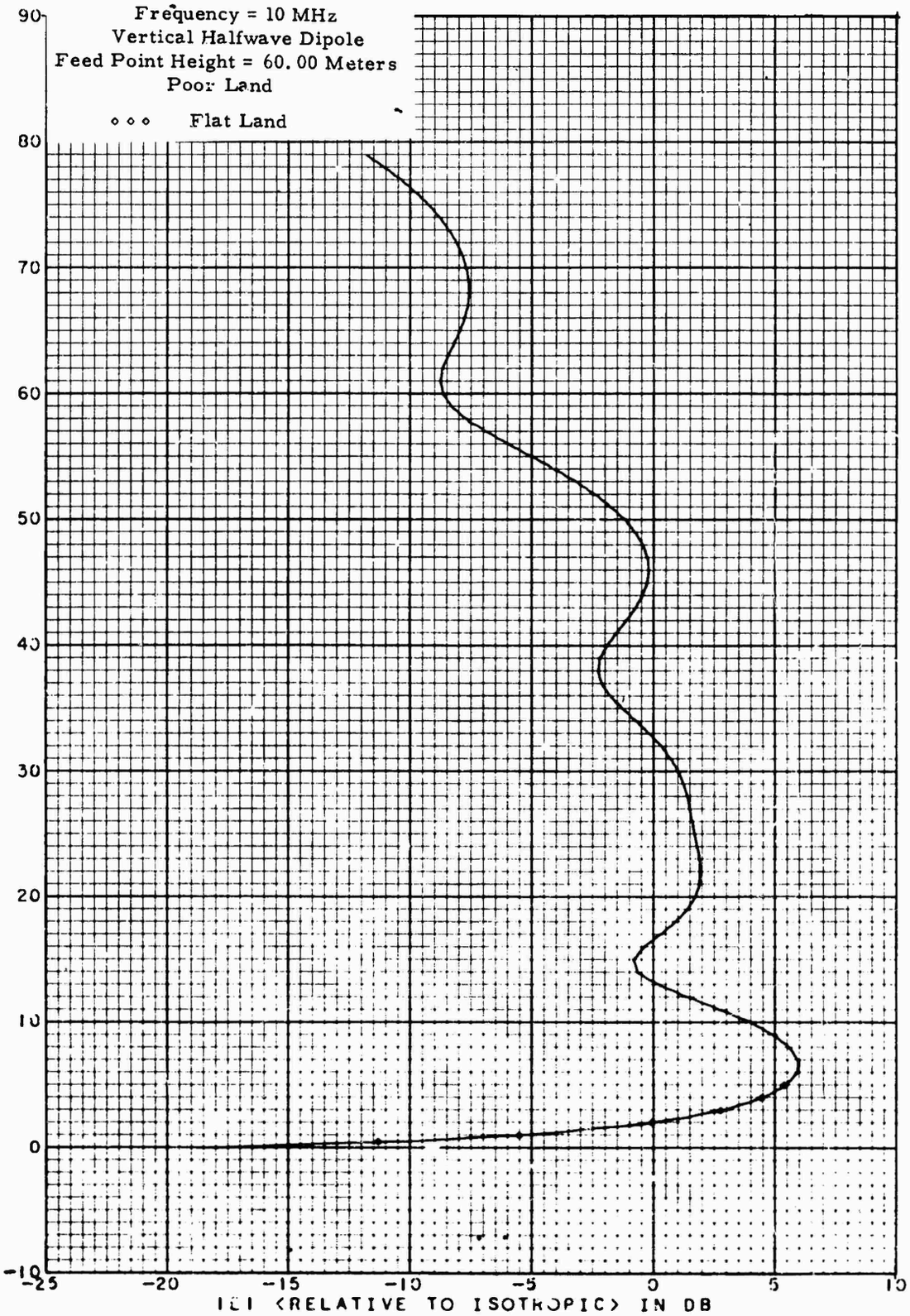

12.5. Vertical radiation pattern of a vertical half-wave dipole located 2λ above poor ground. The frequency is 10 MHz.

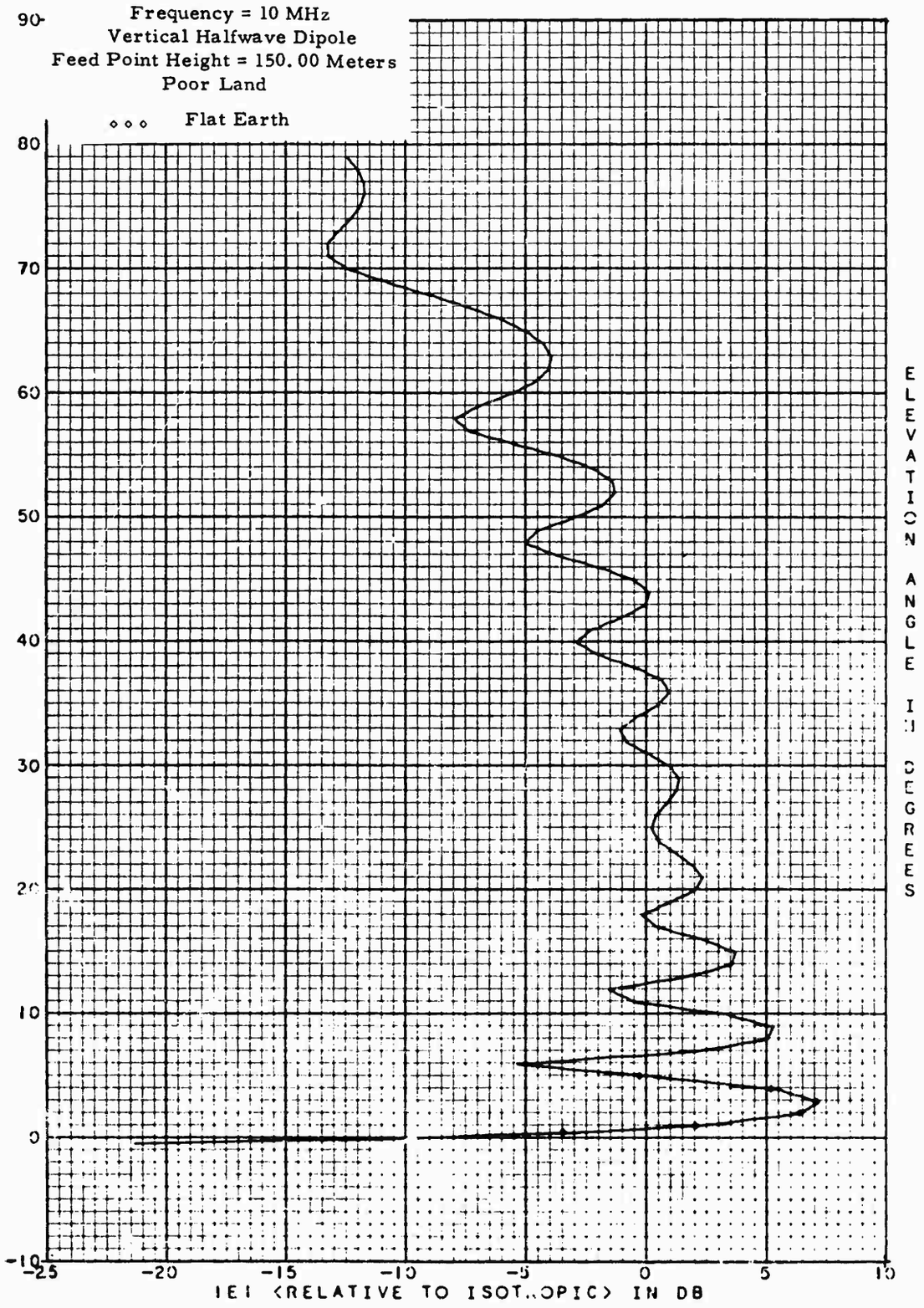

12.6. Vertical radiation pattern of a vertical half-wave dipole located 5λ above poor ground. The frequency is 10 MHz.

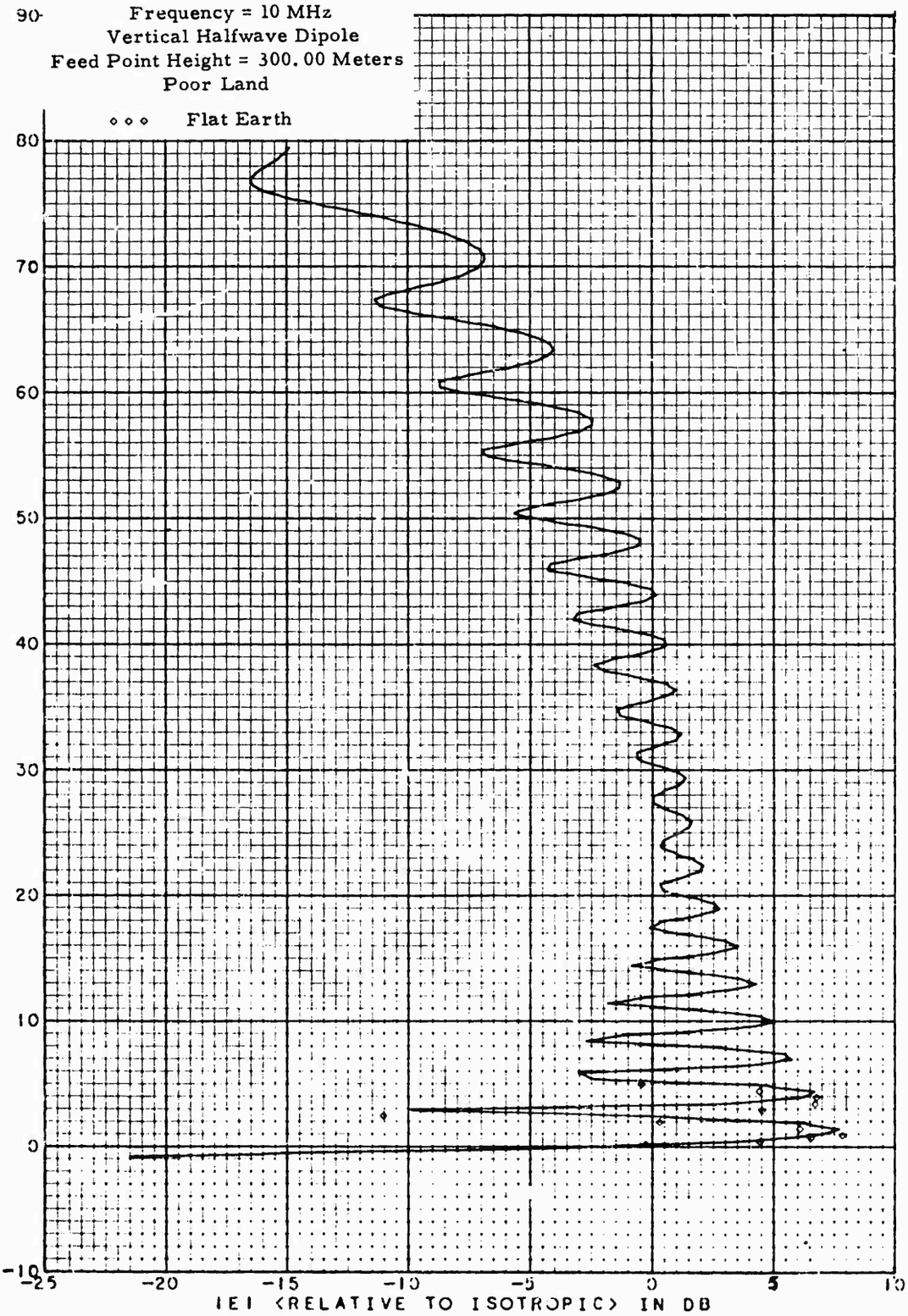

12.7. Vertical radiation pattern of a vertical half-wave dipole located 10λ above poor ground. The frequency is 10 MHz.

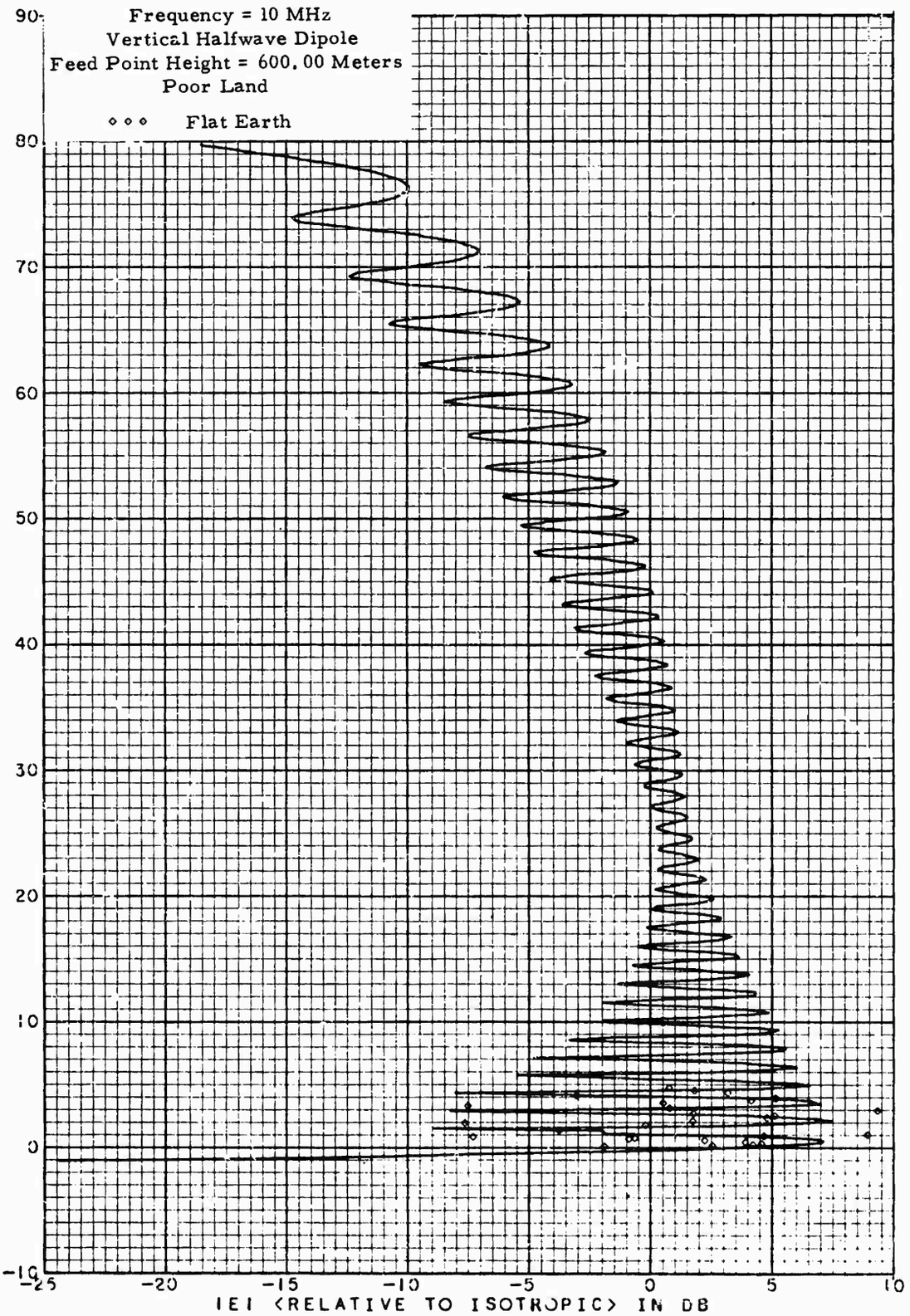

12.8. Vertical radiation pattern of a vertical half-wave dipole located 20λ above poor ground. The frequency is 10 MHz.

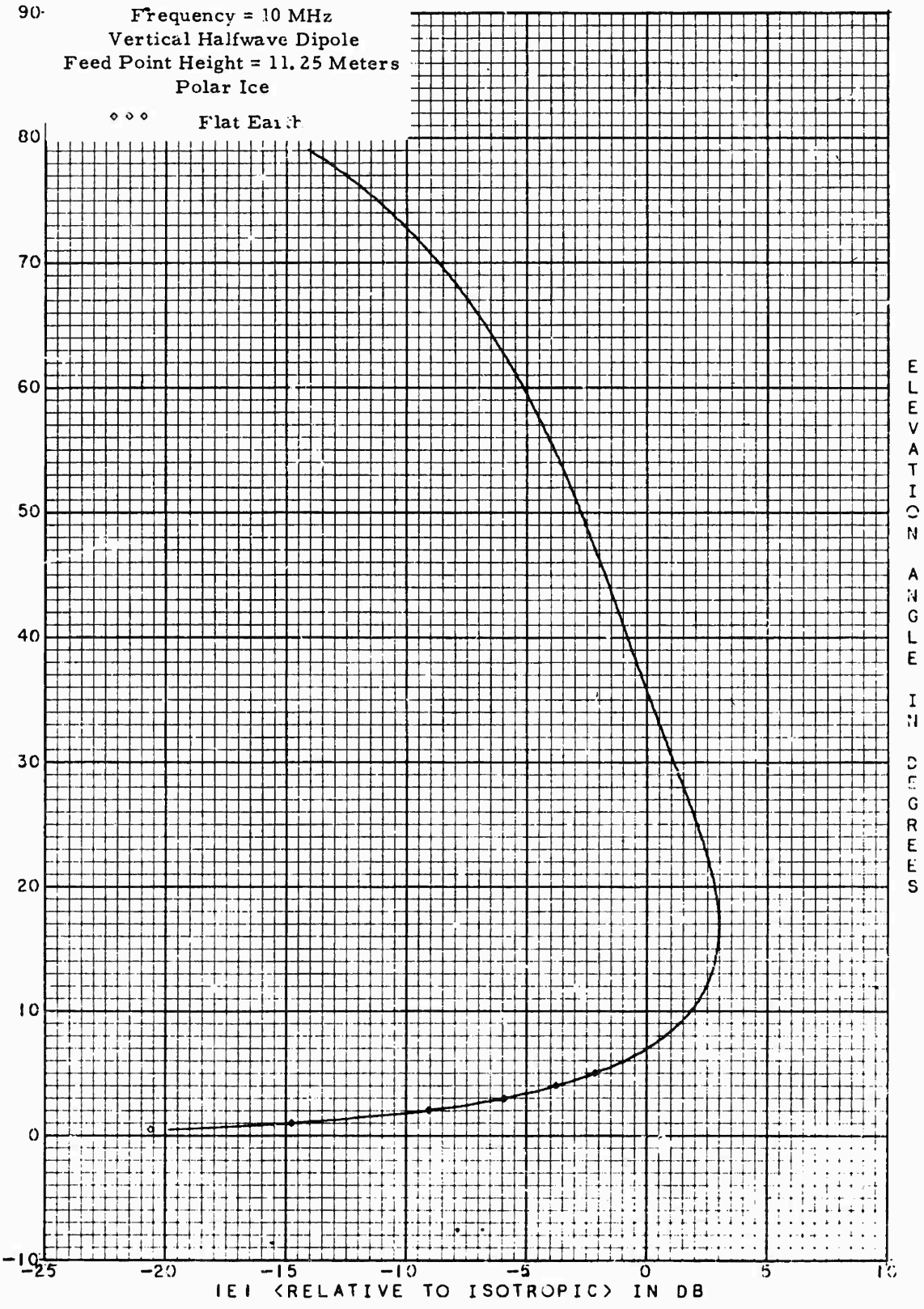

13.1. Vertical radiation pattern of a vertical half-wave dipole located $\frac{3}{8}\lambda$ above polar ice. The frequency is 10 MHz.

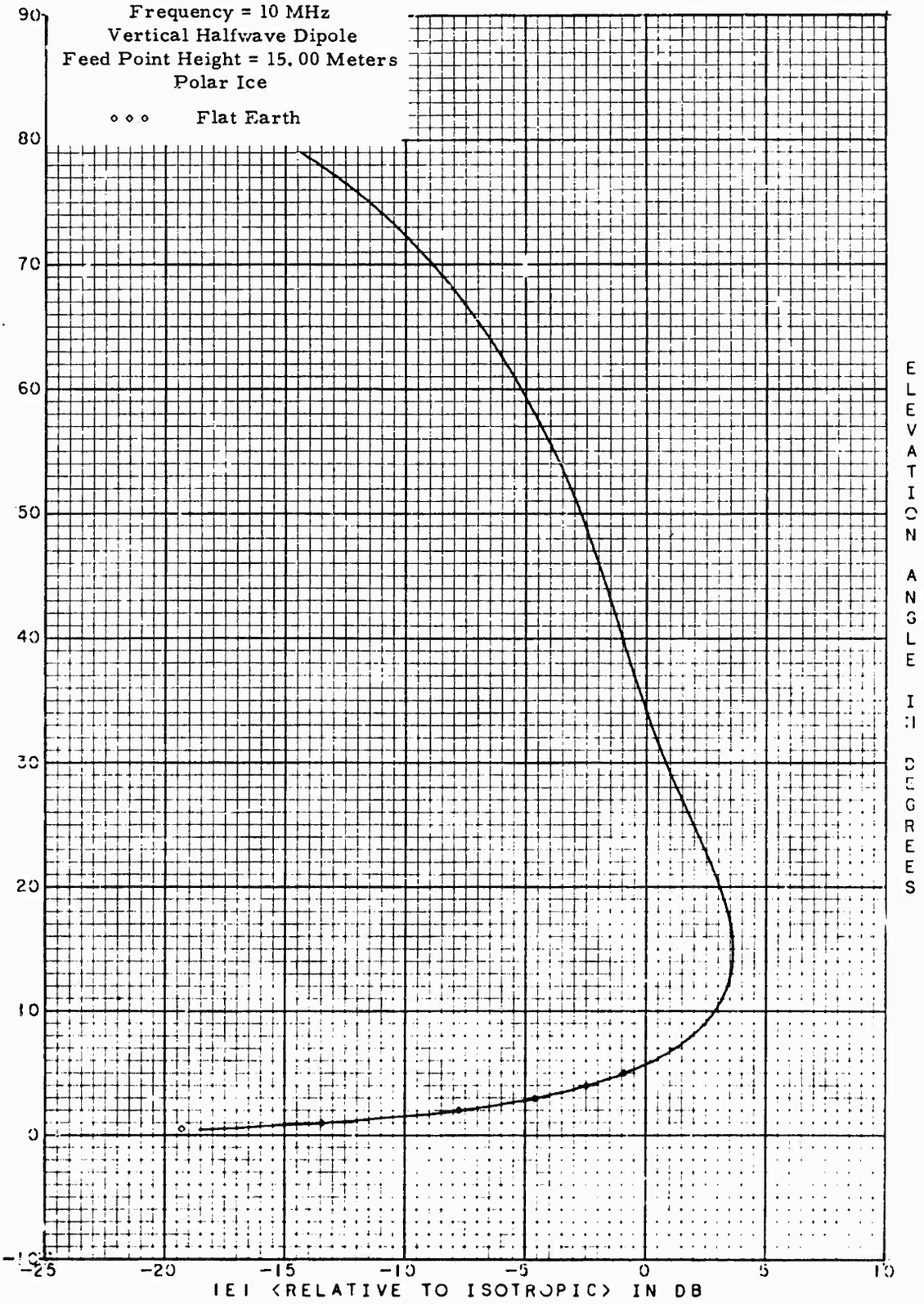

13.2. Vertical radiation pattern of a vertical half-wave dipole located $\lambda/2$ above polar ice. The frequency is 10 MHz.

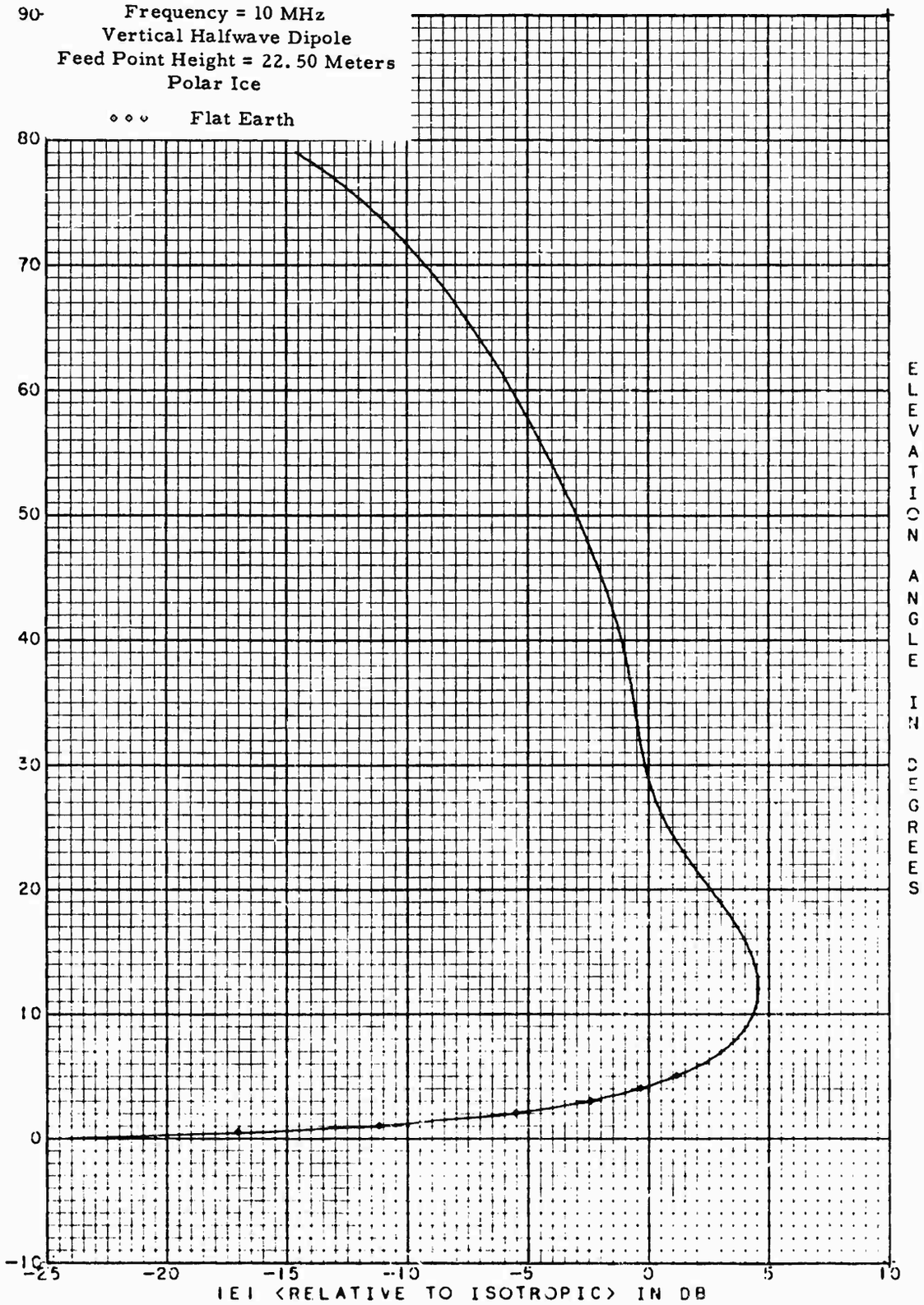

13.3. Vertical radiation pattern of a vertical half-wave dipole located $\frac{3}{4}\lambda$ above polar ice. The frequency is 10 MHz.

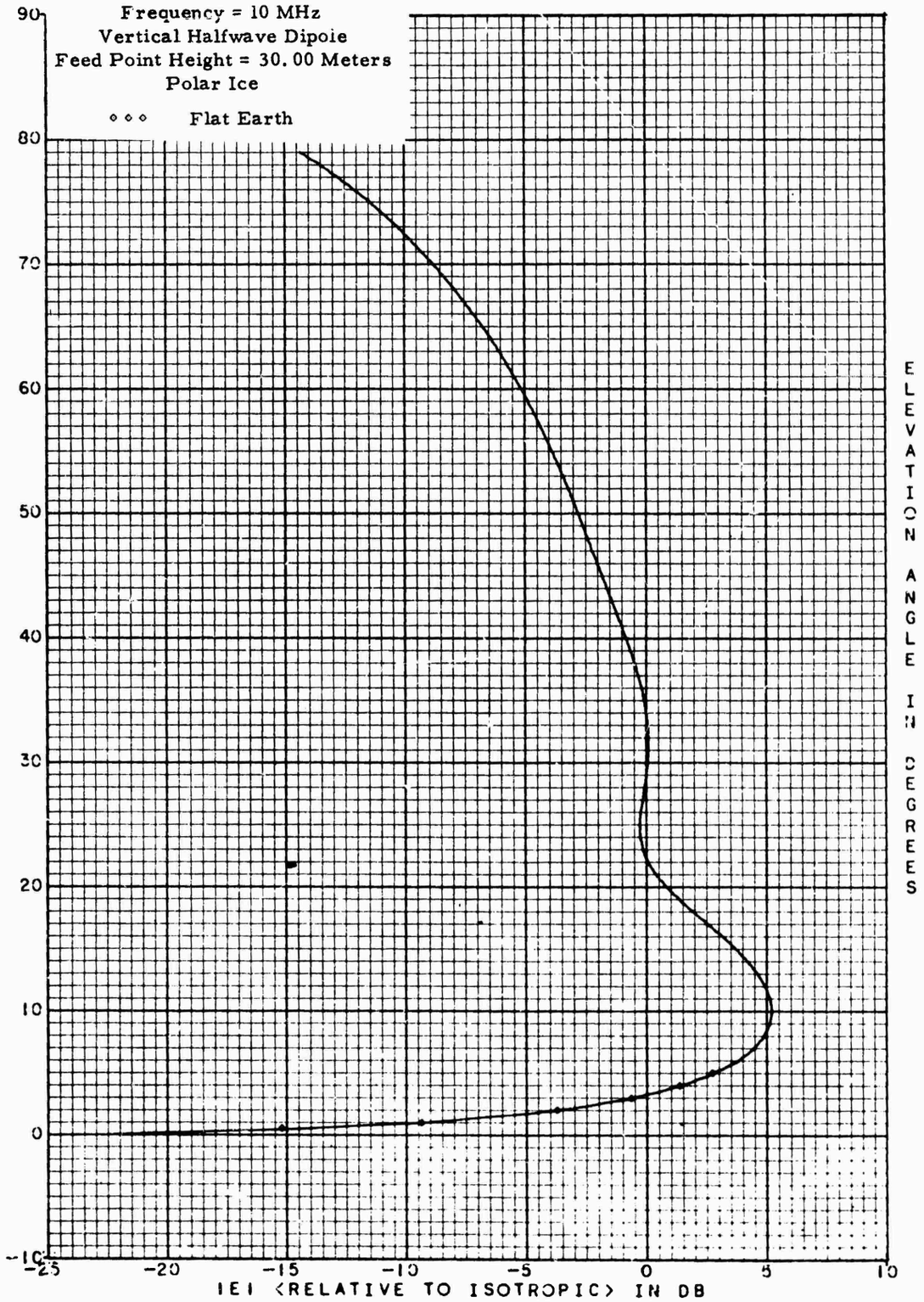

13.4. Vertical radiation pattern of a vertical half-wave dipole located λ above polar ice. The frequency is 10 MHz.

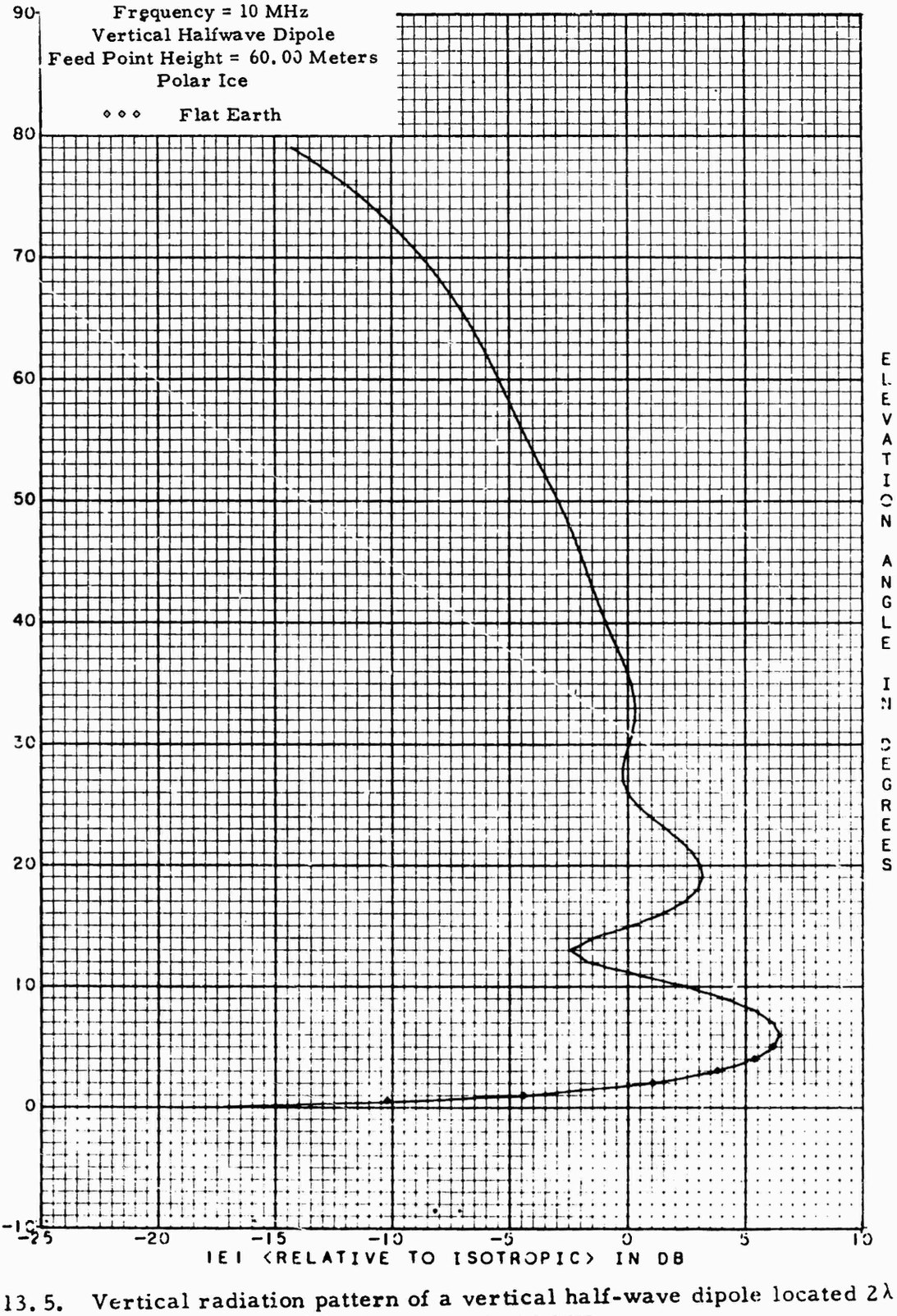

13.5. Vertical radiation pattern of a vertical half-wave dipole located 2λ above polar ice. The frequency is 10 MHz.

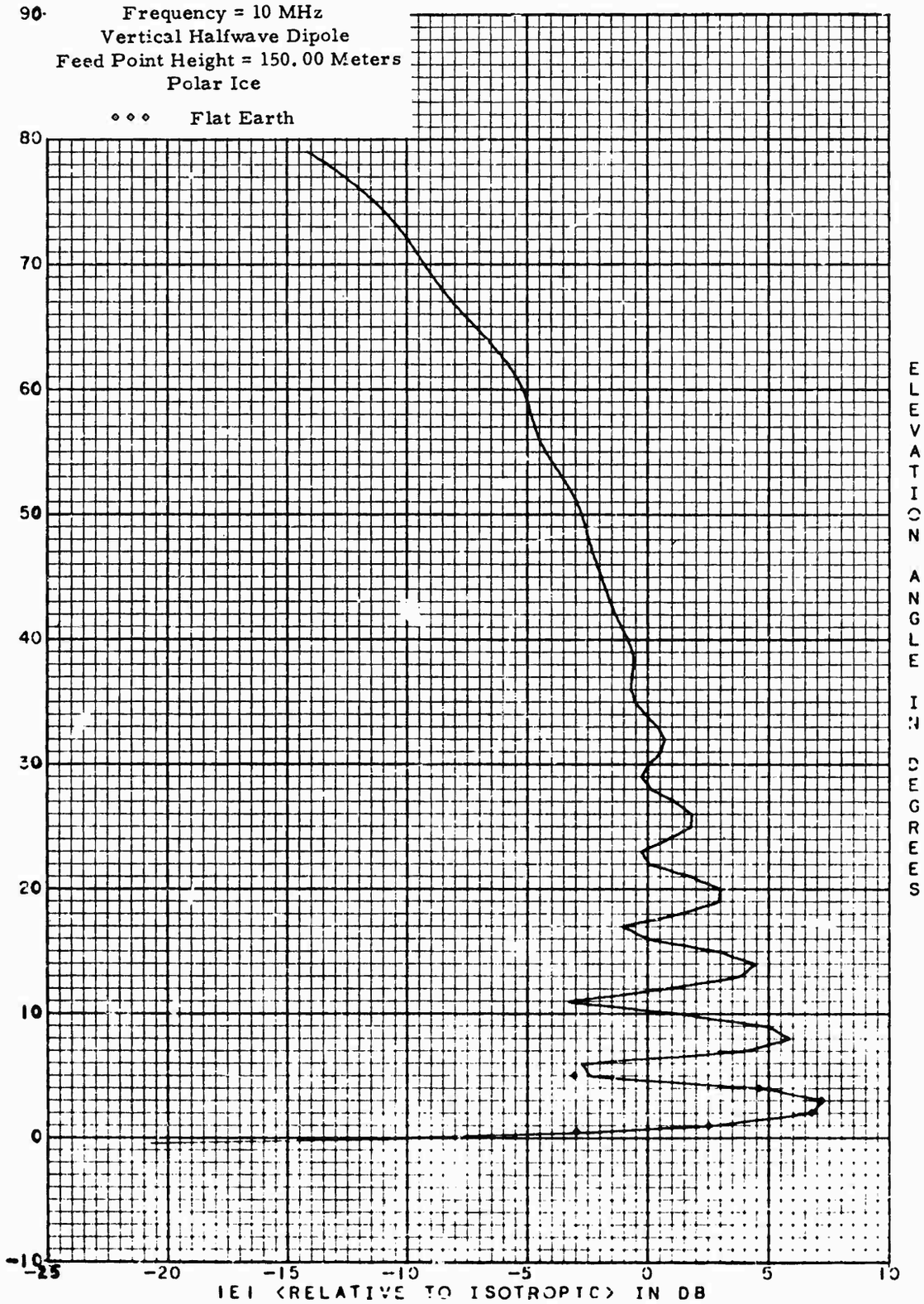

13.6. Vertical radiation pattern of a vertical half-wave dipole located 5λ above polar ice. The frequency is 10 MHz.

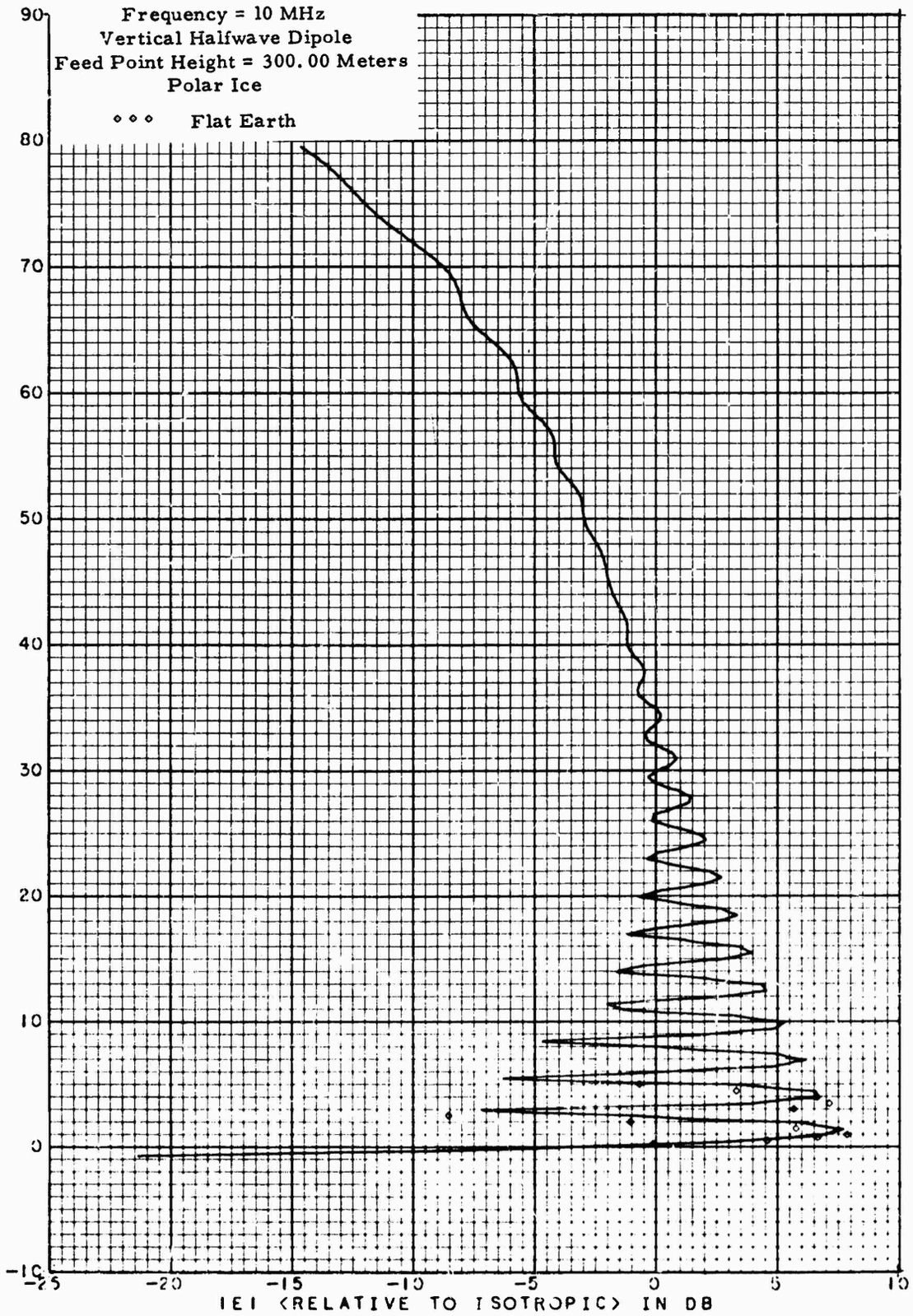

13.7. Vertical radiation pattern of a vertical half-wave dipole located 10λ above polar ice. The frequency is 10 MHz.

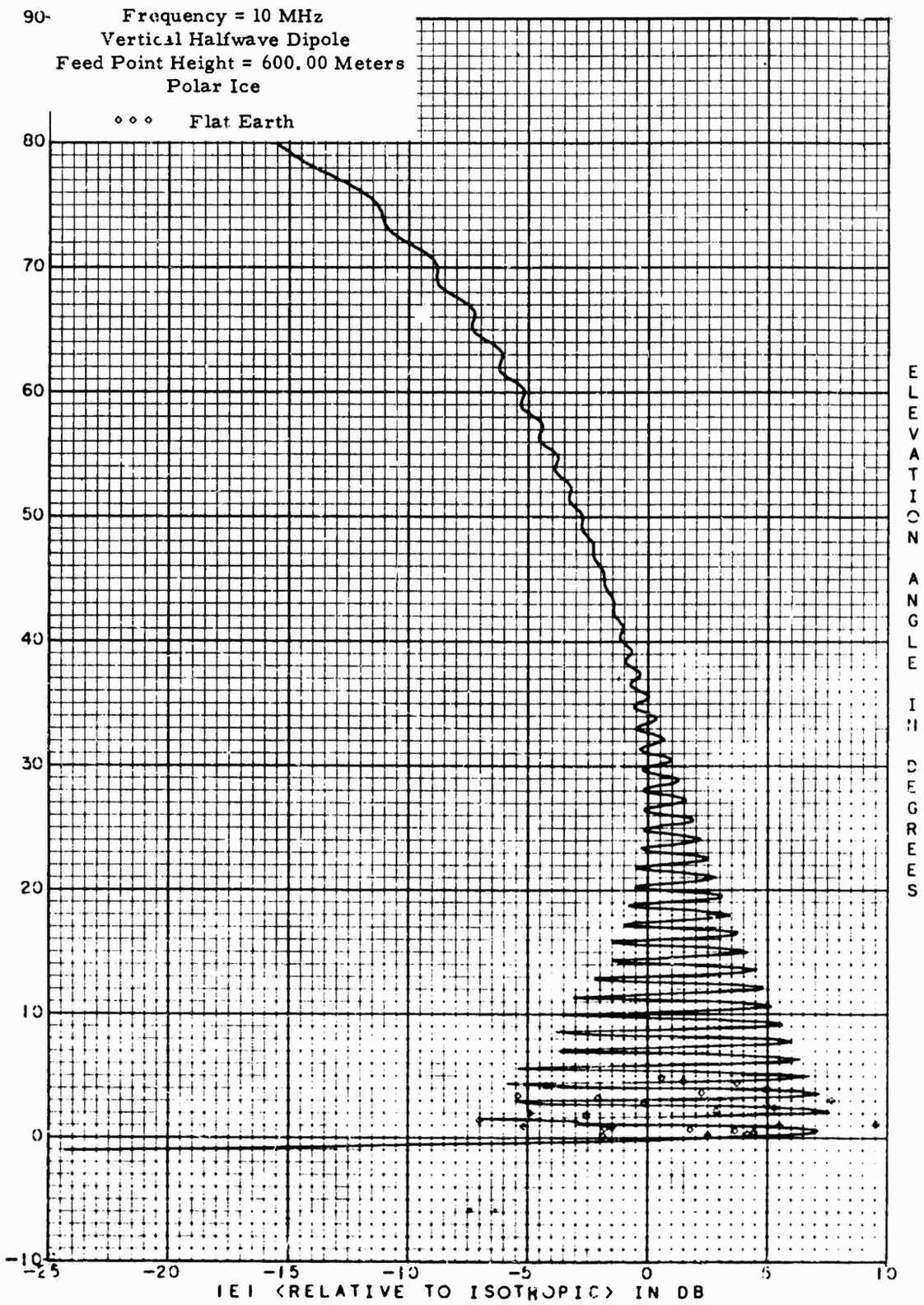

13.8. Vertical radiation pattern of a vertical half-wave dipole located 20λ above polar ice. The frequency is 10 MHz.

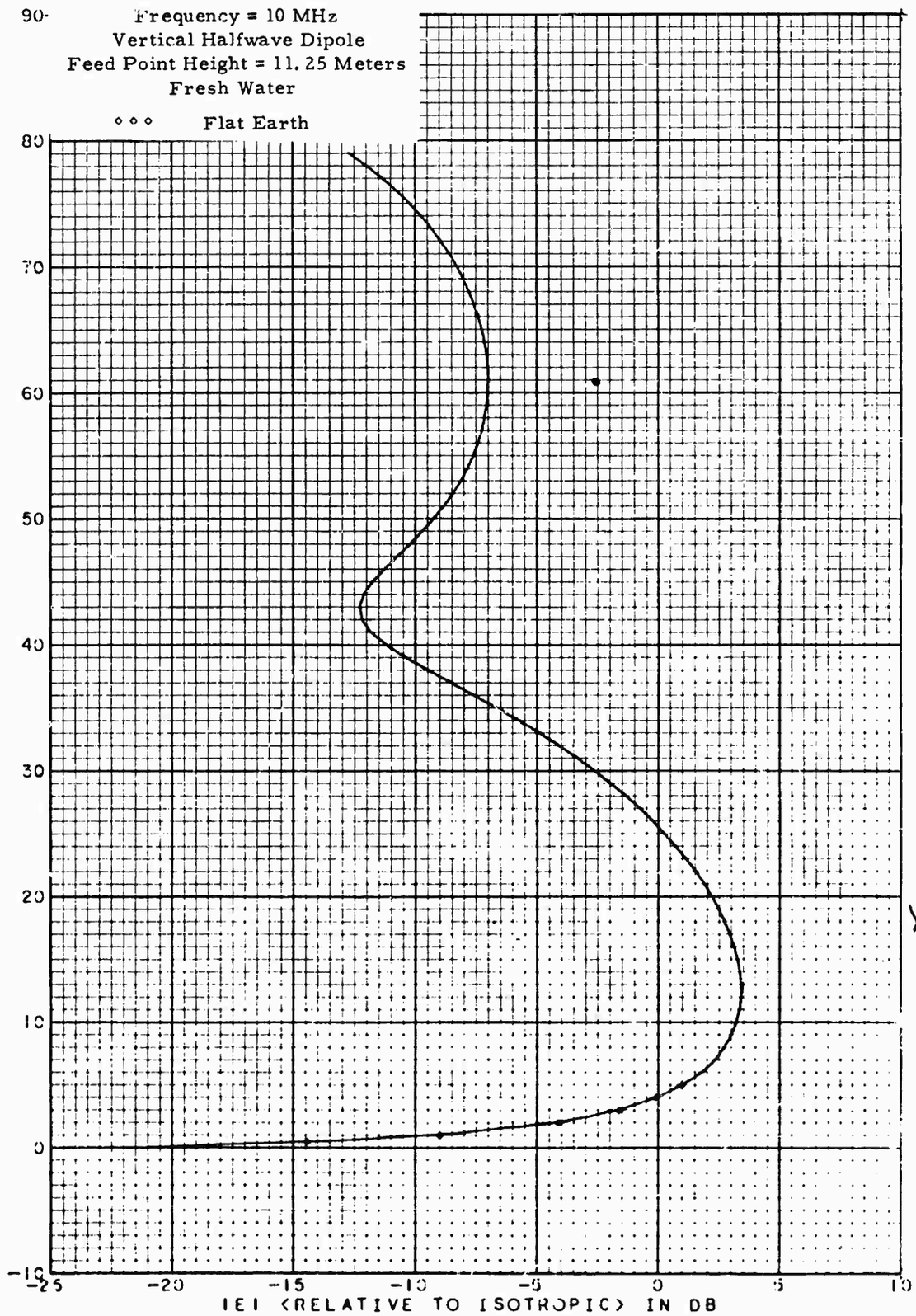

14.1. Vertical radiation pattern of a vertical half-wave dipole located $\frac{3}{8}\lambda$ above fresh water. The frequency is 10 MHz.

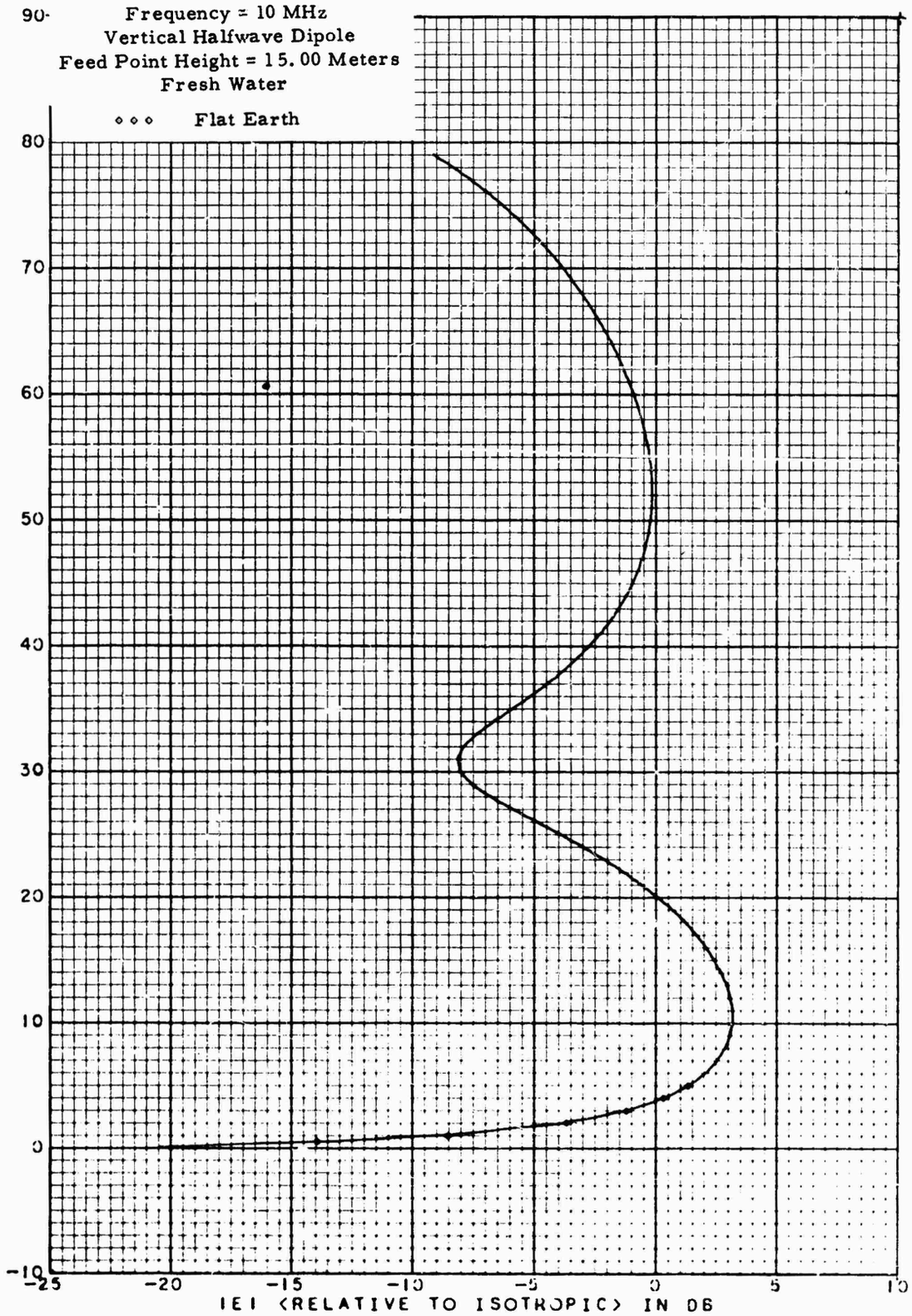

14.2. Vertical radiation pattern of a vertical half-wave dipole located $\lambda/2$ above fresh water. The frequency is 10 MHz.

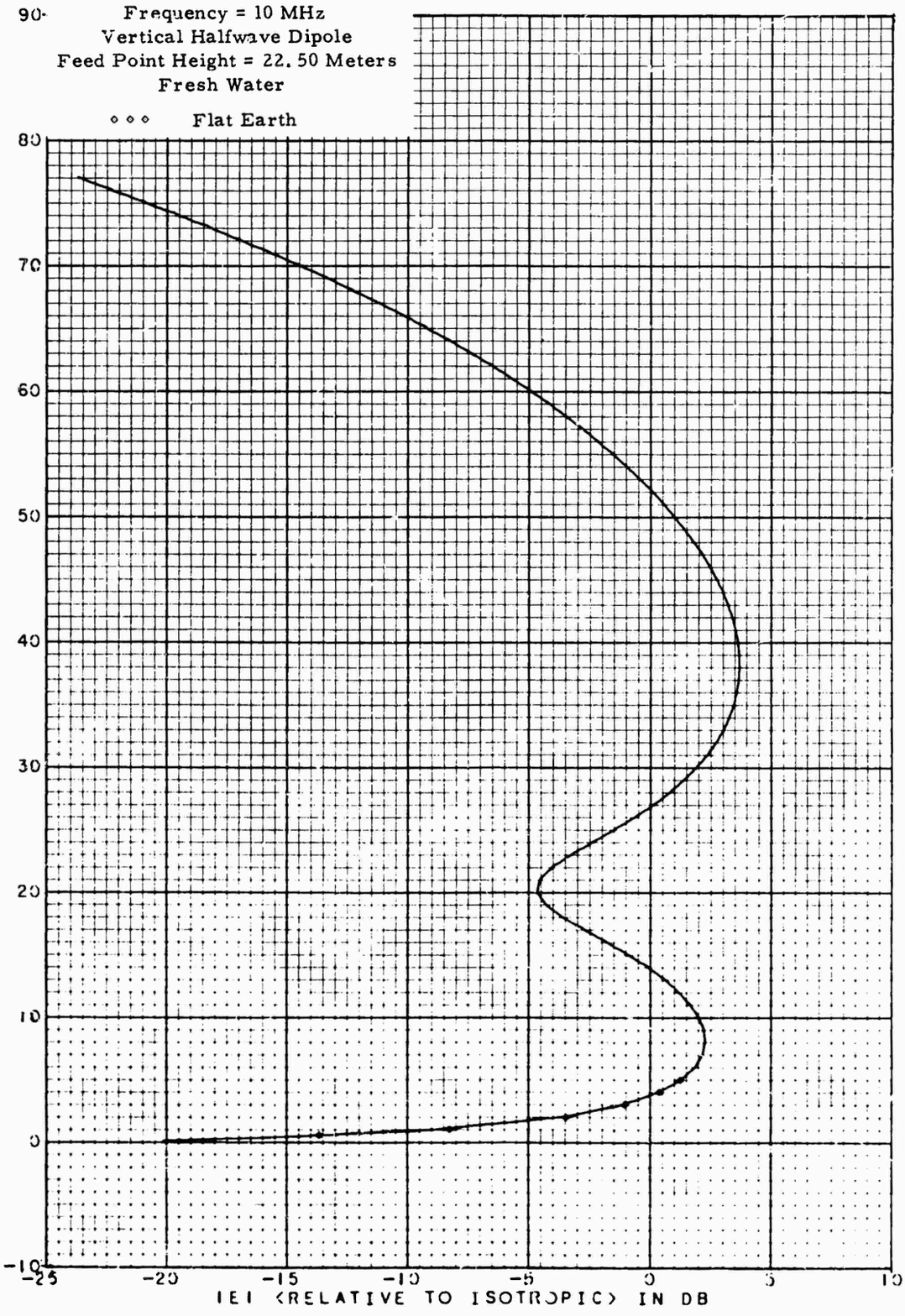

14.3. Vertical radiation pattern of a vertical half-wave dipole located $\frac{3}{4}\lambda$ above fresh water. The frequency is 10 MHz.

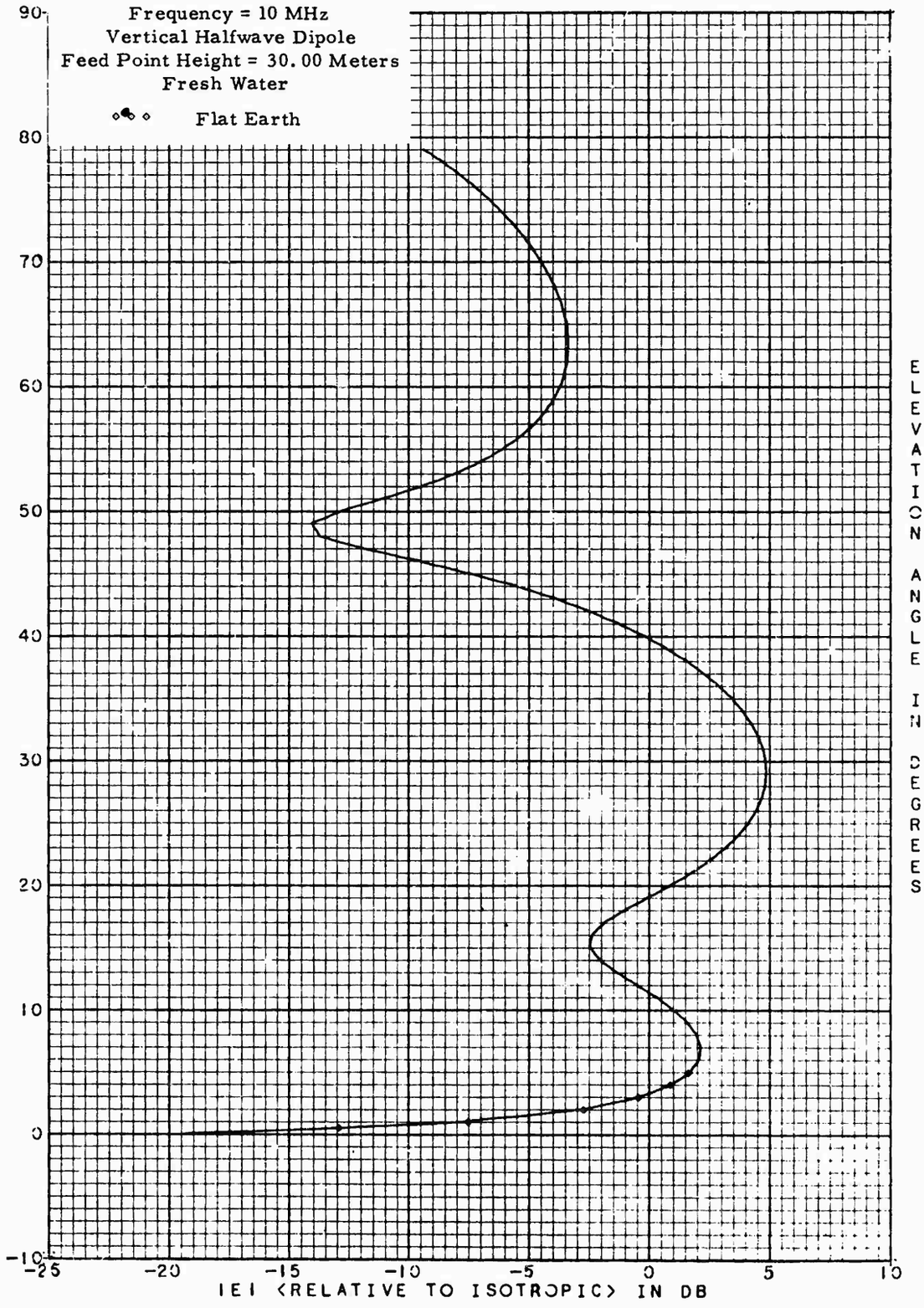

14.4. Vertical radiation pattern of a vertical half-wave dipole located λ above fresh water. The frequency is 10 MHz.

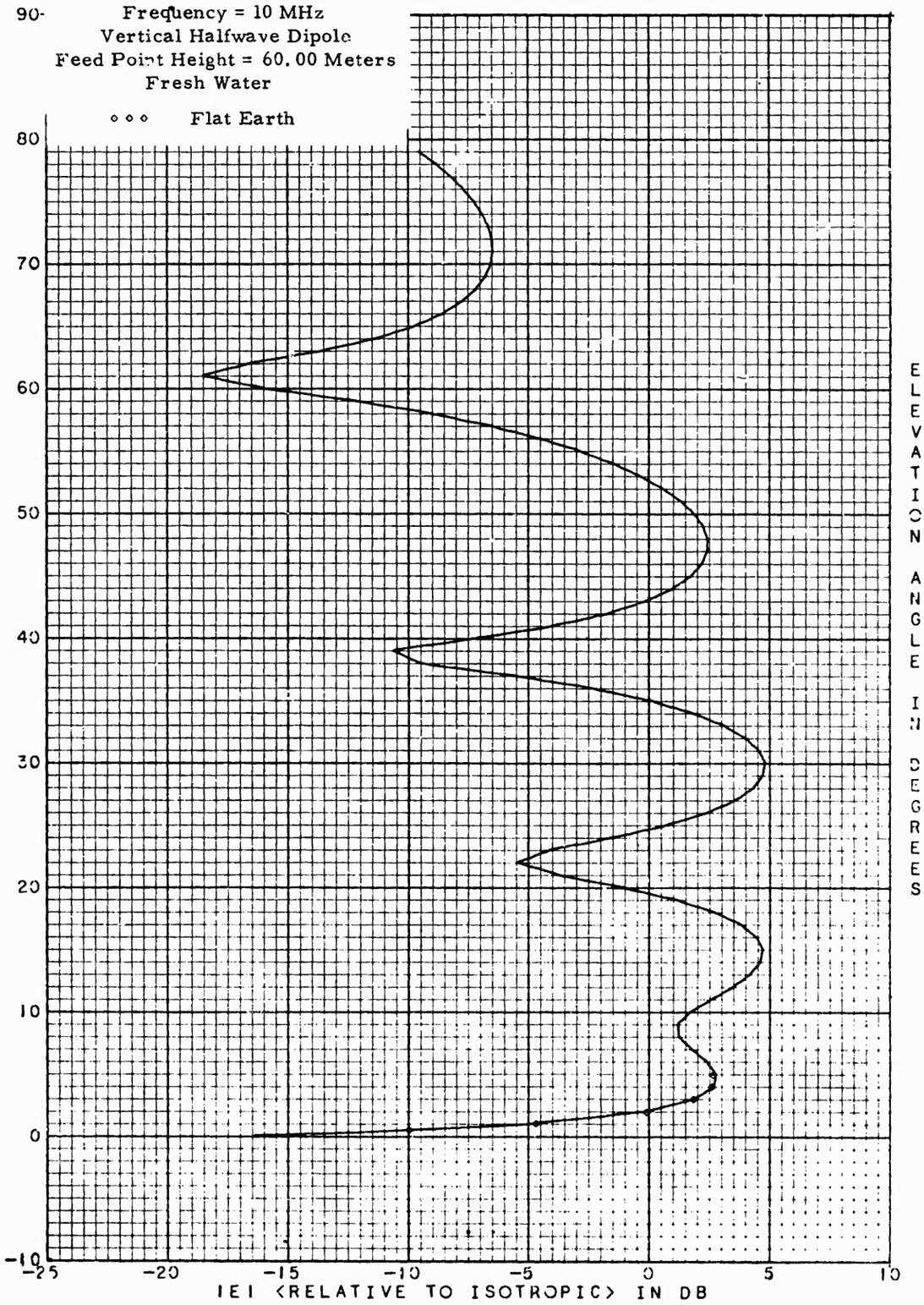

14.5. Vertical radiation pattern of a vertical half-wave dipole located 2λ above fresh water. The frequency is 10 MHz.

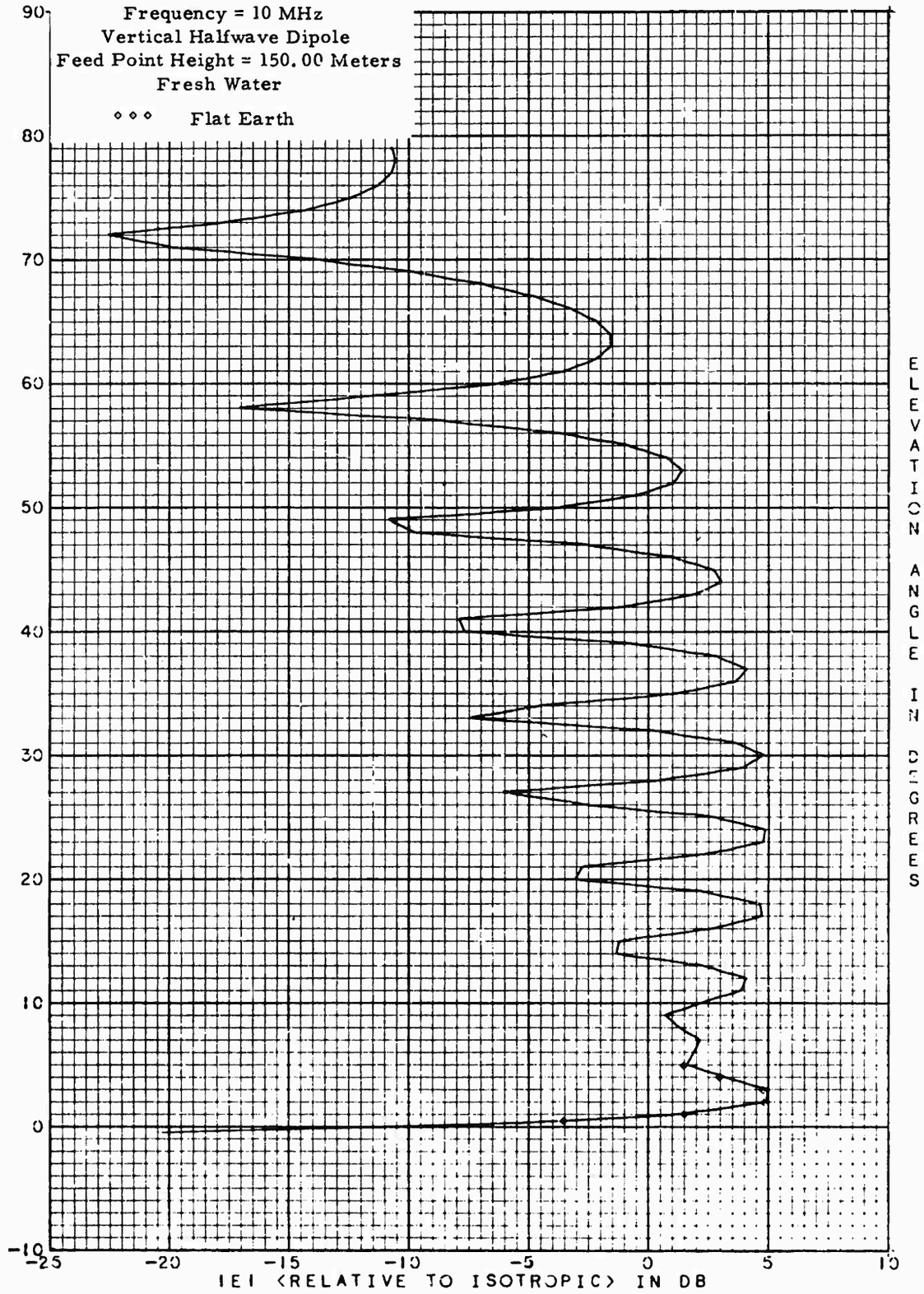

14.6. Vertical radiation pattern of a vertical half-wave dipole located 5λ above fresh water. The frequency is 10 MHz.

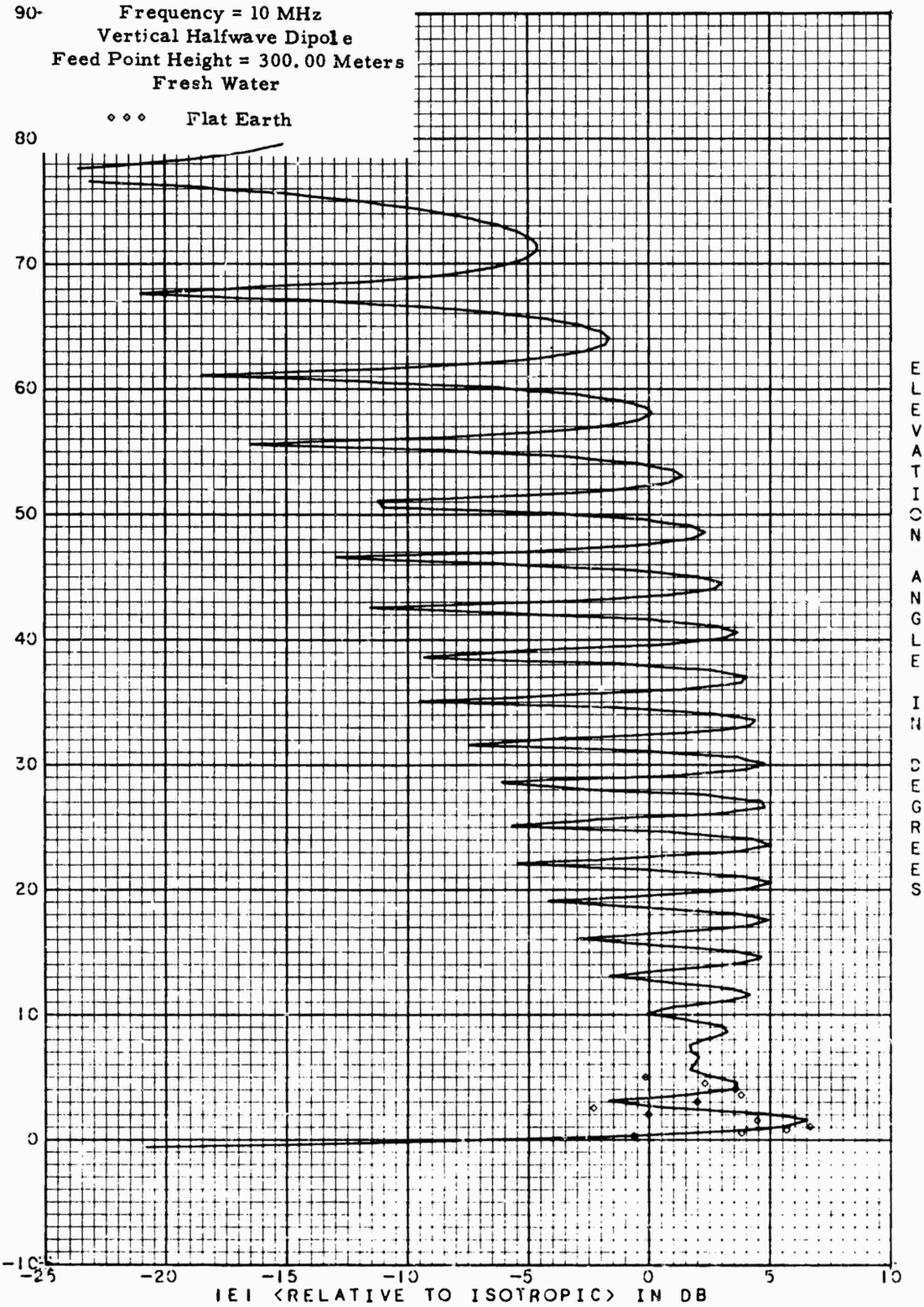

14.7. Vertical radiation pattern of a vertical half-wave dipole located 10λ above fresh water. The frequency is 10 MHz.

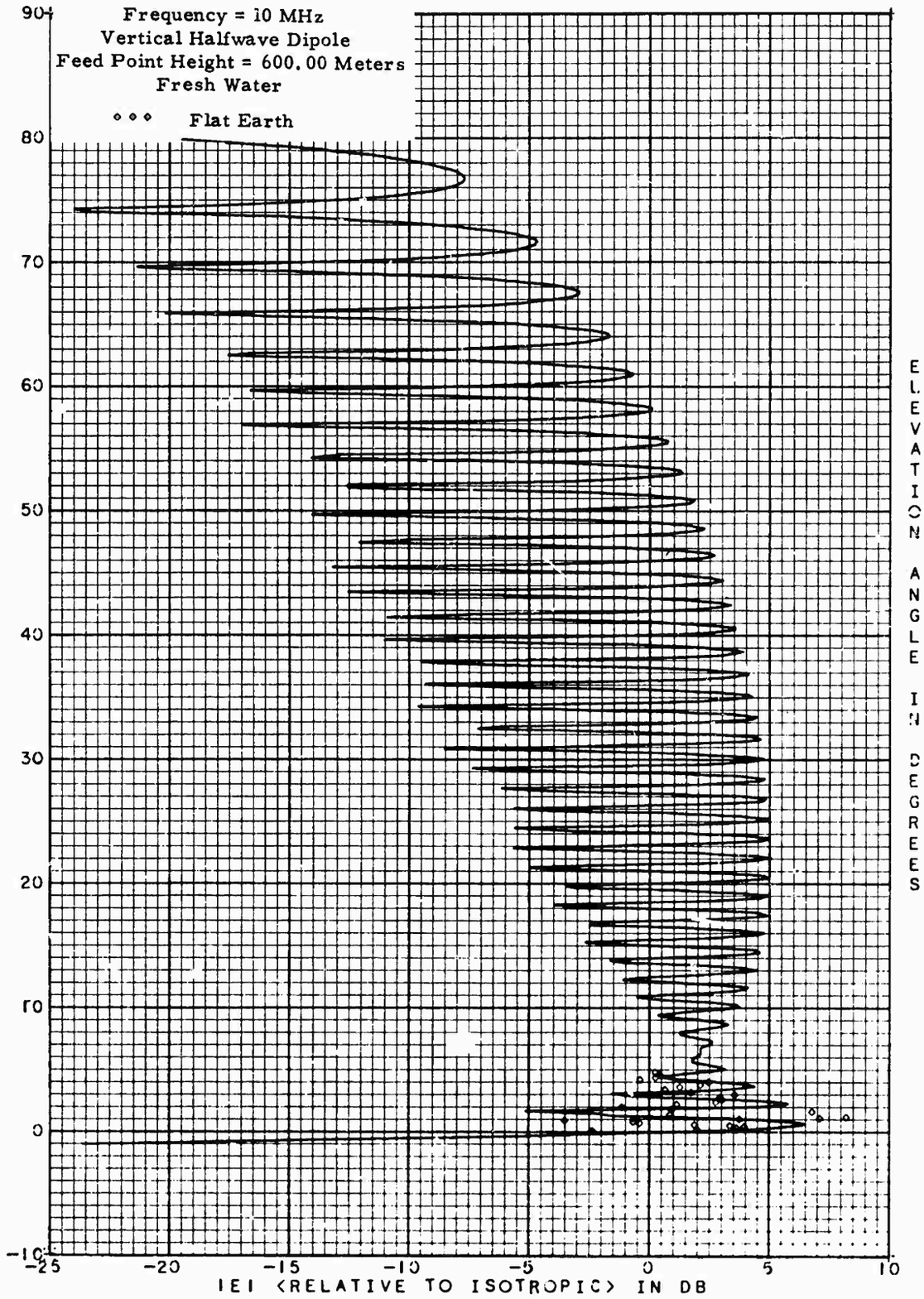

14.8. Vertical radiation pattern of a vertical half-wave dipole located 20λ above fresh water. The frequency is 10 MHz.

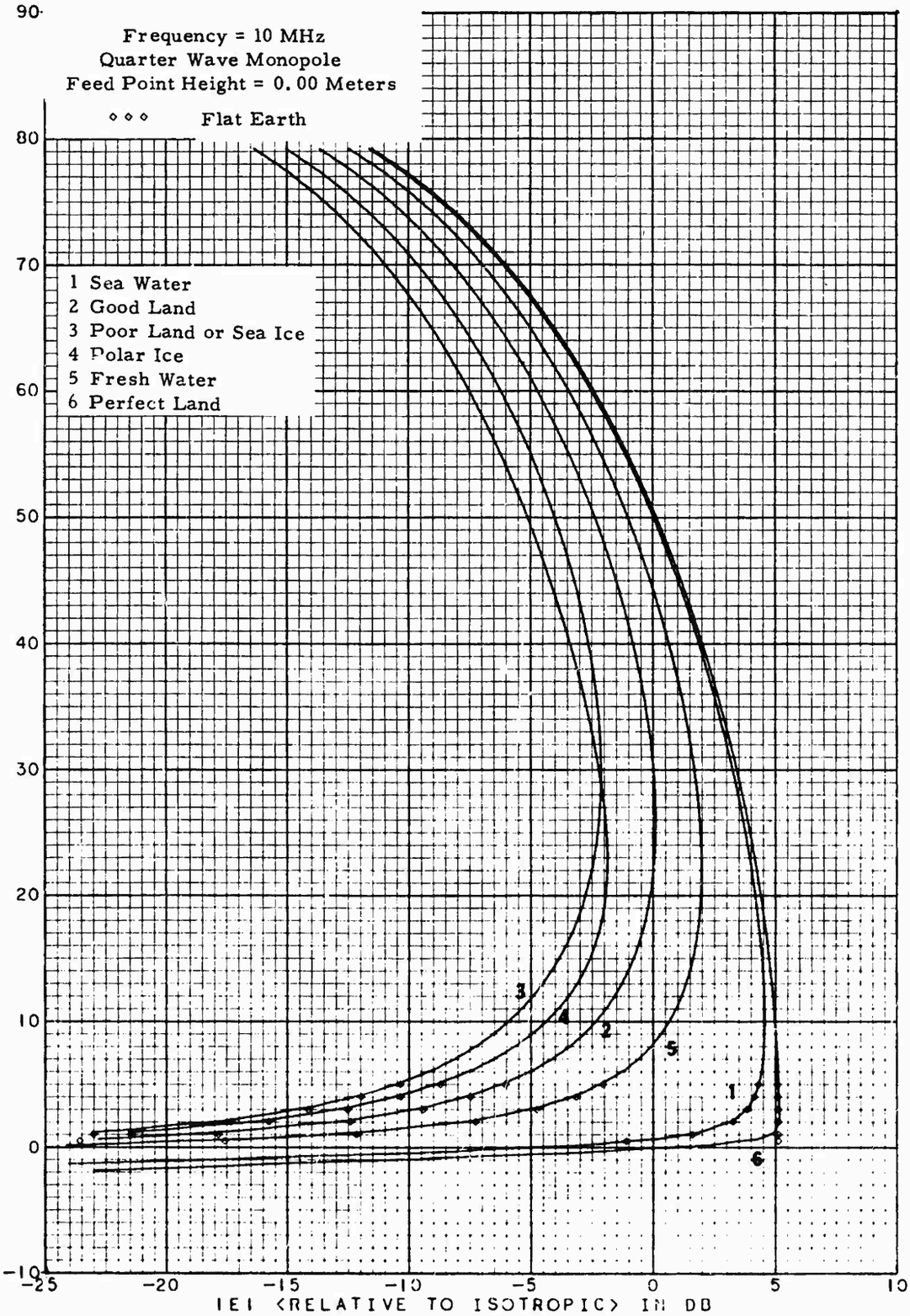

15. Vertical radiation pattern of a quarter-wave grounded antenna with perfect counterpoise on various kinds of ground. The frequency is 10 MHz.

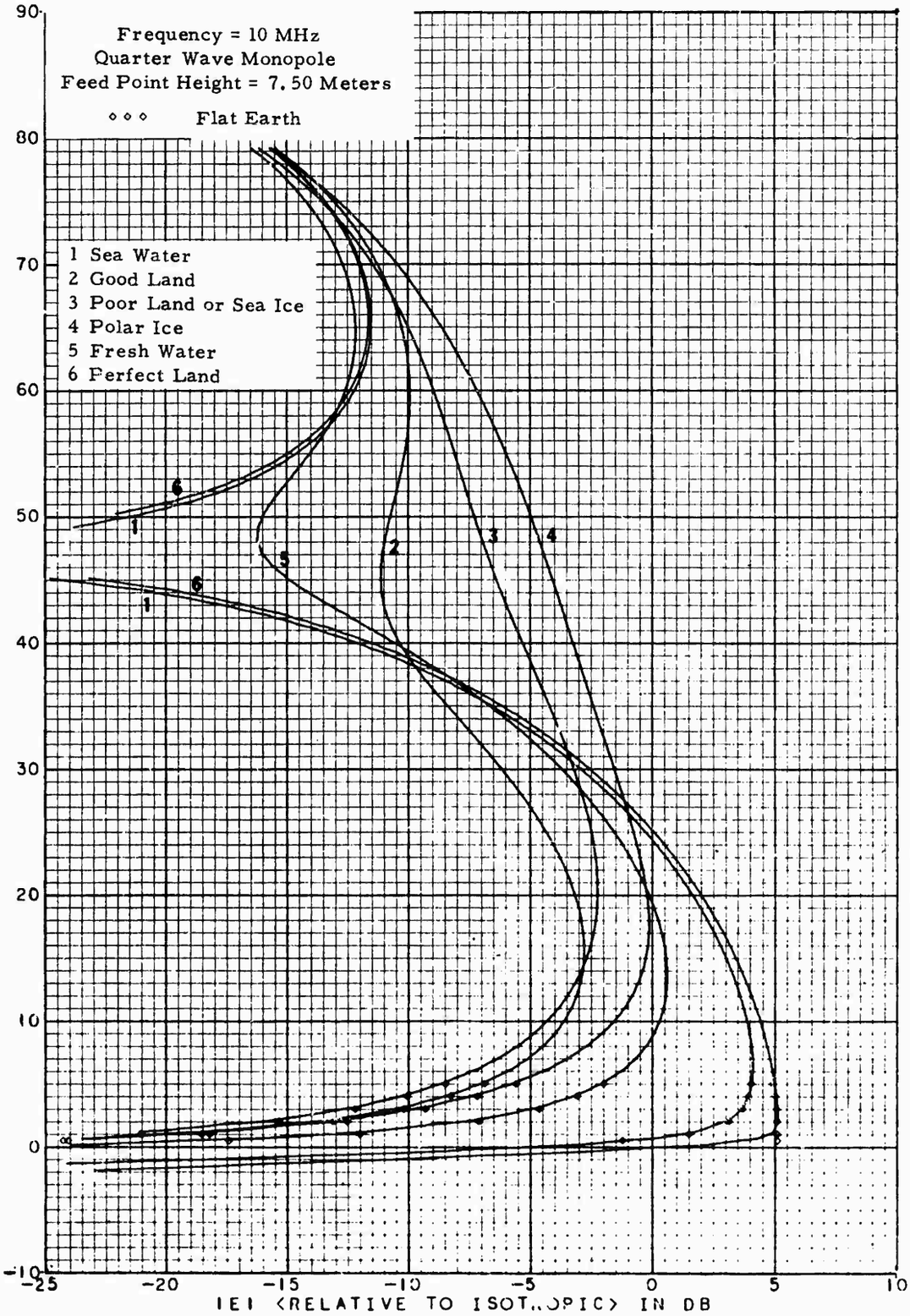

16. Vertical radiation pattern of a quarter-wave antenna with perfect counterpoise located $\lambda/4$ above various types of ground. The frequency is 10 MHz.

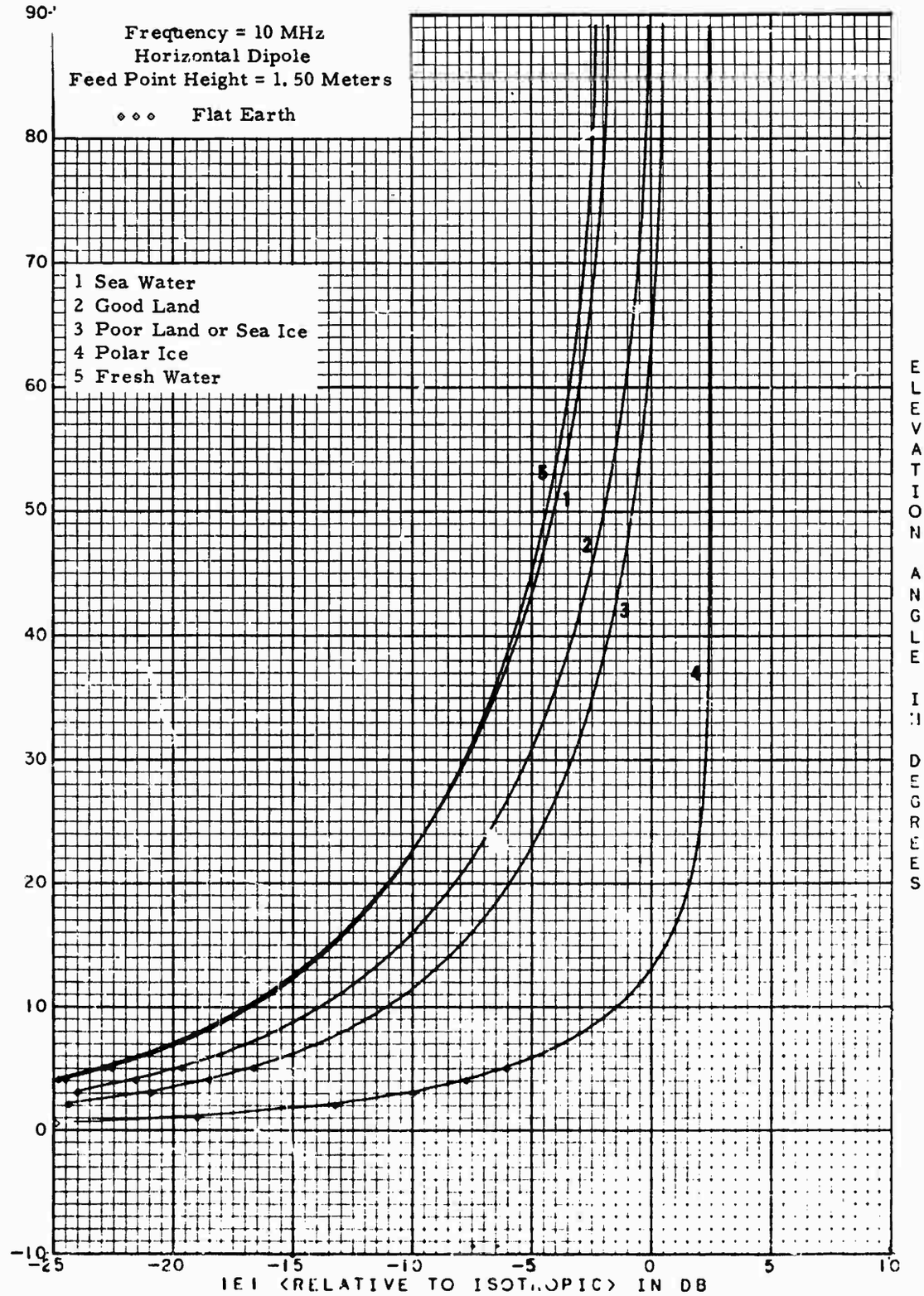

17.1. Vertical radiation pattern of a horizontal half-wave dipole 0.05λ above various kinds of ground. The frequency is 10 MHz.

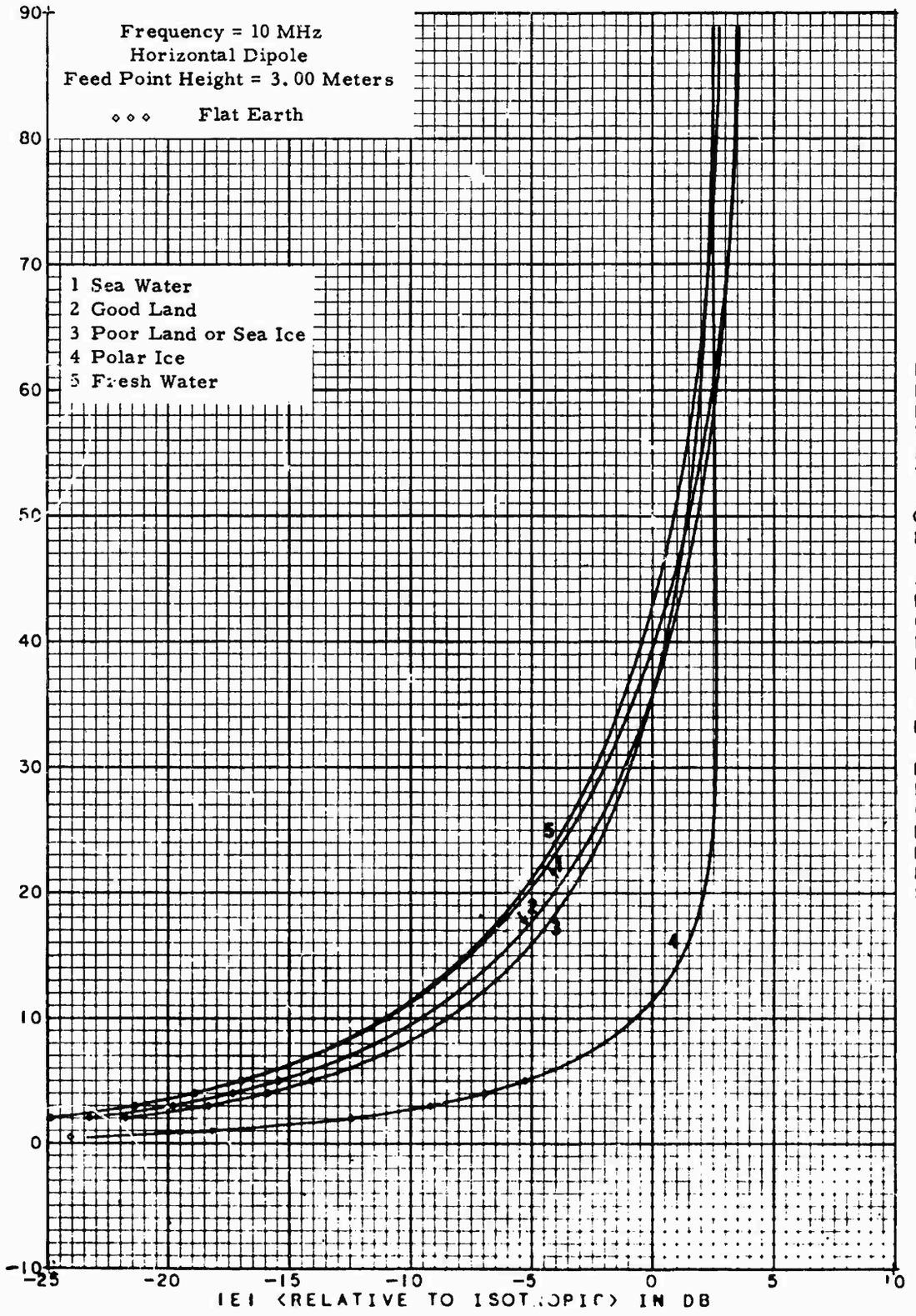

17.2. Vertical radiation pattern of a horizontal half-wave dipole 0.1λ above various kinds of ground. The frequency is 10 MHz.

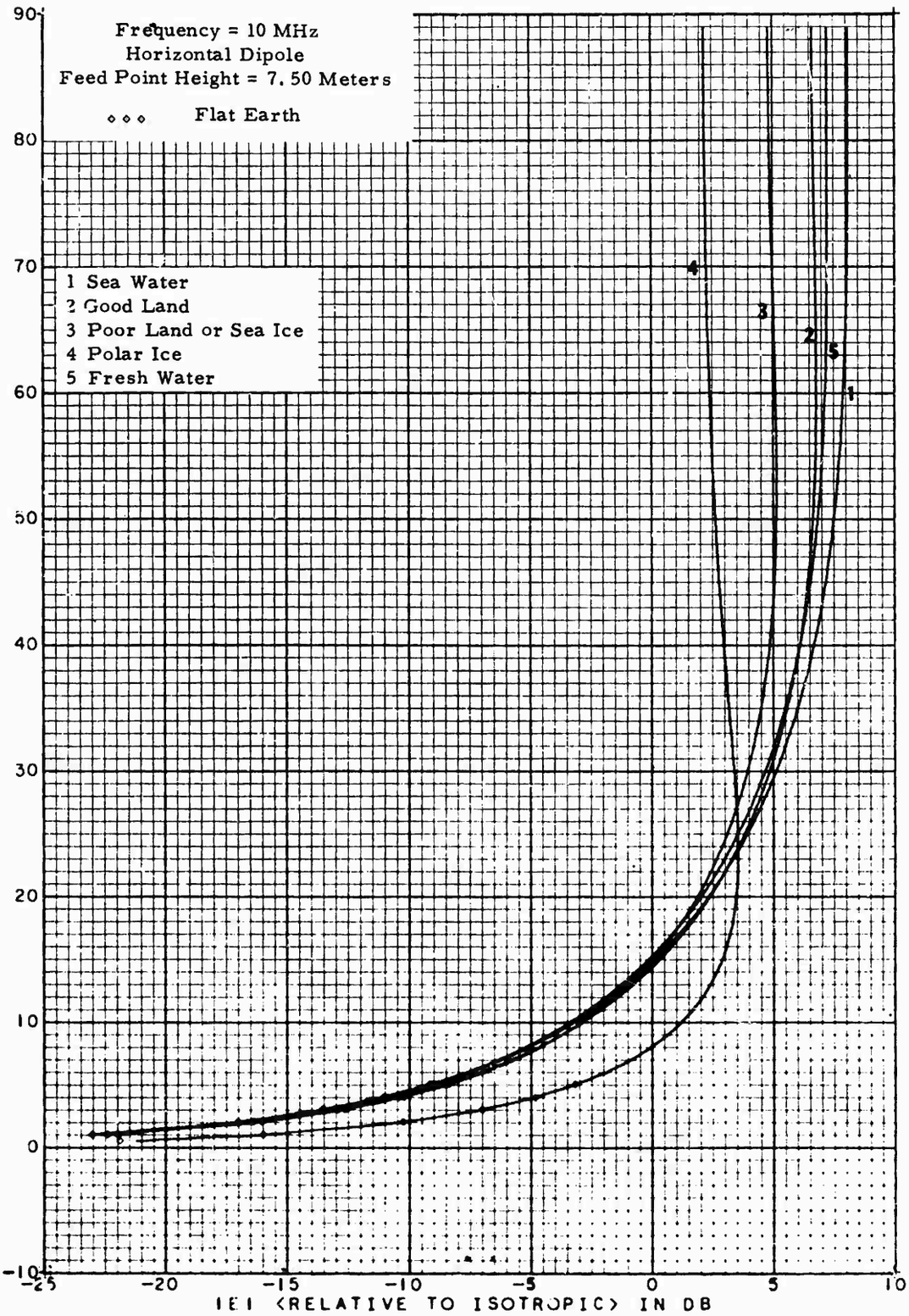

17.3. Vertical radiation pattern of a horizontal half-wave dipole 0.25 λ above various kinds of ground. The frequency is 10 MHz.

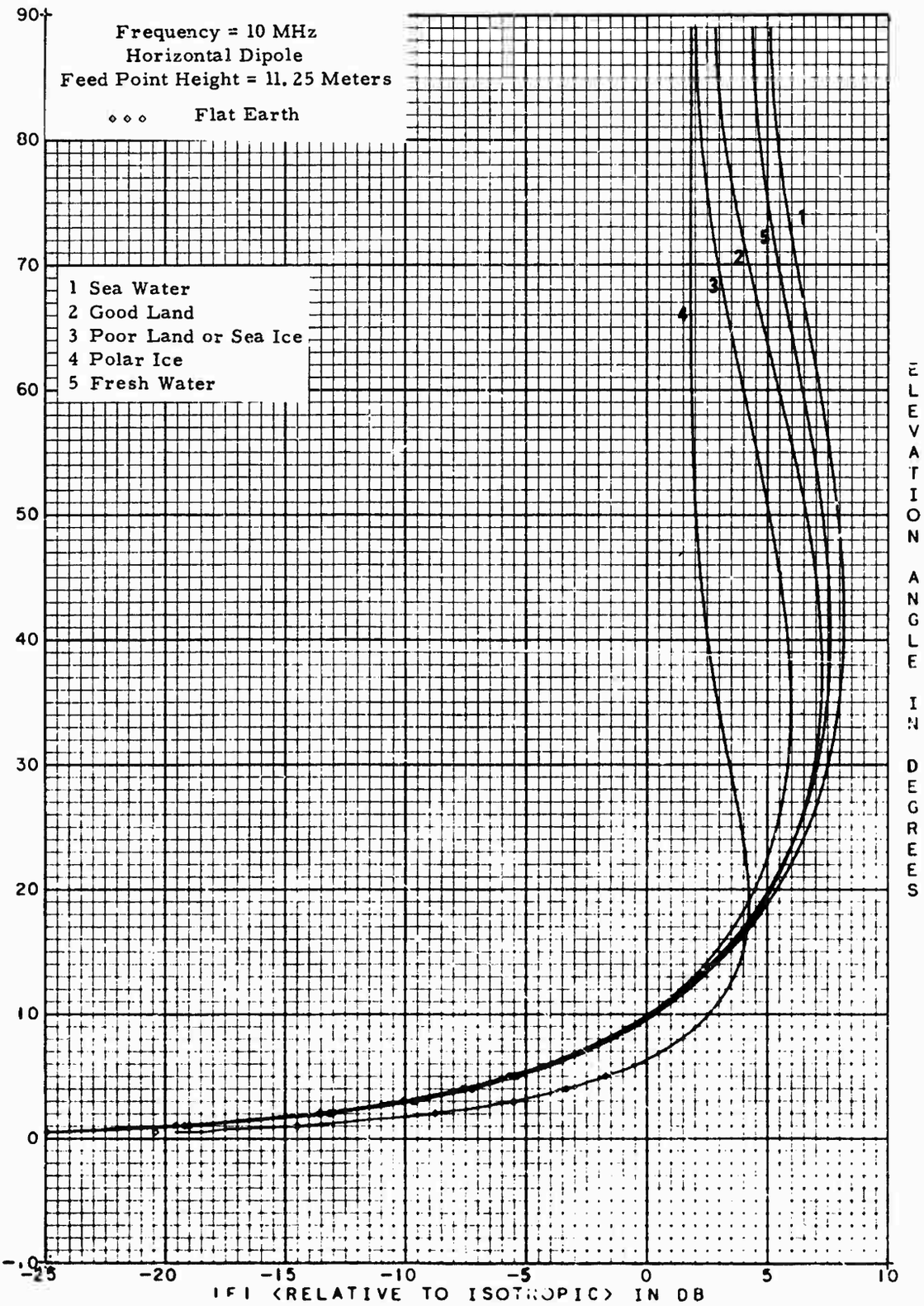

17 Vertical radiation pattern of a horizontal half-wave dipole 0.375λ above various kinds of ground. The frequency is 10 MHz.

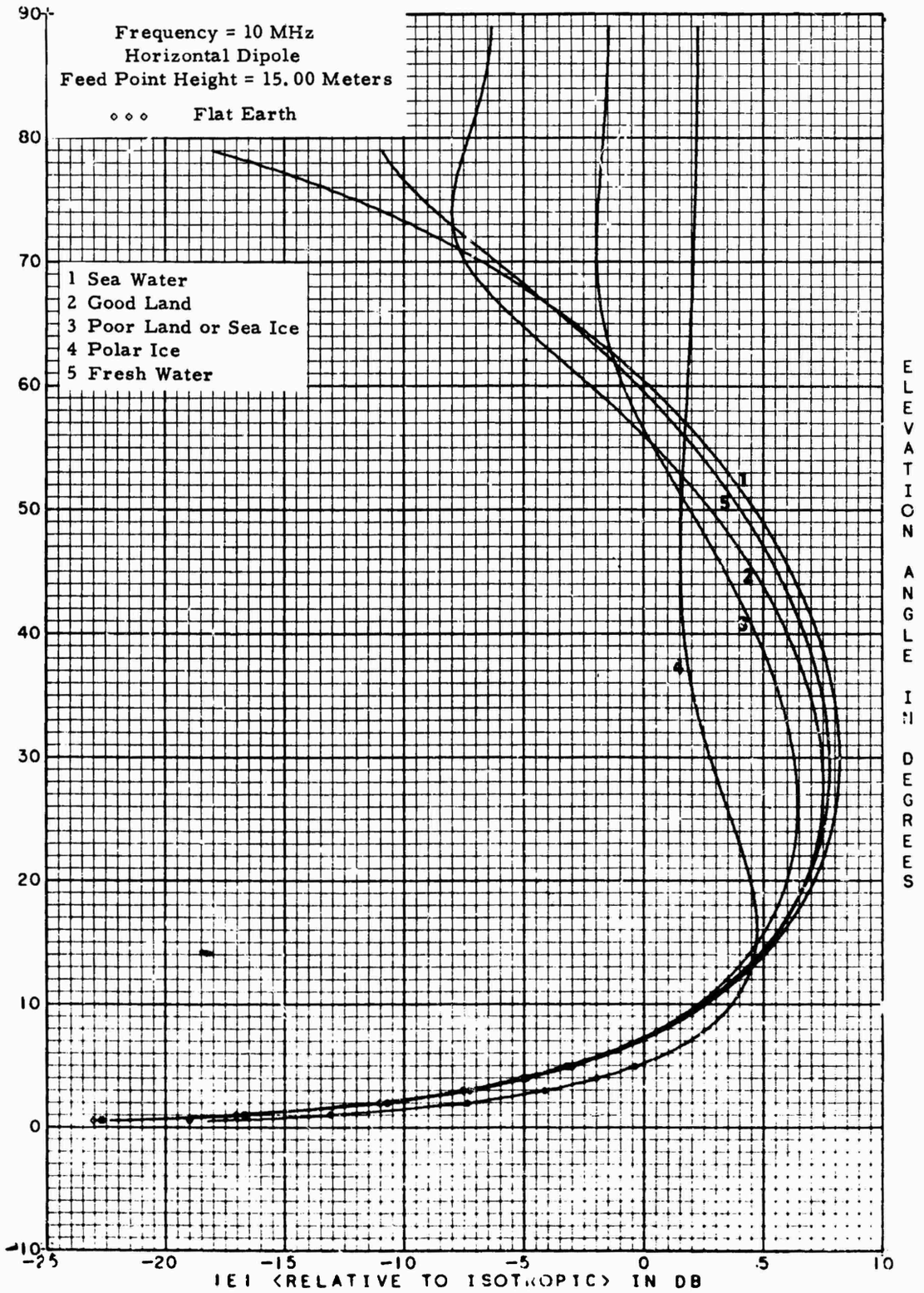

17.5. Vertical radiation pattern of a horizontal half-wave dipole 0.5λ above various kinds of ground. The frequency is 10 MHz.

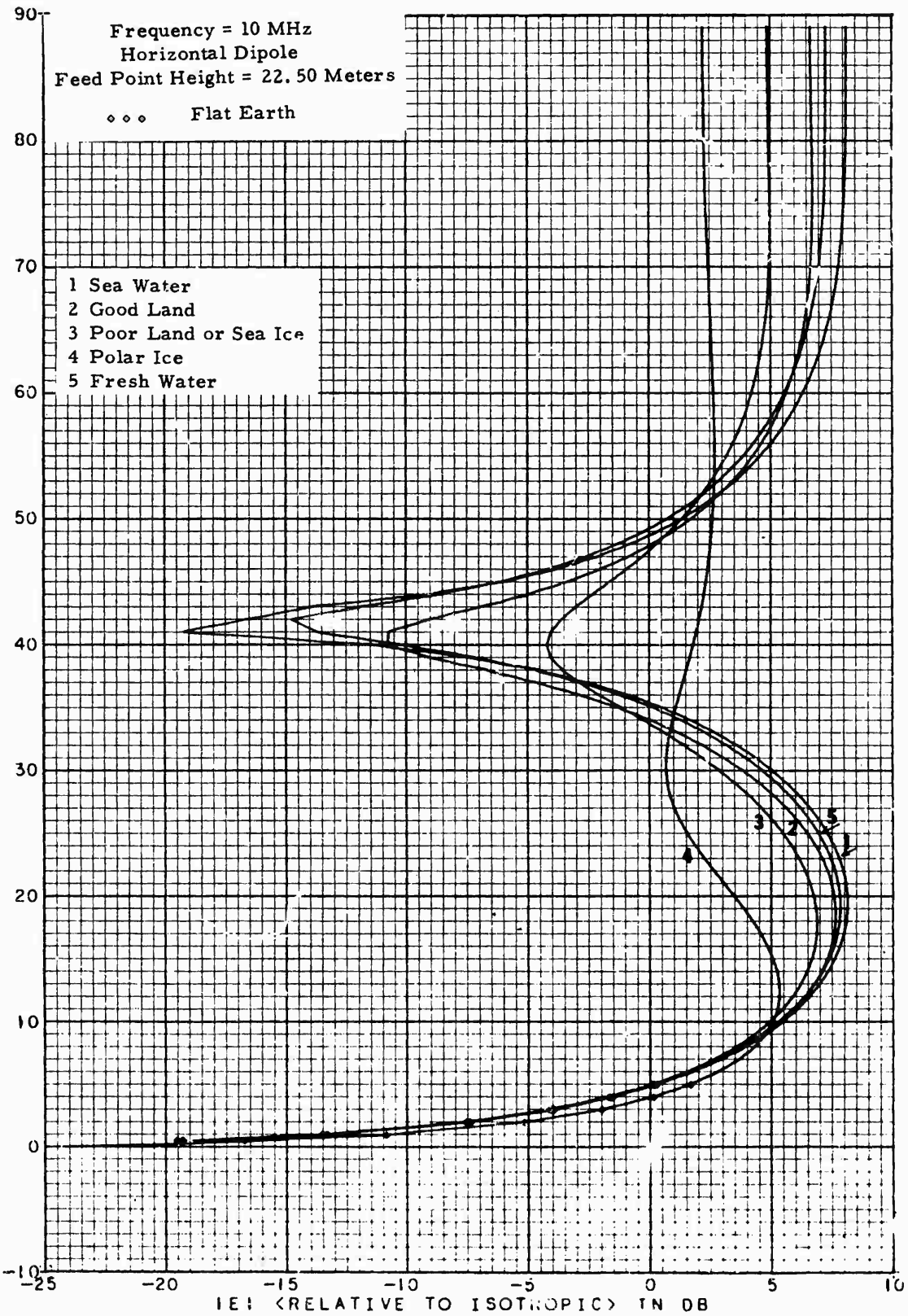

17.6. Vertical radiation pattern of a horizontal half-wave dipole 0.75λ above various kinds of ground. The frequency is 10 MHz.

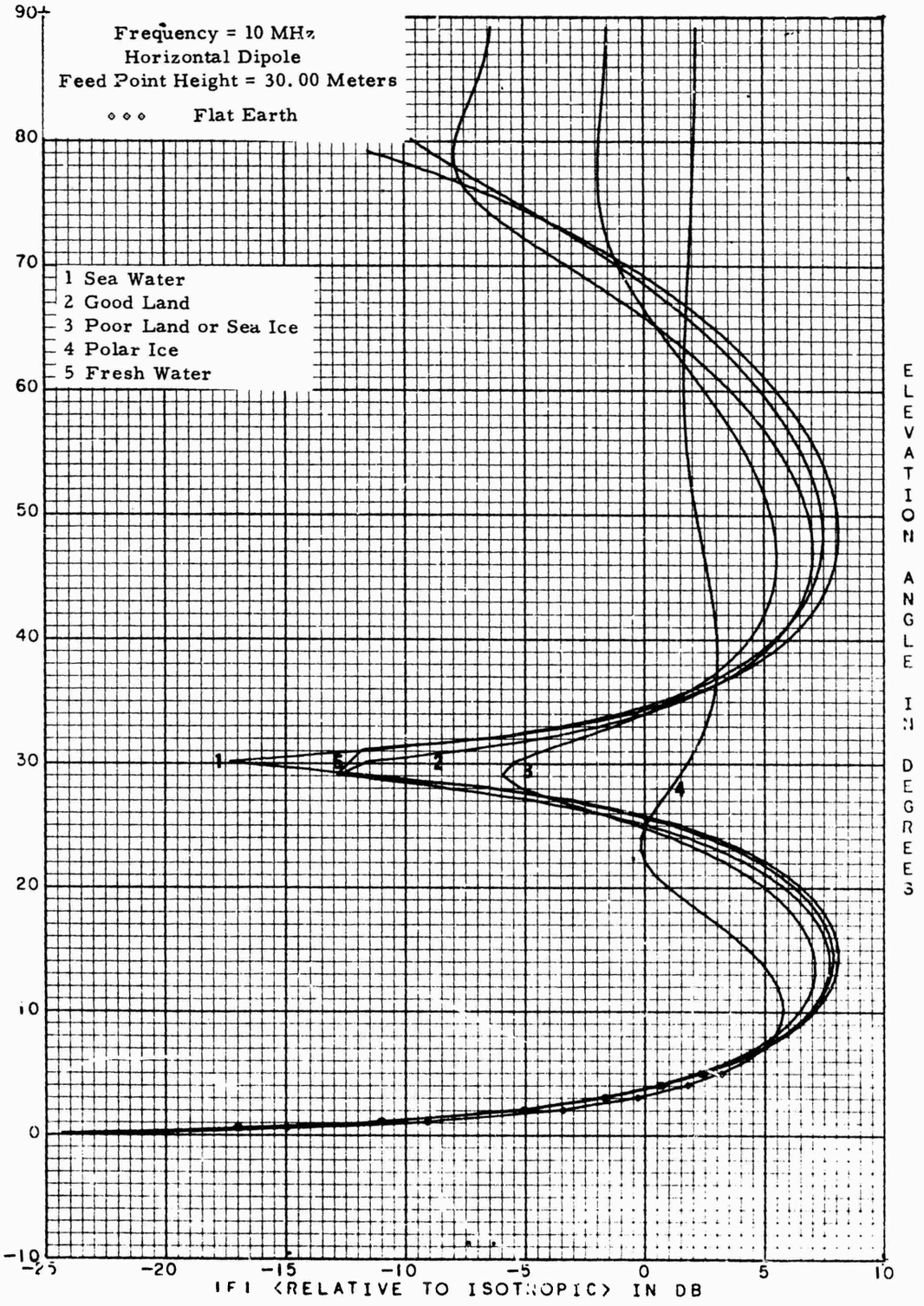

17.7. Vertical radiation pattern of a horizontal half-wave dipole λ above various kinds of ground. The frequency is 10 MHz.

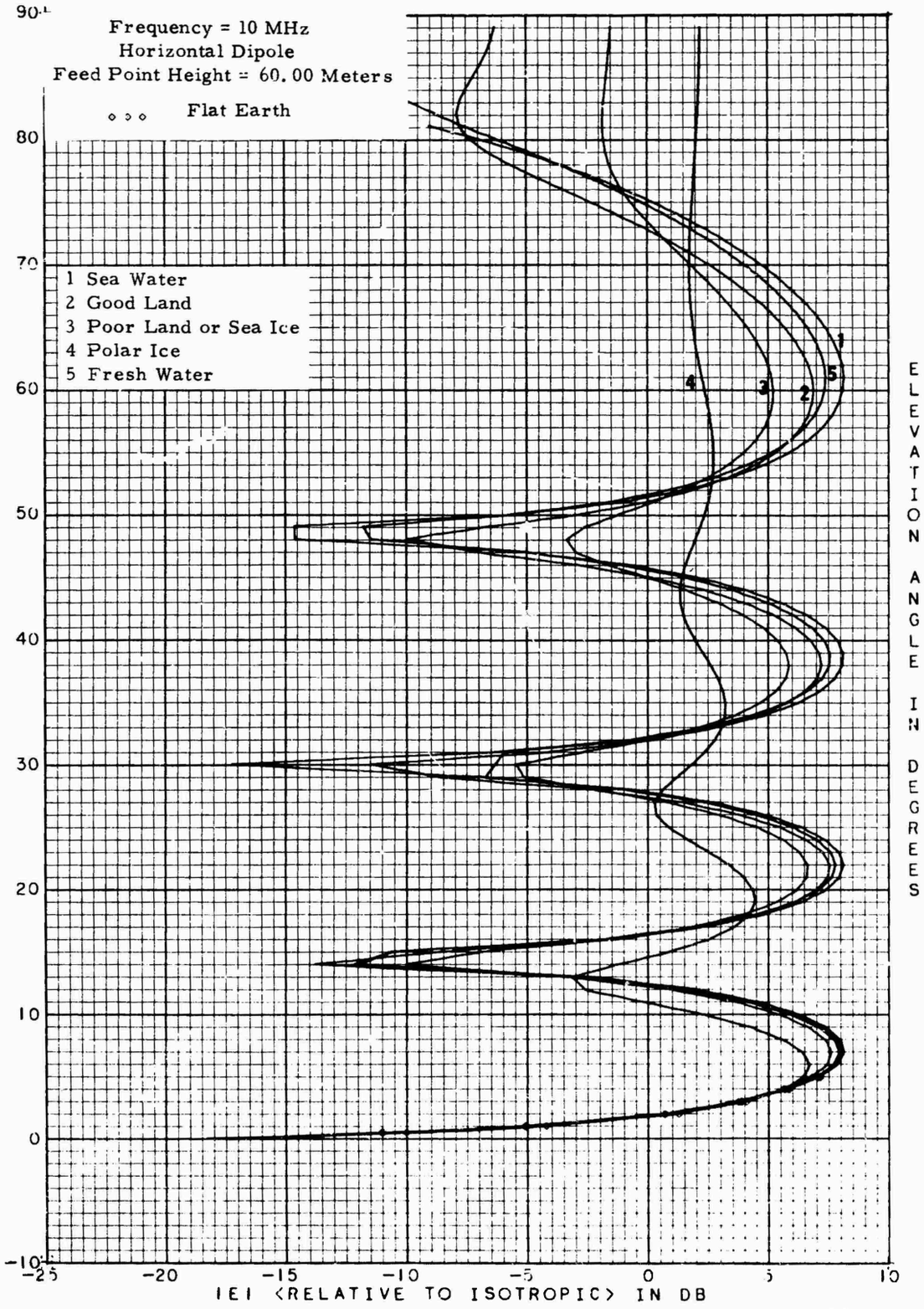

17.8. Vertical radiation pattern of a horizontal half-wave dipole 2λ above various kinds of ground. The frequency is 10 MHz.

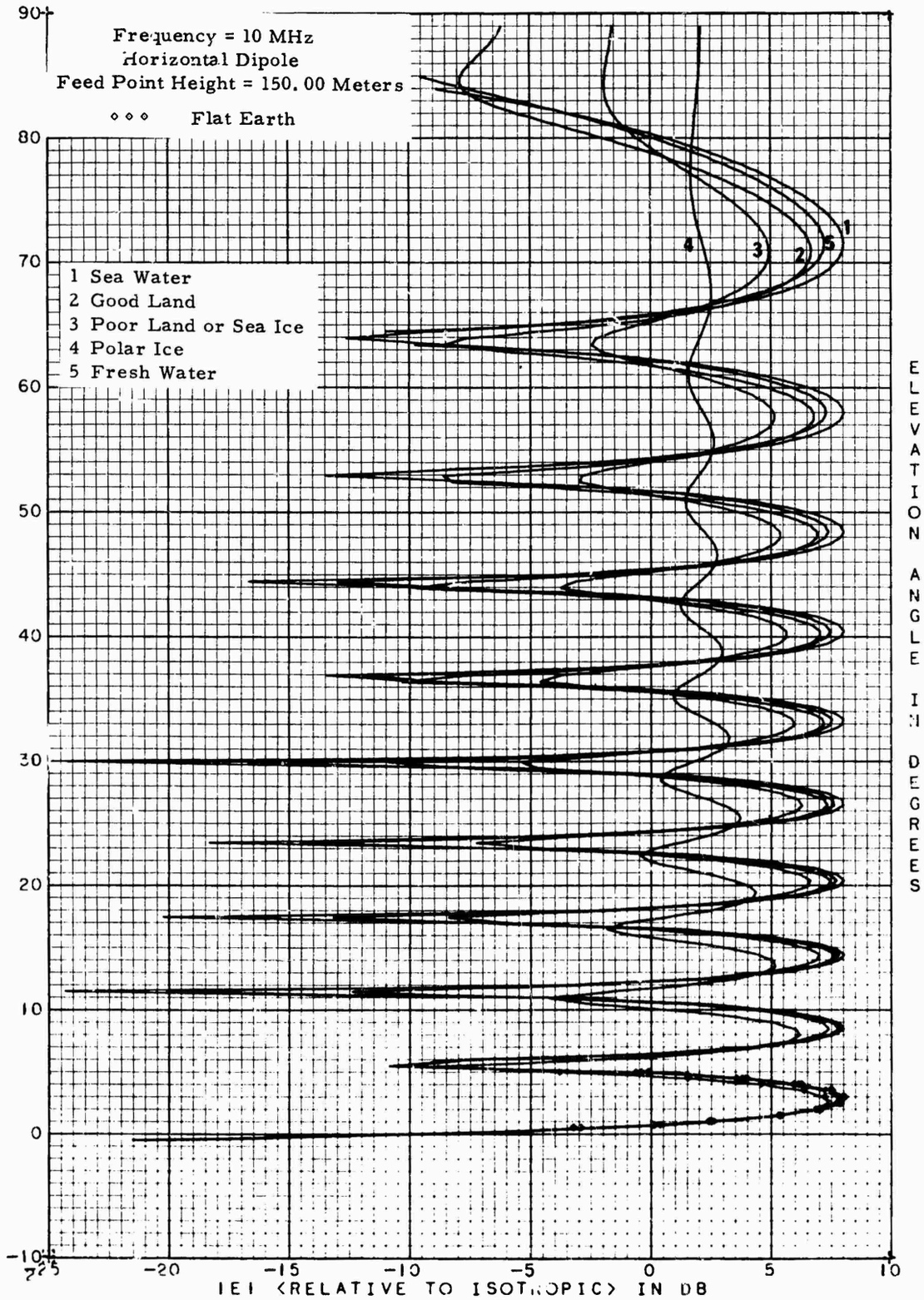

17.9. Vertical radiation pattern of a horizontal half-wave dipole 5λ above various kinds of ground. The frequency is 10 MHz.

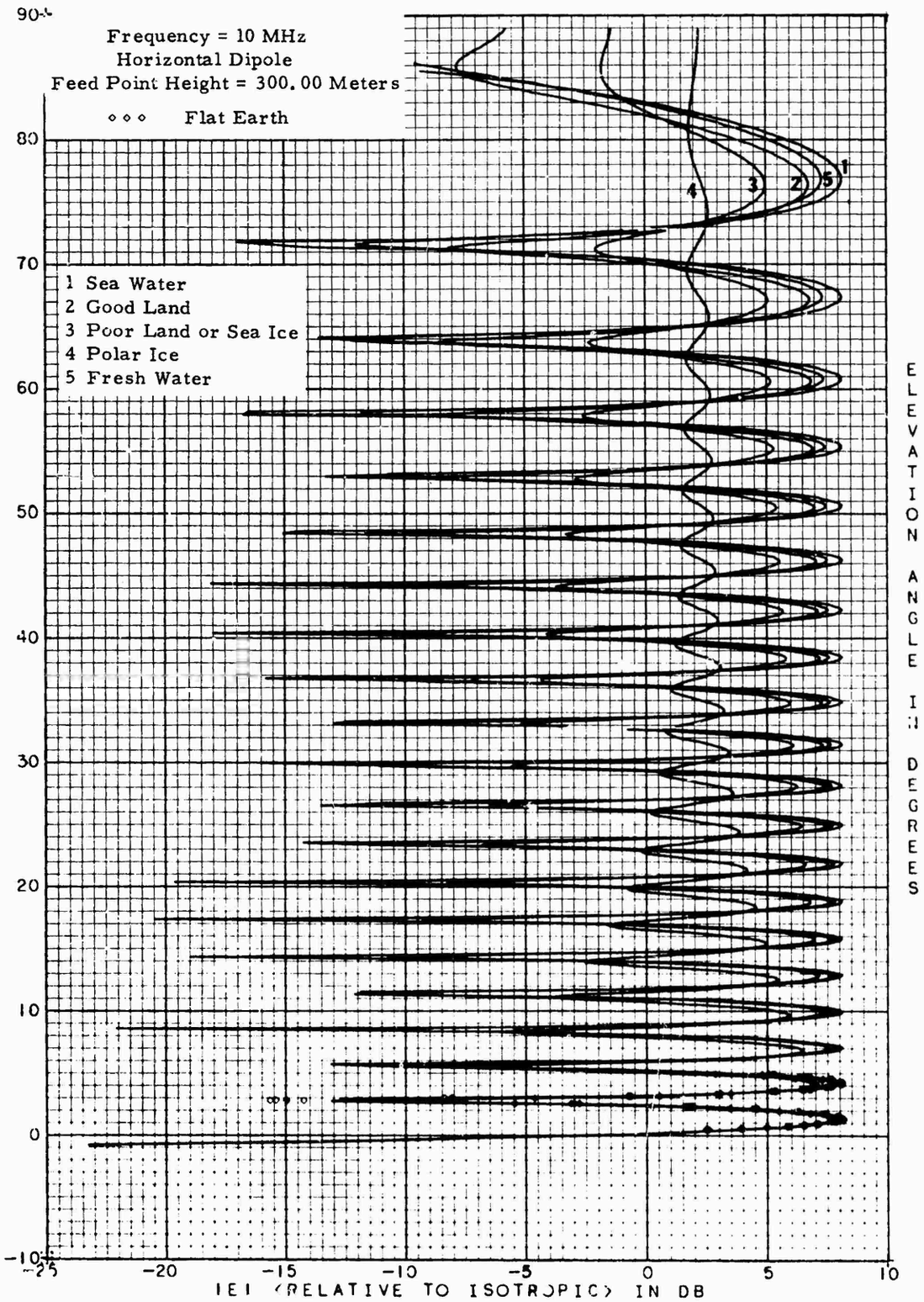

17.10. Vertical radiation pattern of a horizontal half-wave dipole 10λ above various kinds of ground. The frequency is 10 MHz.

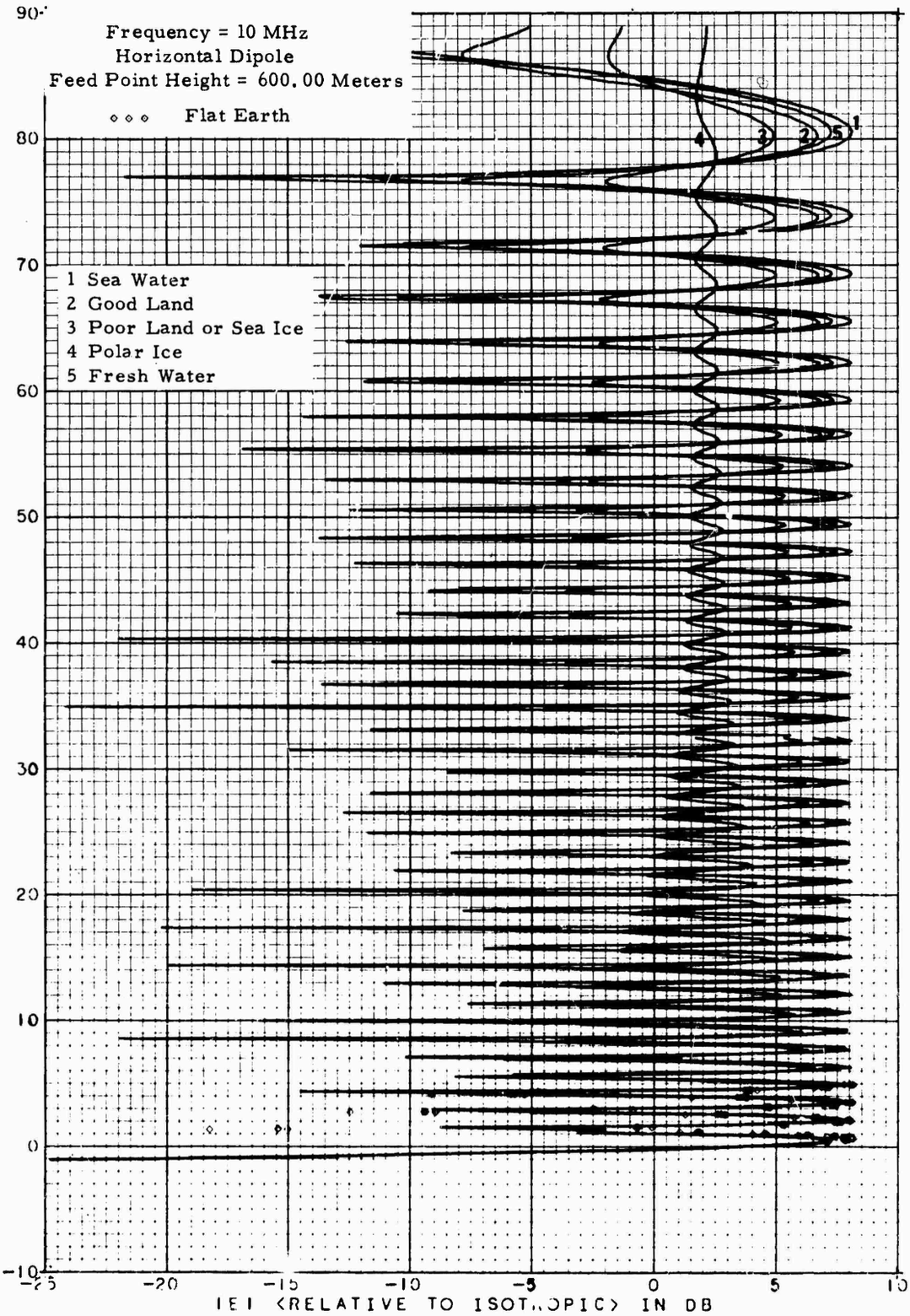

17.11. Vertical radiation pattern of a horizontal half-wave dipole 20λ above various kinds of ground. The frequency is 10 MHz.

GPO 830-575